5-31-2012

Dispersibility of and adsorption on functionalized carbon nanotubes

Susana Addo Ntim
New Jersey Institute of Technology

Copyright Warning & Restrictions

The copyright law of the United States (Title 17, United States Code) governs the making of photocopies or other reproductions of copyrighted material.

Under certain conditions specified in the law, libraries and archives are authorized to furnish a photocopy or other reproduction. One of these specified conditions is that the photocopy or reproduction is not to be "used for any purpose other than private study, scholarship, or research." If a, user makes a request for, or later uses, a photocopy or reproduction for purposes in excess of "fair use" that user may be liable for copyright infringement,

This institution reserves the right to refuse to accept a copying order if, in its judgment, fulfillment of the order would involve violation of copyright law.

Please Note: The author retains the copyright while the New Jersey Institute of Technology reserves the right to distribute this thesis or dissertation

Printing note: If you do not wish to print this page, then select "Pages from: first page # to: last page #" on the print dialog screen

ABSTRACT

DISPERSIBILITY OF AND ADSORPTION ON FUNCTIONALIZED CARBON NANOTUBES

by

Susana Addo Ntim

As the applications of carbon nanotubes (CNTs) proliferate, mass production and widespread use of these nanocarbons will continue to rise. While raw, unrefined, and hydrophobic carbon nanotubes tend to settle out of aqueous media/environments, water dispersible, functionalized CNTs (F-CNTs) will contaminate water resources and will also be highly bioavailable on exposure. Therefore, there is a need to develop an understanding of the fate of F-CNTs in aqueous media.

The colloidal behavior of aqueous dispersions of F-CNTs formed via carboxylation and polymer wrapping with polyvinyl pyrrolidone (PVP) is investigated. The presence of polymer on the nanotube surface provides steric stabilization, and the aggregation behavior of the colloidal system is quite different from its covalently functionalized analog. Based on hydrophobicity index (HI), particle size distribution, zeta potential as well as the aggregation kinetics studies using time-resolved dynamic light scattering, the PVP wrapped CNT is less prone to agglomeration, It is however, less stable in the long term, which is attributed to the partial unwrapping of the polyvinyl pyrrolidone layer on the CNT surface.

CNTs represent a diverse group of nanotubes that vary in size, shape and chirality. Since size alters many of the properties of CNTs, it may also affect their fate and transport and is an important parameter when CNTs are in consideration as pollutants. Size dependent colloidal behavior of aqueous dispersions of carboxylated

multiwall carbon nanotubes (c-MWCNTs) is presented. While the aspect ratio does not show any definite correlation, the HI, zeta potential and aggregation kinetics show dependence on the length of the c-MWCNTs. The shorter c-MWCNTs show significantly lower HI values, smaller particle aggregates, higher absolute zeta potential values and higher critical coagulation concentrations (*ccc*) in the presence of electrolytes. The diameter of the short c-MWCNTs does not appear to influence their aggregation behavior. The longer c-MWCNTs however, show a dependence on diameter where stability decreases with increasing CNT diameter.

The potential for contaminant specific functionalization of CNTs for water purification is explored. The adsorptive removal of arsenic from water using multiwall carbon nanotube-metal oxide hybrids (MWCNT-ZrO_2 and Fe-MWCNT) is presented. The synthesis of the sorbent was facilitated by the high degree of nanotube functionalization using a microwave assisted process, and controlled assemblies of iron oxide and zirconia are possible where the MWCNT serve as an effective support for the oxides. Metal oxide loadings of up to 11% per carbon atom are achieved and the hybrids are effective in arsenic removal to below drinking water standard levels of 10 μg L^{-1}. Equilibrium and kinetic modeling indicate a pseudo-second order sorption process fitting both the Langmuir and Freundlich isotherms. Regeneration data show that both sorbent materials can be used for effective arsenic removal in a cyclable fashion.

DISPERSIBILITY OF AND ADSORPTION ON FUNCTIONALIZED CARBON NANOTUBES

by
Susana Addo Ntim

A Dissertation
Submitted to the Faculty of
New Jersey Institute of Technology
in Partial Fulfillment of the Requirements for the Degree of
Doctor of Philosophy in Environmental Science

Department of Chemistry and Environmental Science

May 2012

.

APPROVAL PAGE

DISPERSIBILITY OF AND ADSORPTION ON FUNCTIONALIZED CARBON NANOTUBES

Susana Addo Ntim

Dr. Somenath Mitra, Dissertation Advisor — Date
Distinguished Professor of Chemistry and Environmental Science, NJIT

Dr. Carol A. Venanzi, Committee Member — Date
Distinguished Professor of Chemistry and Environmental Science, NJIT

Dr. Edgardo Farinas, Committee Member — Date
Associate Professor of Chemistry and Environmental Science, NJIT

Dr. Haidong Huang, Committee Member — Date
Assistant Professor of Chemistry and Environmental Science, NJIT

Dr. Pradyot Patnaik, Committee Member — Date
Consultant, Radiance, Burlington, New Jersey

BIOGRAPHICAL SKETCH

Author: Susana Addo Ntim

Degree: Doctor of Philosophy

Date: May 2012

Undergraduate and Graduate Education:

- Doctor of Philosophy in Environmental Science,
  New Jersey Institute of Technology, Newark, NJ, 2012

- Master of Science in Marine Estuarine Environmental Science,
  University of Maryland Eastern Shore, Princess Anne, MD, 2006

- Bachelor of Science in Chemistry,
  Kwame Nkrumah University of Science and Technology, Kumasi, Ghana, 2002

Major: Environmental Science

Peer Reviewed Publications:

ADDO NTIM, S. & MITRA, S. 2011. Removal of trace arsenic to meet drinking water standards using iron oxide coated multiwall carbon nanotubes. *J Chem Eng Data,* 56, 2077-2083.

ADDO NTIM, S. & MITRA, S. 2012a. Adsorption of arsenic on multiwall carbon nanotube–zirconia nanohybrid for potential drinking water purification. *J Colloid Interface Sci,* 375, 154-159.

ADDO NTIM, S. & MITRA, S. 2012b. Aggregation behavior of carbon nanotubes in aqueous and physiological media and its influence on toxicity. *Int J Biomed Nanosci Nanotechnol,* In Review.

ADDO NTIM, S., SAE-KHOW, O., DESAI, C. & MITRA, S. 2012. Size dependent aqueous dispersibility of carboxylated multiwall carbon nanotubes. *Nanoscale,* In Review.

ADDO NTIM, S., SAE-KHOW, O., WITZMANN, F. A. & MITRA, S. 2011. Effects of polymer wrapping and covalent functionalization on the stability of mwcnt in aqueous dispersions. *J Colloid Interface Sci,* 355, 383-388.

ANAND, B., ADDO NTIM, S., SAI MUTHUKUMAR, V., SIVA SANKARA SAI, S., PHILIP, R. & MITRA, S. 2011. Improved optical limiting in dispersible carbon nanotubes and their metal oxide hybrids. *Carbon,* 49**,** 4767-4773.

DESAI, C., ADDO NTIM, S. & MITRA, S. 2012. Antisolvent precipitation of hydrophobic functionalized multiwall carbon nanotubes in an aqueous environment. *J Colloid Interface Sci,* 368**,** 115-120.

LAKSHMAN, K. V., ADDO NTIM, S., SAE-KHOW, O., JANARDHANA, C., LAKSHMINARAYANAN, V. & MITRA, S. 2012. Electrocatalytic activity of multiwall carbon nanotube–metal (Pt/Pd) nanonhybrids synthesized for fuel cells applications. *Carbon,* In review.

LI, C., CHEN, Y., ADDO NTIM, S. & MITRA, S. 2010. Fullerene-multiwalled carbon nanotube complexes for bulk heterojunction photovoltaic cells. *Appl Phys Lett,* 96**,** 143301-143303.

ROY, S., ADDO NTIM, S., MITRA, S. & SIRKAR, K. K. 2011. Facile fabrication of superior nanofiltration membranes from interfacially polymerized CNT-polymer composites. *J Mem Sci,* 375**,** 81-87.

WANG, X., XIA, T., ADDO NTIM, S., JI, Z., GEORGE, S., MENG, H., ZHANG, H., CASTRANOVA, V., MITRA, S. & NEL, A. E. 2010. Quantitative techniques for assessing and controlling the dispersion and biological effects of multiwalled carbon nanotubes in mammalian tissue culture cells. *ACS Nano,* 4**,** 7241-7252.

WANG, X., XIA, T., ADDO NTIM, S., JI, Z., LIN, S., MENG, H., CHUNG, C.-H., GEORGE, S., ZHANG, H., WANG, M., LI, N., YANG, Y., CASTRANOVA, V., MITRA, S., BONNER, J. C. & NEL, A. E. 2011. Dispersal state of multiwalled carbon nanotubes elicits profibrogenic cellular responses that correlate with fibrogenesis biomarkers and fibrosis in the murine lung. *ACS Nano,* 5**,** 9772-9787.

WEI, L., THAKKAR, M., CHEN, Y., ADDO NTIM, S., MITRA, S. & ZHANG, X. 2010. Cytotoxicity effects of water dispersible oxidized multiwalled carbon nanotubes on marine alga, dunaliella tertiolecta. *Aquat Toxicol,* 100**,** 194-201.

Conference Presentations:

ADDO NTIM, S. & MITRA, S. "Iron oxide coated multiwall carbon nanotubes for the removal of arsenic from water," NJIT GSA Research Day, Newark, NJ, November 2011.

ADDO NTIM, S. & MITRA, S. "Iron oxide coated multiwall carbon nanotubes for the removal of arsenic from water," NJIT GSA Research Day, Newark, NJ, November 2010.

ADDO NTIM, S. & MITRA, S. "Iron oxide coated multiwall carbon nanotubes for the removal of arsenic from water," 240th American Chemical Society National Meeting & Exposition, Boston, MA, August 2010.

ADDO NTIM, S. & MITRA, S. "Iron oxide coated multiwall carbon nanotubes for the removal of arsenic from water," 4th Passaic River Symposium, Montclair State University, Montclair, NJ, June 2010.

ADDO NTIM, S. & MITRA, S. "Iron oxide coated multiwall carbon nanotubes for the removal of arsenic from water," The 10th National Conference on Science, Policy, and the Environment, Washington, DC, January 2010.

ADDO NTIM, S. & MITRA, S. "Adsorptive removal of arsenic from drinking water using carbon nanotube-metal oxide hybrids," Department of Chemistry and Environmental Science, NJIT, Fall Seminar Series. Newark, NJ, November 2011.

ADDO NTIM, S. & MITRA, S. "Carbon nanotube–metal oxide nanohybrids for water purification," The Dana Knox Research Showcase, NJIT Newark, NJ, April 2012

ADDO NTIM, S., ANAND, B., MUTHUKUMAR, S. S., SANKARA SAI, S. S., PHILIP, R. & MITRA, S. "Improved optical limiting in dispersible carbon nanotubes and their metal oxide hybrids," 243rd American Chemical Society National Meeting & Exposition, San Diego, CA, March 2012.

ADDO NTIM, S., RAMAMURTHY, S. S. CHEN, Y., JANARDHANA, C. & MITRA, S. "Carbon nanotube–metal oxide nanohybrids for water purification," 243rd American Chemical Society National Meeting & Exposition, San Diego, CA, March 2012.

ADDO NTIM, S., SAE-KHOW, O. WANG, X. WITZMANN, F. A. NEL, A. & MITRA, S. "Aggregation behavior of multiwall carbon nanotubes in aqueous and physiological media and their toxicological effects," 243rd American Chemical Society (ACS) National Meeting & Exposition, San Diego, CA, March 2012.

LI, C., CHEN, Y., ADDO NTIM, S. & MITRA, S. "Fullerene-multi walled carbon nanotube complexes for bulk heterojunction photovoltaic cells" – 239th ACS National Meeting in San Francisco, CA March 21st – 25th 2010

To my late mum, Ms. Margaret Oye Asante for cheering me on while you could, and my late aunt, Ms. Violet Manko Asante for picking up where my mum left off. To my brother, Michael Ntim-Addo; my sister, Ewurama Korantema Addo; and my nieces and nephews, Julida Naana Tenkorama Asante, Michael Nana Opare Addo, Aaron Nyamekye Addo and Emmanuella Nana Oye Addo, your undying love and support have been invaluable to me throughout this process.

ACKNOWLEDGMENT

I would like to express my sincere gratitude to my advisor, Dr. Somenath Mitra, for providing invaluable guidance, support, encouragement, and opportunities during the course of my doctoral study. Special thanks go to Dr. Carol A. Venanzi, Dr. Edgardo T. Farinas, Dr. Haidong Huang and Dr. Pradyot Patnaik for their contributions as members of my dissertation committee.

I greatly appreciate the help of Dr. Ronald Kane, Dr. Marino Xanthos, Ms. Clarisa González-Lenahan, and Mr. Jeffrey Grundy, as well as the staff of the Graduate Studies Office and the Office for International Students and Faculty throughout my stay at NJIT. I am immensely grateful to the Schlumberger foundation faculty for the future fellowship, National Institute of Environmental Health Sciences (NIEHS) and the US Army for their financial support. My appreciation also goes to the Department of Chemistry and Environmental Science for offering Teaching Assistantship.

Additionally, I would like to thank Dr. Larisa Krishtopa, Dr. Young Pu, Yogesh Gandhi, Gayle Katz and Genti Price for their assistance during my study at NJIT. I also would like to thank my colleagues, Dr. Chutarat Saridara, Dr. Cheng Li, Dr. Yuhong Chen, Dr. Ornthida Sae-Khow, Dr. Xiangxin Meng, Dr. Chaudhery Hussain, Dr. Sagar Roy, Chintal Desai, Xinbo Cui, Smruti Ragunath, Zheqiong Wu, and Zhiqian Wang for their friendship, collaboration, and exchange of thoughts and ideas. Finally, I would like to take the opportunity to thank my wonderful family for their love and support throughout my life.

TABLE OF CONTENTS

TABLE OF CONTENTS
(Continued)

TABLE OF CONTENTS
(Continued)

Chapter **Page**

TABLE OF CONTENTS
(Continued)

Chapter **Page**

LIST OF TABLES

LIST OF FIGURES

LIST OF FIGURES
(Continued)

LIST OF FIGURES
(Continued)

CHAPTER 1

INTRODUCTION

1.1 Overview

Carbon nanotubes (CNTs) are characterized by some highly desirable mechanical, thermal and electrical properties, which make them attractive for a wide range of applications ranging from field emission to reinforcements in nanocomposites (Kong et al., 2000, Petrov et al., 2004, Yun et al., 2006, Murugesan et al., 2006). They are essentially graphene sheets that have been seamlessly rolled into cylindrical tubes. They can be single-walled (SWCNTs), double-walled (DWCNTs) or multi-walled (MWCNTs) depending on the number of concentric rings (Iijima, 1991, Iijima, 2002, Zhou et al., 2002). The applicability of CNTs is often limited by their inherent incompatibility with solvents and polymers.

With largely defect-free sidewalls CNTs are rather inert to chemical attack, tend to be hydrophobic, and difficult to disperse or dissolve in water and other organic solvents. Some level of functionalization is therefore, required prior to their utilization in real-world applications. This has mandated a plethora of studies on the solubilization of CNTs using diverse techniques (Tasis et al., 2006).The three main approaches that have been used to solubilize CNTs are; surfactant-based solubilization (Islam et al., 2003), non-covalent wrapping/adsorption, where soluble polymers have been wrapped on the CNTs (Lin et al., 2003), and covalent functionalization involving chemical modification of the CNT surface (Mickelson et al., 1999, Huang et al., 2002, Pompeo and Resasco, 2002, Peng et al., 2009, Wang et al., 2005a, Chen and Mitra, 2008). The latter techniques

include covalent tethering, such as, fluorination (Mickelson et al., 1999), amidation (Huang et al., 2002), glucosamine attachment, and sidewall carboxylic acid functionalization (Peng et al., 2009).

1.2 Carbon Nanotube Functionalization

Carbon nanotubes in their pristine form are generally chemically stable and insoluble in water or organic solvents. This limits their applicability in systems that require the preparation of homogenous mixtures of CNTs with different organic, inorganic, and polymeric materials. Some level of functionalization is therefore, necessary where certain molecules or functional groups are physically or chemically attached to their sidewalls without significantly changing their physical/electronic properties. Several routes to CNT functionalization have been reported (Hirsch and Vostrowsky, 2005) however, non-covalent wrapping/adsorption and covalent tethering are the two main routes which have been extensively investigated. Covalent functionalization is based on covalent linkage of functional entities onto the nanotube's carbon scaffold, either at the end caps of the tubes or sidewalls. This can involve either a direct covalent functionalization where a change in hybridization from sp^2 to sp^3 and a simultaneous loss of conjugation occurs, or defect functionalization where chemical transformations occur at defect sites already present at the open ends or the sidewalls, or pentagon and heptagon irregularities in the graphene framework. Non-covalent functionalization on the other hand involves supramolecular complexation using various adsorption forces, such as van der Waals' and π-stacking interactions.

Various covalent reactions have been developed to functionalize carbon nanotubes, oxidation being one of the most common. CNT oxidation is carried out with oxidizing agents such as nitric acid (Niyogi et al., 2007, Chen and Mitra, 2008). During the process, carboxyl groups are formed at the ends of tubes as well as at the defects on the sidewalls. Further modification can be achieved by attaching hydrophilic polymers such as poly(ethylene glycol) (PEG) to oxidized CNTs, yielding CNT-polymer conjugates stable in biological environments (Zhao et al., 2005, Liu et al., 2007, Schipper et al., 2008). Another widely used type of covalent reaction to functionalize CNTs is the cylcoaddition reaction. [2+1] cycloadditions can be conducted by photochemical reaction of CNTs with azides (Moghaddam et al., 2003, Lee et al., 2005) or carbene generating compounds via the Bingel reaction (Coleman et al., 2003, Umeyama et al., 2007). A 1,3-dipolar cycloaddition reaction on CNTs developed by Tagmatarchis and Prato is now a commonly used reaction (Georgakilas et al., 2002, Tagmatarchis and Prato, 2004). An azomethine-ylide generated by condensation of an α-amino acid and an aldehyde is added to the graphitic surface, forming a pyrrolidine ring coupled to the CNT sidewall. Functional groups (e.g., amino terminated PEG) introduced via a modified α-amino acid can be used for further conjugation of biological molecules such as peptides or drugs (Lam et al., 2004, Pastorin et al., 2006).

In contrast to covalent functionalization, noncovalent functionalization of CNTs can be carried out by coating CNTs with amphiphilic surfactant molecules or polymers. Taking advantage of the π-π interaction between pyrene and the nanotube surface, pyrene derivatives have been used to noncovalently functionalize carbon nanotubes (Chen et al., 2001, Wu et al., 2008). Polymers such as poly-aminobenzoic sulfonic acid (PABS),

polyimide, polyvinyl alcohol (PVA) and polyvinyl pyrrolidone (PVP) (O'Connell et al., 2001, Addo Ntim et al., 2011) have been attached to CNT surfaces. Chen et al. showed that proteins can be immobilized on SWCNTs functionalized by an amine-reactive pyrene derivative (Chen et al., 2001). A recent study conducted by Wu et al. also used pyrene conjugated glycodendrimers to solublize carbon nanotubes (Wu et al., 2008). Beside pyrene derivatives, single-stranded DNA molecules have been widely used to solubilize SWCNTs by virtue of the π-π stacking between aromatic DNA base units and the nanotube surface (Tu and Zheng, 2008). Fluorescein (FITC) terminated PEG chains have also been used to solubilize SWCNTs with the aromatic FITC domain π-π stacked on the nanotube surface, yielding SWCNTs having visible fluorescence which are useful for biological detection and imaging (Nakayama-Ratchford et al., 2007). Noncovalent functionalization of SWCNTs by PEGylated phospholipids (PL-PEG) have also been reported (Liu et al., 2007, Liu et al., 2008).

1.3 Physicochemical Characterization

The key physicochemical properties of the CNTs are often determined by electron microscopy (SEM and TEM), Atomic Force Microscopy (AFM), thermogravimetric analysis (TGA), Raman Spectroscopy and Fourier Transform Infrared spectroscopy (FTIR). Saleh et al. used a high resolution transmission electron microscope to image MWCNT and SWCNT samples to determine the diameter and length distribution (Saleh et al., 2008, Saleh et al., 2010). The TEM data showed significant debundling and shortening of the MWCNTs after sonication and dark spherical features on the image which they presumed to be catalyst particles. Isolated single MWCNTs were also

observed which they attributed to a high degree of dispersion due to the sonication treatment. The diameter and length distribution reported based on the TEM analysis was not in agreement with the data supplied by the MWCNT manufacturer (Saleh et al., 2008). A similar tube shortening with sonication was observed from the TEM images of the SWCNTs (Saleh et al., 2010). It was also observed that the majority of the tubes were SWCNTs, with few larger diameter tubes, most likely doublewalled or multiwalled (Saleh et al., 2010). Several other studies have used high resolution TEM to study the morphology of CNTs mainly confirming tube structure before and after processing (Jiang et al., 2003, Sinani et al., 2005, Shieh et al., 2007, Heister et al., 2010).

In instances where TEM was not used SEM was used to characterize tube morphology (Jiang et al., 2003, Shieh et al., 2007, Wang et al., 2010, Addo Ntim et al., 2011, Desai et al., 2012). Wang et al. used Scanning Electron Microscope equipped with an energy-dispersive X-ray analyzer (EDS) to demonstrate that MWCNTs after acid functionalization retained their tube structure with minimal visible damage. The EDS system attached to the SEM was used to analyze the elemental composition in the as-prepared and functionalized MWCNTs (Wang et al., 2010).

In most of the studies involving functionalized CNTs, FTIR is used to confirm the presence of functional groups (Shieh et al., 2007, Wang et al., 2010). The carboxylic (C=O) stretching frequency in oxidized MWCNTs is often reported to occur around 1700 cm^{-1} with the O–H vibration occurring around 3400 cm^{-1} (Shieh et al., 2007, Wang et al., 2010). The purity of CNTs studied, and in some instances percentage of functional groups present, are investigated using TGA. TGA is carried out either under an air or nitrogen flow at specified flow and heating rates. As-prepared MWCNTs often

decompose between 500–600°C with SWCNTs decomposing around 450°C (Saleh et al., 2010).

Raman spectroscopy has been used to estimate SWCNT diameter and also to obtain information about its defect levels. A typical Raman spectra of SWCNTs exhibits two active Raman signature modes, namely, the radial breathing mode (RBM, near 200 cm^{-1}) and a high-energy mode (HEM or "G" band, near 1600 cm^{-1}), and another electric resonance mode originating from double resonance called the "D" band (near 1300 cm^{-1}). The Raman shift frequency at the RBM mode is correlated with SWCNT diameter using semiempirical relationships. Saleh et al. (2010) estimated the diameter of SWCNTs based on their Raman spectra to be 0.87-1.42 nm. It was also reported that the defect density in SWCNTs estimated by the G/D ratio was lower in sonicated SWCNTs than in as-prepared SWNTs indicating an increase in defect density due to successive sonication of the SWCNT samples, consistent with previous observation with MWCNTs (Saleh et al., 2008). Heister et al. used Raman spectra to confirm diameter of SWCNT and to demonstrate that NaOH washing of oxidized SWCNTs removes oxidative debris resulting in slightly lower D/G ratio, indicating the removal of defective material from the sample (Heister et al., 2010).

1.4 Dispersibility of Carbon Nanotubes

Extensive use of CNTs in industry and the consumer market will increase the likelihood of CNT exposure to the natural environment. CNTs can be released into the environment via wastewater discharge as point source emissions from manufacturing industries (Wiesner et al., 2006). Upon release, they will interact with the aquatic environment and

biological species. Depending on the interplay between electrostatic and van der Waals interactions, they may aggregate or persist in aqueous media as homogenous dispersions (Thess et al., 1996). The aggregation state of CNTs therefore, has a strong influence on their fate and transport in the environment. Therefore, understanding the factors governing the aggregation behavior of CNTs is key to evaluating their potential interaction with biological species. Literature on CNT aggregation has mostly been centered on enhancement of their aqueous solubility, either by dispersing CNTs by surfactant (Jiang et al., 2003, Lisunova et al., 2006), polymer adsorption (Jung et al., 2004), or by introducing oxygen containing functional groups on the surface through acid treatment (Wang et al., 2005a, Chen and Mitra, 2008, Peng et al., 2009). However, in recent years the number of studies evaluating the aggregation behavior of CNTs in the presence of electrolytes has increased significantly, where time-resolved dynamic light scattering (TRDLS), Raman spectroscopy, zeta-potential measurements, and UV-Visible spectroscopy have been used to investigate the aggregation kinetics of CNTs in aqueous and physiological media (Smith et al., 2009, Peng et al., 2009).

The dispersal state of CNTs is also one of the most important physicochemical characteristics that need critical attention during cytotoxicological studies because this determines their bioavailability and therefore, interactions at the nano-bio interface. Therefore, understanding the mechanisms involved in controlling the state of CNT agglomeration in physiological media is very important to assess the toxic effects expressed by aggregated tubes as opposed to the dispersed ones. Since there is a high propensity for CNTs to aggregate due to electrostatic attractions, efforts have been aimed at achieving well dispersed CNT formulations for toxicological analysis using surfactants

and dispersing agents. Some dispersants such as fetal bovine serum, tween and bronchoalveolar lavage (BAL) of rodents have been successfully used in dispersing CNTs in tissue culture media (Shvedova et al., 2003, Warheit et al., 2004, Jia et al., 2005, Muller et al., 2005, Sager et al., 2007, Porter et al., 2008). Synergistic effects of proteins and surfactants in CNT dispersion have also been reported (Chen et al., 2001, Li et al., 2004). The effect of the dispersal state of CNTs on their cytotoxicity has also been reported with varied impacts on cell activity and proliferation observed (Shvedova et al., 2005, Wick et al., 2007, Mercer et al., 2008).

1.4.1 CNT Electrokinetic Properties

A charged colloidal particle suspended in an electrolyte solution is surrounded by a cloud of counterions which contribute to a set of surface charges and countercharges called the electric double layer. This plays an essential role in various interfacial electrical phenomena on the particle surface and in the particle–particle interaction in the colloid suspension. The surface potential on colloid particles is generally difficult to measure. However, the potential near the particle surface called the zeta (ζ) potential is measurable. The ζ-potential provides useful information regarding the stability of colloidal suspensions in diverse applications including food preparations, agriculture, pharmaceuticals, paper industry, ceramics, paints, coatings, photographic emulsions, etc. Zeta potential has been used to study the stability of MWCNT dispersions and the influence of counterions on their aggregation behavior (Peng et al., 2009). In some cases electrophoretic mobility (EPM) which is essentially the migration of charged colloidal particles through a solution under the influence of an applied electric field has been used

instead of zeta potential (Saleh et al., 2008, Smith et al., 2009, Saleh et al., 2010). Generally CNTs exhibit negative surface potential in aqueous systems (Jiang et al., 2003, Saleh et al., 2008, Peng et al., 2009, Smith et al., 2009, Saleh et al., 2010). While the negative surface charge in functionalized CNTs is attributed to the presence of acidic groups introduced through acid treatment, the origin of surface charge is not fully understood for unfunctionalized carbon-based nanomaterials such as fullerenes and CNTs.

Jiang et al. reported that adsorption of sodium dodecyl sulfate (SDS) improved the zeta potential of CNT dispersions at pHs below 8. This was however, not observed at higher pH values where the zeta potential values were essentially the same for both dispersion systems (with and without SDS) (Jiang et al., 2003). This was attributed to the presence of acidic sites on the surface of the CNTs purified by acid treatment which can be dissociated in the alkaline solutions. It was demonstrated that the presence of SDS resulted in more negative zeta potential values (-40 mV) translating to better stabilized MWCNT dispersions, than was observed in the dispersions without SDS (-30 mV). This was true for the entire pH range studied (3-11). The effect of SDS was attributed to the electrostatic repulsion provided by adsorbed surfactants which stabilized the CNTs against van der Waals attraction (Vigolo et al., 2000). In a similar study by Saleh et al. (2008) the EPM of MWCNTs dispersions was reported to decrease, becoming less negative with increasing salt concentration. The presence of defects on the surface of CNTs in the form of pentagon and heptagon irregularities at their carbon scaffold and also incomplete carbon rings at the end termini make the sidewalls and tube-ends susceptible to oxidation to form carboxyl and hydroxyl functional groups (Hirsch and

Vostrowsky, 2005). These functional groups present on the CNT surface accounts for the strong dependence of EPM on solution pH. Saleh et al. (2008) observed that the presence of Suwannee River humic acid (SRHA) did not significantly affect the EPM of the MWCNT dispersions under the solution chemistries investigated. In another study involving SWCNTs in the presence of biomacromolecules and humic acid, Saleh et al. (2010) reported a similar decrease in EPM with increasing salts concentration as was observed for the MWCNTs (Saleh et al., 2008). The SWCNTs were observed to have a negative surface charge which the authors attributed to mechanochemistry (Saleh et al., 2010). The presence of biomacromolecules and humic acid did not significantly increase in the EPM values of the SWCNTs contrary to previous observations where adsorbed surfactants and polyelectrolytes reportedly enhanced the EPM of SWCNTs (Liu et al., 2007, White et al., 2007).

Smith et al. (2008) investigated the influence of pH on the EPM of oxidized MWCNT in the presence of 64 mM NaCl. The EPM values decreased with increasing pH from pH 3 to 5 with the values remaining fairly stable above pH 6, independent of the electrolyte concentration (Smith et al., 2009). This was consistent with previously reported EPM measurements of oxidized carbon nanotubes (Esumi et al., 1996, Hu et al., 2005). A similar observation was made by Peng et al. while investigating the effect of electrolytes on the stability of oxidized MWCNTs (Peng et al., 2009).

1.4.2 Aggregation Behavior in Aqueous Media and the Effect of Electrolytes

The aggregation behavior of both as-prepared and functionalized carbon nanotubes in aqueous media have been studied, with particular emphasis on the influence of dissolved

salts and pH. In some instances the effects of natural organic matter and biomacromolecules have also been investigated. Precipitation of CNTs under the influence of different salts often show dependence on the charge on the cations, and in general these nanoparticles have followed the well-established Derjaguin-Landau-Verwey-Overbeek (DLVO) theory (Derjaguin and Landau, 1993, Verwey and Overbeek, 1999). In aqueous systems, electrolyte ions are known to coagulate certain colloidal sols. It is well-known that the critical coagulation concentration (*ccc*), the minimum concentration of ions necessary to cause rapid coagulation of colloids follows the Schulze-Hardy rule

$$ccc \sim \left(\frac{1}{z}\right)^{n} \tag{1.1}$$

where *z* is the valence of the electrolyte counterions. Typically, *n* is 6 in three dimensions (3D) and 9 in two dimensions (Sano et al., 2000). According to the DLVO theory, the Schulze-Hardy rule results from interplay between van der Waals attraction and electric double-layer repulsion (Israelachvili, 2010).

Sano et al. were among the first group to investigate the colloidal nature of SWCNTs in electrolyte solutions particularly emphasizing the dependence on the Schulze-Hardy rule (Sano et al., 2001). The aggregation behavior of 0.6mg/mL dispersions of shortened, oxidized SWCNTs was studied in the presence of Na^{+}, K^{+}, Mg^{2+}, Ca^{3+}, La^{3+} and Ce^{3+} by first dispersing the SWCNTs in an electrolyte solution by utrasonication and then measuring the UV absorbance of the supenantant after allowing the dispersions to sit undisturbed for 12 hrs at room temperature. The *ccc* values obtained

for Na^{+}, K^{+}, Mg^{2+}, Ca^{3+}, La^{3+} and Ce^{3+} were 37, 26, 0.31, 0.20, 0.050 and 0.052, respectively. A clear inverse relationship between the *ccc* values and the counterion valence *z* was observed, and a plot of the double logarithm of the *ccc* values against valence *z* produced a straight line with a slope of -6 (Sano et al., 2001). It was therefore, concluded that SWCNTs followed the 3D Schulze-Hardy rule.

Jiang et al. used a UV-Visible spectrophotometric method to compare the stability of CNT dispersion made with and without SDS (Jiang et al., 2003). CNT dispersions at 0.2 wt% were made with and without SDS (0.1wt%) at pH 9 and the UV-Visible absorbance of the dispersions was measured as a function of time over a period of 500 h. It was observed that in both dispersions, CNT concentration reduced with time, with the SDS stabilized dispersion showing better stability (Jiang et al. 2003). The optimal conditions necessary to make stable homogenous CNT dispersions were reported to be 0.5 wt% CNT and 2.0 wt% SDS. Aqueous dispersions of SWCNTs containing individual tubes can be achieved using SDS. Once intertube van der Waals attraction is overcome by intense sonication, free SDS adsorbs to SWCNT surfaces and creates a net surface density of negative charge, which prevents SWCNT reaggregation. Any change in the surface charge density or solubility of the surfactant that eliminates the electrostatic repulsion between the nanotubes will cause SWCNTs to aggregate and coagulate (Tan and Resasco, 2005). Niyogi et al. demonstrated that by controlling the interplay between intermolecular and surface forces of SDS in water it was possible to engineer the resultant Van de Waals attraction between SWCNTs to achieve selective aggregation (Niyogi et al., 2007). The absorbance and emission spectra of SDS assisted SWCNT dispersions were studied after the addition of NaCl and it was observed that the addition

of Na^+ decreased the electrostatic repulsion between SDS molecules resulting in an increase in their aggregation number. Thus, manipulation of SDS equilibria results in loss of free SDS in solution through precipitation or further micellization, causing a loss in SWCNT-bound in response. This results in nanotube aggregation as electrostatic repulsion is reduced (Niyogi et al., 2007). A dependence on the DLVO theory of the SWCNT aggregation was observed where an increase in salt concentration resulted in a corresponding increase in CNT aggregation. The valence of counterions also affected the SWCNT aggregation according to the Schulze-Hardy rule.

Sinani et al. studied the stability of positively charged suspensions of SWCNTs and MWCNTs in water and/or mixed polar solvents, investigating the influence of CNT manufacturer on suspension stability, SWCNTs from three different vendors were studied (Sinani et al., 2005). Several block copolymers namely poly(*N*-cetyl-4-vinylpyridinium bromide-*co*-*N*-ethyl-4-vinylpyridinium bromide-*co*- 4-vinylpyridine) (16/75/9), poly(vinylpyrro-lidone-*co*-allylamine), poly(*N*-ethyl-4-vinylpyridinium bromide-*co*-4-vinylpyridine) (94/6), poly(*N*-ethyl-4-vinylpyridinium bromide-*co*-4-vinylpyridine) (30/70), and poly-(*N*-dodecyl-4-vinylpyridinium bromide-*co*-*N*-ethyl-4-vinylpyridinium bromide-*co*-4-vinyl-pyridine (36/51/13) were examined as CNT dispersing agents. It was observed that only poly(*N*-cetyl-4-vinylpyridinium bromide-*co*-*N*-ethyl-4-vinylpyridinium bromide-*co*- 4-vinylpyridine) (16/75/9) and poly-(*N*-dodecyl-4-vinylpyridinium bromide-*co*-*N*-ethyl-4-vinylpyridinium bromide-*co*-4-vinyl-pyridine (36/51/13) displayed efficient solubilization of the CNTs. It was speculated that those two polymers could potentially be used as universal dispersing agents based on the fact

that they successfully produced stable dispersions of both SWCNT and MWCNT and also the difference in CNT vendors did not affect the stability of the colloidal system.

Saleh et al. (2008) investigated the initial aggregation kinetics of as-prepared MWNCTs using time-resolved dynamic light scattering (TRDLS) (Saleh et al., 2008). They evaluated the influence of pH, concentration of monovalent (NaCl) and divalent ($CaCl_2$ and $MgCl_2$) salts and the presence of natural organic matter (Suwannee River humic acid, SRHA) on the aggregation kinetics of the MWCNTs. A TRDLS method was used to study the initial aggregation kinetics of MWCNT in the presence of electrolytes and natural organic matter where the hydrodynamic radius of the MWCNTs in the dispersion was measured as function of time over a period of 3 hours to obtain approximately 30% increase in the original hydrodynamic radius of the MWCNTs. The attachment efficiency of the MWCNTs was then determined based on the initial aggregation rate constant *k* of MWNTs which is proportional to the initial rate of increase in the hydrodynamic radius, R_h, with time, *t*, and the inverse of MWNT concentration N_0 (Chen and Elimelech, 2007):

$$k \propto \frac{1}{N_o}\left(\frac{dR_h(t)}{dt}\right)_{t\to 0} \tag{1.2}$$

For MWCNT dispersions with the same nanotube concentration, the attachment efficiency, α, (which is also the inverse of the Fuchs stability ratio, *W*, commonly used in colloidal stability studies) is obtained by dividing the initial slope of the aggregation profile of a given solution chemistry by the initial slope obtained under favorable (fast) aggregation conditions:

$$\alpha = \frac{\left(\frac{dR_h(t)}{dt}\right)_{t\to 0}}{\left(\frac{dR_h(t)}{dt}\right)_{t\to 0,fast}} \quad (1.3)$$

where the subscript "fast" represents favorable solution conditions, under which rapid, diffusion-limited aggregation takes place. The *ccc* values are then obtained from the intersection of the slow and fast aggregation regimes of the attachment efficiency/electrolyte concentration profile.

Saleh et al. (2008) observed an increase in MWCNT aggregation with increasing salt concentration and counterion valence consistent with the DLVO theory and the Schulze-Hardy rule. The *ccc* value obtained for the monovalent NaCl was 25mM, slightly lower than the value obtained by Sano and coworkers for SWCNT (37mM) [17]. For the divalent salts however, the *ccc* values (2.6 mM Ca^{2+} and 1.5 mM Mg^{2+}) were higher than those for SWCNT (0.2 mM Ca^{2+} and 0.3 mM Mg^{2+}) (Sano et al. 2001). The attachment efficiencies of the MWCNTs were observed to significantly decrease in the presence of SRHA for aqueous solutions containing monovalent and divalent salts. This was attributed to non-DLVO, steric stabilization due to the presence of adsorbed humic macromolecules (Saleh et al., 2008) and was consistent with previous observations (Tipping and Ohnstad, 1984, Buffle et al., 1998, Heidmann et al., 2004, Chen and Elimelech, 2007). Humic and fulvic acid molecules have been reported to associate with fullerenes and MWCNTs through π-π interactions between the cross-linked aromatic networks (Terashima and Nagao, 2007, Hyung et al., 2007, Hyung and Kim, 2008), Saleh et al. (2010) investigated the effect of biomacromolecules and humic acid on the aggregation kinetics of SWCNTs in the presence of electrolytes. The biomacromolecules

used were sodium alginate, bovine serum albumin (BSA), a microbial culture medium [Luria-Bertani (LB) broth], and Suwannee River humic acid (SRHA), in the presence of NaCl and $CaCl_2$ salts. SWCNT stability curves were constructed using the aggregation kinetics data from which the critical coagulation concentrations for the monovalent and divalent salts were determined. The SWCNT preparation protocol and the aggregation studies were conducted in the same manner as the MWCNTs (Saleh et al., 2008). It was demonstrated that the mechanism of stabilization of the SWCNTs in aqueous media followed DLVO type interactions. The *ccc* values reported were 20 mM NaCl and ~2 mM $CaCl_2$, which were lower than reported values in literature the for SWCNTs and MWCNTs (Saleh et al., 2008, Sano et al., 2001). The authors reported an observed reduction in the aggregation rate of SWCNTs in the presence of biomacromolecules and SRHA, in the order; BSA>SRHA>LB>alginate. It was further observed that for the salt concentrations examined, none of the stability profiles with biomacromolecules or SRHA reached the favorable aggregation regime, demonstrating that the presence of biomacromolecules and SRHA enhanced the stability of SWNTs even at high salt concentrations. The authors observed at high $CaCl_2$ concentrations, the aggregation of SWCNTs increased in the presence of alginate resulting in attachment efficiencies greater than 1. This was attributed to alginate molecule bridging of SWNTs with Ca^{2+}.

Smith et al conducted a similar study with oxidized MWCNTs prepared by refluxing pristine MWCNTs in nitric acid, reporting a similar influence of counterion concentration and valence on the observed aggregation behavior (Smith et al., 2009). Their work differed from that of Saleh and coworkers (Saleh et al., 2008) only in the oxidation of the MWCNTs. The influence of natural organic matter was not investigated.

The *ccc* values obtained using TRDLS in the presence of Na^{+}, Mg^{2+} and Ca^{2+} were 93±5 mM, 1.8 mM and 1.2 mM, respectively. While these values were similar to those reported by Saleh and coworkers (Saleh et al., 2008) in the case of the divalent salts, the monovalent NaCl gave a much higher *ccc* value. Peng et al. used UV-visible absorption to study the stability of nitric acid oxidized MWCNTs over a 30 day period and investigated the influence of salts. Their investigations showed that during the 30 day aging time, the oxidized MWCNT dispersion showed characteristic UV–vis absorbance peaks at 252nm with the MWCNTs concentration reducing to 85% of the initial concentration after 30 days (Peng et al., 2009). An apparent dependence on counterion valence was observed in agreement with the Schulze-Hardy rule. The minimum concentration of Na^{+}, K^{+}, Mg^{2+}, Ca^{2+}, Fe^{3+} and Al^{3+} required to cause precipitation in the MWCNT dispersions were determined based on a previously reported procedure (Peng et al., 2009) and termed precipitation value. This value is similar to *ccc* values however, their determination may not be as accurate as the procedure for *ccc* determination. Oxidized CNT dispersions were mixed with different concentrations of salt solutions at pH 6.0±0.2 after 2 hrs of standing. The minimum salt concentration at which oxidized CNTs precipitated was determined as the precipitation value (Peng et al., 2009). The reported values for Na^{+}, K^{+}, Mg^{2+}, Ca^{2+}, Fe^{3+} and Al^{3+} were 185 mM, 125 mM, 1.05 mM, 0.55 mM, 0.15 mM, and 0.036 mM, respectively.

While the *ccc* values in the presence of divalent and trivalent salts appear to be reproducible across these studies, the values obtained for monovalent salts vary quite a bit (Sano et al., 2001, Saleh et al., 2008, Smith et al., 2009, Saleh et al., 2010, Addo Ntim

and Mitra, 2011). Generally values obtained for as-prepared CNTs were lower than oxidized ones.

1.4.3 Aggregation Behavior in Biological Media

Physiological fluids contain various proteins and other organic molecules, as well as high salt concentrations, and sometimes variation in pH, making it extremely important for CNT dispersions intended for *in vitro* or *in vivo* experiments to be stable under the prevailing conditions. The review of the aggregation behavior of CNTs in the presence of electrolytes has established that the solubility of CNTs depends on the pH, decreases with increasing salt concentration, and the presence of biomacromolecules may influence their aggregation behavior. Some of the key factors involved in CNT aggregation are hydrophobicity, attractive van der Waals forces, and the potential influence of electrical double layer formation on the surface of functionalized CNTs (Girifalco et al., 2000). The hydrophobic surface properties of CNTs make them associate readily with biological macromolecules, such as proteins (Shim et al., 2002, Karajanagi et al., 2004, Shi Kam et al., 2004) and antibodies (Sager et al., 2007), as well as natural organic matter, such as humic substances (Hyung et al., 2007). The interaction of CNTs with macromolecules is inevitable in biological systems including culture media that contain macromolecules such as enzymes, proteins, DNA, and polysaccharides. Dispersing agents have been used in the preparation of relatively well dispersed CNT suspensions. A number of investigators have studied the aggregation behavior of CNTs in culture media with particular emphasis on the effect of macromolecules, polymers and surfactants.

In an effort to develop quantitative methods for assessing CNT dispersibility in water and tissue culture media, Wang et al. (2010) investigated the dispersibility of three MWCNT derivatives: as-prepared (AP-MWCNT), purified (PD-MWCNT) and carboxylated (COOH-MWCNT). It was demonstrated that partitioning coefficient, suspension stability index, attachment efficiency, and dynamic light scattering (DLS) could be used systematically in preparing stable MWCNT suspensions through the use of the protein Bovine Serum Albumen (BSA) and the phospholipid Dipalmitoylphosphatidylcholine (DPPC). The hydrophobicity index for the different MWCNT derivatives was calculated using the light absorbance of the CNT dispersions in distilled H_2O, phenol red-free Dulbecco's Modified Eagle's Medium (DMEM) and Bronchial Epithelial Basal Medium (BEBM) before and after n-octanol extraction. It was demonstrated that AP-MWCNTs and PD-MWCNTs had relatively higher hydrophobicity indices than the COOH-MWCNTs, which was in agreement with their zeta potential values, where COOH-MWCNT had a relatively higher negative value compared to AP-MWCNT and PD-MWCNT. This was attributed to electrostatic repulsion by surface carboxyl groups present in COOH-MWCNT which was non-existent in others. Following the addition of BSA, the zeta potential values of the aqueous dispersions of AP-MWCNT and PD-MWCNT were observed to significantly increase, which was attributed to direct binding of BSA to the hydrophobic tube surfaces providing steric stabilization (Chen et al., 2003) and also electrosteric hindrance as a result of the anionic nature of BSA at neutral pH. The influence of BSA on the stability of the more hydrophilic COOH-MWCNT was however, attributed to steric hindrance.

The aggregation kinetics of COOH-MWCNT in PBS was investigated with and without BSA, and it was observed that the presence of BSA resulted in significantly lower attachment efficiencies indicating a significant contribution of BSA towards stabilizing COOH-MWCNT. This was attributed to a combination of steric and electrosteric hindrances from attached BSA and possible Ca^{2+} bridging of the protein to the CNT surface. UV-visible spectroscopy was used to establish a stability index for the CNTs in Bronchial epithelial growth medium (BEGM) and DMEM and after addition of BSA and DPPC to assess their influence on the stability of the MWCNT derivatives (Wang et al., 2010). It was observed that while BSA significantly improved the stability of the CNTs, DPPC showed no improvement. A combination of BSA and DPPC was observed to synergistically improve the stability of the more hydrophobic CNTs.

Kim et al. investigated the macrodispersion of SWCNTs and MWCNTs in the presence of BSA, Tween 80, DPPC, and dimethylsulfoxide (DMSO) using a light absorbance method (Kim et al., 2011b). The dispersion stability of the dispersed CNTs evaluated over a period of 16 weeks indicated that BSA was the best among the dispersants studied for both SWCNT and MWCNT which was in agreement with the data reported by Wang et al. (2010). Heister et al. demonstrated an influence of CNT dimensions and surface functionalities on their aqueous dispersibility and *in vitro* behavior. The effect of CNT dimensions and surface properties on their dispersion stability was investigated in salt solutions at different pHs and concentrations and in biological fluids, such as cellular growth media and human plasma, and their toxicity toward cancer cells. It was also demonstrated that oxidation debris arising from the functionalization process tends to enhance stability of CNTs in dispersions by acting as a

pseudosurfactant or charge buffer (Heister et al., 2010). The influence of MWCNT dispersal state on their toxicity has been reported where CNTs that were well-dispersed with BSA and DPPC induced TGF-β1 and Platelet-Derived Growth Factor AA (PDGF-AA) production in the lung in parallel with prominent granulomatous inflammation and fibrosis around small airways, which was not as pronounced in the case of their non-dispersed counterparts(Wang et al., 2011).

While significant effort has gone into these studies, much is unknown as far as colloidal stability as a function CNT size, morphology and surface functionalization.

1.5 Adsorption on Carbon Nanotubes for Potential Water Purification

The water resources of the world have been contaminated with widespread natural and anthropogenic pollution, leading to the scarcity of potable water. These problems range from Arsenic in natural waters to emerging contaminants such as pharmaceutical residues in drinking water (Vidyasagar, 2007). While millions of people are at risk from Arsenic pollution in India and Bangladesh, and the US-EPA has published a 10 ppb (0.01 mg/L) standard for arsenic in drinking water, no standards exist for pharmaceutical residues, which also pose significant threat to public health (Vidyasagar, 2007). In short, water pollution problems are diverse with each posing a unique challenge.

Conventional technologies for water treatment are oxidation, coagulation/co-precipitation, nanofiltration, reverse osmosis, electro dialysis, adsorption, ion exchange, foam flotation, solvent extraction and bioremediation (Václavíková et al., 2009). Most of these techniques are well developed and have their advantages and disadvantages that may range from the generation of toxic waste to low removal efficiency and high cost

(Václavíková et al., 2009). Adsorption has proven to be an efficient method for water treatment and a wide range of materials including zeolites, metals, metal oxides, clay, biological materials, polymeric resins, activated carbons, alumina, metal coated sand, and natural ores have been studied (Václavíková et al., 2009). New high performance sorbent materials are needed to meet the challenge of providing clean water to the world. These should have specifically designed structures that will allow them to selectively bind targeted contaminants from complex water matrices, and then they need be regenerated in a controlled fashion for cyclability.

The selection of sorbent materials for water purification applications is usually carried out by trial-and-error, such as the testing of a variety of commercially available activated carbons or zeolites. The development of next-generation sorption materials requires a rational design based on a fundamental understanding of the sorption mechanisms, and the ability to synthesize diverse materials in a controlled fashion. Such new strategies for formulating optimized architectures can be translated into revolutionary new materials for improved water purification. For example, high-surface-area activated carbons are prepared using a top-down approach employing chemical, pyrolytic or physical activation which leads to a wide (even random) distribution in pore sizes. Alternate synthesis routes incorporating a bottom-up strategy may be implemented to achieve tailored materials where enhanced, selective sorption is achieved by surface modification. Specific functional groups such as metal oxides or metal nano particles (or clusters) with terminal functionality will not only enhance sorption but simultaneously simplify solute release for regeneration.

1.5.1 Conventional Sorbents for Water Treatment

Sorbents such as activated carbon, sand, activated alumina, silica gel, molecular sieve carbon, molecular sieve and ion exchange resins have conventionally been used for water treatment (Václavíková et al., 2009). Activated carbon, which is one of the most widely used sorbents, has been used in both the granular and powdered forms for the removal of organic as well inorganic pollutants. They are a crude form of graphite with a random, amorphous, highly porous structure with a broad range of pore sizes (Sud et al., 2008). Activated carbons have been prepared from materials such as coconut shells, wood char, lignin, petroleum coke, and bone-char, and their pore structure as well as surface characteristics vary widely (Sud et al., 2008). Sand has been employed in the removal of lead, arsenic cadmium and zinc however, heavy metal adsorption on sand is often slow with low adsorption capacities (Yadanaparthi et al., 2009). Activated alumina (AA), prepared by thermal dehydration of aluminum hydroxide, has high surface area and a distribution of both macro- and micro-pores. They have been used for the successful removal of chromium (IV), arsenic and fluoride (Bishnoi et al., 2004, Tripathy et al., 2006, Sud et al., 2008). Zeolites have received increasing attention for pollution control. Both ion exchange and adsorption properties of zeolites have been exploited for the selective separation of cations from aqueous solutions. Heavy metals removal from industrial waste streams by the use of natural zeolites has long been applied in medium and large scale installations with variable success (Dąbrowski et al., 2004). Ion exchange polymers are known to be the most efficient of all sorbents for the removal of ions but tend to be expensive (Romo-Herrera et al., 2006). While the above mentioned sorbents show some excellent properties for water purification, novel sorbent structures with

higher capacity and easier regeneratability is of great importance as water emerges as a valuable and a scarce resource in the future.

1.6 Objectives

The objectives of this research are to;

- Investigate the influence of surface functionalization on the aggregation behavior of functionalized CNTs in an ionic environment, comparing polymer wrapped CNTs (MWCNT-PVP) and its carboxylated analog (MWCNT-COOH).
- Investigate the influence of tube dimensions on the aggregation kinetics of carboxylated multiwall carbon nanotubes (c-MWCNTs) in electrolytic environments.
- Synthesize MWCNT-metal oxide nanohybrids (Fe-MWCNT and MWCNT-ZrO_2) using highly functionalized carbon nanotubes and study the removal of μg L^{-1} levels of arsenic from water, to meet the US EPA drinking water standard of 10 μg L^{-1} and investigate the cyclability of the spent sorbent.

CHAPTER 2

EFFECTS OF POLYMER WRAPPING AND COVALENT FUNCTIONALIZATION ON THE STABILITY OF MWCNT IN AQUEOUS DISPERSIONS

As the applications of carbon nanotubes (CNTs) proliferate, mass production and widespread use of these nanocarbons will continue to rise. In addition to the likelihood of occupational exposure, there is the potential for environmental contamination. While raw, unrefined, and hydrophobic carbon nanotubes tend to settle out of aqueous media/environmentss into solid phases such as river sediments (Lin and Xing, 2008), water dispersible, F-CNTs will contaminate water resources and will also be highly bioavailable on exposure**.** Therefore, there is a need to develop an understanding of the fate of F-CNTs in aqueous media.

Several different routes to aqueous dispersion of CNTs have been explored. The most common approach includes the use of surfactants, and the covalent functionalization of CNT surface using different oxidizing agents (Aitchison et al., 2007, Yu et al., 2007). In addition, non-covalent interactions with different groups have been utilized to generate water dispersible CNTs. Well established approaches include DNA wrapping (Daniel et al., 2007, Wang et al., 2007b, Kharisov et al., 2008, Noguchi et al., 2008) and composite formation with polymers such as polyvinyl pyrrolidone (PVP), polyvinyl alcohol (PVA), polyethylene glycol (PEG) and poly(ethylene oxide)-*b*-poly [2-(*N*,*N*-dimethylamino)ethyl methacrylate] (PEO-*b*-PDMA) (Wise and Rayment, 2004, Wang et al., 2007b, Hu et al., 2008).

The colloidal behavior of CNT dispersions is important in understanding their fate and transport in the aquatic environment, and several publications have addressed this issue (Elimelech et al., 1995, Yurekli et al., 2004, Saleh et al., 2008). Aggregation kinetics of CNTs have been studied using time-resolved dynamic light scattering (TRDLS), Raman spectroscopy, zeta-potential measurements, and UV-Visible spectroscopy (Chiang et al., 2001, Peng et al., 2009). Precipitation of the carboxylated CNTs under the influence of different salts has shown (Manivannan et al., 2009, Smith et al., 2009) that precipitation is dependent on the charge of the cations. In general these nanoparticles have followed the well-established Derjaguin-Landau-Verwey-Overbeek (DLVO) theory (Derjaguin and Landau, 1993, Verwey and Overbeek, 1999).

The polymer-wrapped CNTs were prepared from purified MWCNTs which had no surface modification and therefore, hydrophobic in nature. In an aqueous solution they tend to agglomerate via van der Waals interactions. The grafting of the polymer onto the surface eliminates these forces. Polyvinyl pyrrolidone is a highly water soluble polymer which has been non-covalently grafted onto the CNTs surface. The polymer is attached to the CNT surface at one end, and the long chains float in water repelling each other to prevent aggregation. In an aqueous environment, these hydrophilic molecules prefer to interact with water. Therefore, the presence of PVP on the CNT surface provides steric stabilization and the aggregation behavior of the colloidal system may be quite different from the carboxylated CNTs. Since the stabilization is not caused by the electrical double layer, zeta potential data for such systems provide limited information. It has been shown that while systems stabilized with ionic polymers tend to obey the DLVO theory, non-ionic polymeric systems with low zeta potential may exhibit high stability (Troy, 2005).

Therefore, the aggregation behavior of oxidized CNTs and those wrapped with a polymer are expected to differ due to their modes of stabilization. The water dispersibility of covalently functionalized CNTs originates from electrostatic repulsive forces between negative surface charges, whereas a polymer wrapped CNT is stabilized sterically by the presence of the hydrophilic polymer on the surface.

This Chapter presents the aggregation behavior of polymer modified CNTs in an ionic environment showing how it differs from its carboxylated analog. Particularly focusing on poly(vinylpyrrolidone) (PVP) wrapped MWCNTs, which have been used extensively as aqueous dispersible CNTs.

2.1. Preparation of the F-CNTs:

Carboxylated multiwalled carbon nanotubes **(**MWCNT-COOH) were functionalized in a Microwave Accelerated Reaction System (Mode: CEM Mars) fitted with internal temperature and pressure controls according to an experimental procedures previously published by our laboratory (Chen et al., 2007b, Chen and Mitra, 2008). Weighed amounts of purified MWCNTs were treated with a mixture of concentrated H_2SO_4 and HNO_3 solution by subjecting them to microwave radiation at 140 °C for 20 min. This led to the formation of carboxylic groups on the surface, leading to high aqueous dispersibility. The resulting solid was filtered through a 10 μm membrane filter, washed with water to a neutral pH and dried under vacuum at 80 °C to a constant weight.

MWCNT-PVP was prepared according to previously reported procedures (O'Connell et al., 2001). Purified MWCNT was dispersed in deionized water at a concentration of 50 mg L^{-1} with the aid of 1% sodium dodecyl sulfate (SDS) and 1 % by

weight of PVP was added to the mixture, which was then incubated at 50 °C for 12 hrs. The carbon nanotubes were then filtered through a 10 μm membrane filter and washed with deionized water. This was followed by three cycles of ultrasonic redispersion in deionized water to remove any residual SDS. The sample was filtered and dried under vacuum at room temperature to a constant weight.

2.1.1 Characterization of the F-CNTs

The materials were characterized by scanning electron microscope (SEM), thermogravimetric analysis (TGA), and Fourier Transform Infrared spectroscopy (FTIR). SEM Data was collected on a LEO 1530 VP Scanning Electron Microscope equipped with an energy-dispersive X-ray analyzer. TGA was performed using a Pyris 1 TGA from Perkin-Elmer Inc from 30 °C to 900 °C under a flow of air at 10 mL min^{-1}, at a heating rate of 10 °C per min. FTIR measurements were carried out in purified KBr pellets using a Perkin-Elmer (Spectrum One) instrument.

2.1.2 Hydrophobicity and Stability Measurements

50 mg L^{-1} stock solutions of MWCNT-COOH and MWCNT-PVP were prepared by sonicating weighed amounts of the F-CNTs in deionized water. Various concentrations of F-CNTs used in this study were then prepared by diluting the stock solution by ultrasonication. 400 mM stock solutions of sodium chloride (NaCl), sodium acetate (NaOAc) and magnesium chloride ($MgCl_2$) were prepared by dissolving weighed amounts of salt in MilliQ water and dilution was carried out on an as-needed basis.

The hydrophobicity of MWCNT-COOH and MWCNT-PVP was determined in deionized water and in the presence of 25 mM and 100 mM salt solutions by measuring the UV absorbance at 252 nm before and after extraction with 1-octanol. The stability of 25 mg L^{-1} dispersions of the F-CNTs over a 24-hr period was determined in the presence of 25 mM solutions of sodium chloride, sodium acetate and magnesium chloride using UV absorbance at 252 nm. This was measured at 0, 1, 2, 4, 6, and 24 hrs. the concentration of carbon nanotubes at each point in time was determined based on calibration standards.

2.1.3 Dynamic Light Scattering and Zeta Potential Measurements

The hydrodynamic diameter of 1mg L^{-1} dispersions of the F-CNTs were measured as a function of salt concentration at 25 ^{o}C using dynamic light scattering (Beckman Coulter N4 Plus submicron particle size analyzer, operated at 90^{o} detector angle), where the salt concentrations ranged from 10 to 200 mM. The zeta potential of the F-CNT dispersions was measured at a concentration of 5 mg L^{-1} at 25 ^{o}C using a Malvern Instrument (Zetasizer nano ZS90). Measurements were made in deionized water and as a function of electrolyte concentration. Data on CNT aggregation was collected using 1 mg L^{-1} dispersions of MWCNT-COOH and MWCNT-PVP in the presence of electrolyte solutions whose concentrations ranged between 10 and 200 mM. The measurements were performed for a time period ranging from 180 s to 3 hrs.

2.2 Results and Discussion

2.2.1 Characterization

SEM images of MWCNT-COOH and MWCNT-PVP are presented in Figure 2.1. These show that the CNTs remained intact after functionalization with minimal visible tube damage.

The FTIR spectrum (Figure 2.2) confirmed the presence of functional groups in the purified MWCNT, MWCNT-COOH and MWCNT-PVP. The carboxylic stretching frequency in MCWNT-COOH occurred at 1716 cm^{-1}. The stretching (O-H) vibration occurred at 3440 cm^{-1} in the MWCNT-COOH spectrum (Figure 2.2b), which was clearly absent from the purified MWCNT spectrum (Figure 2.2a). The carbonyl stretching frequency from the amide group in PVP occurred at 1645 cm^{-1} (Figure 2.2c). In all the samples, the peak around 1576 cm^{-1} was assigned to the C=C stretching of the carbon skeleton.

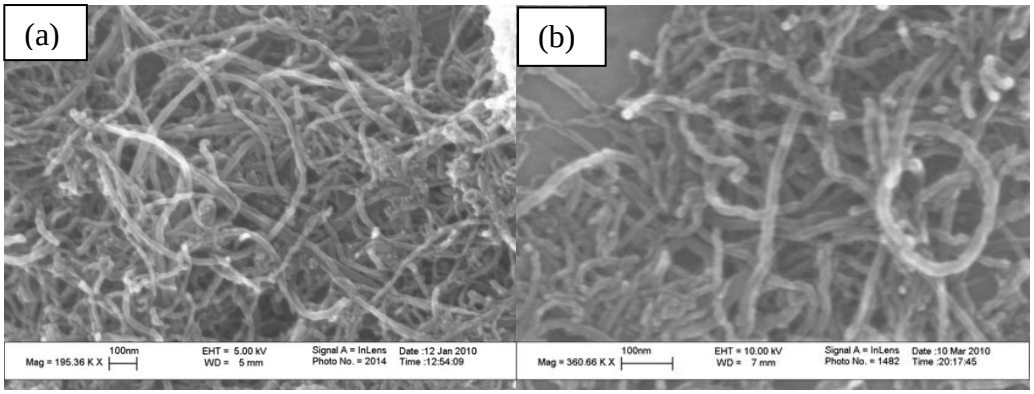

Figure 2.1 Scanning Electron microscope images of (a) MWCNT-COOH and (b) MWCNT-PVP.

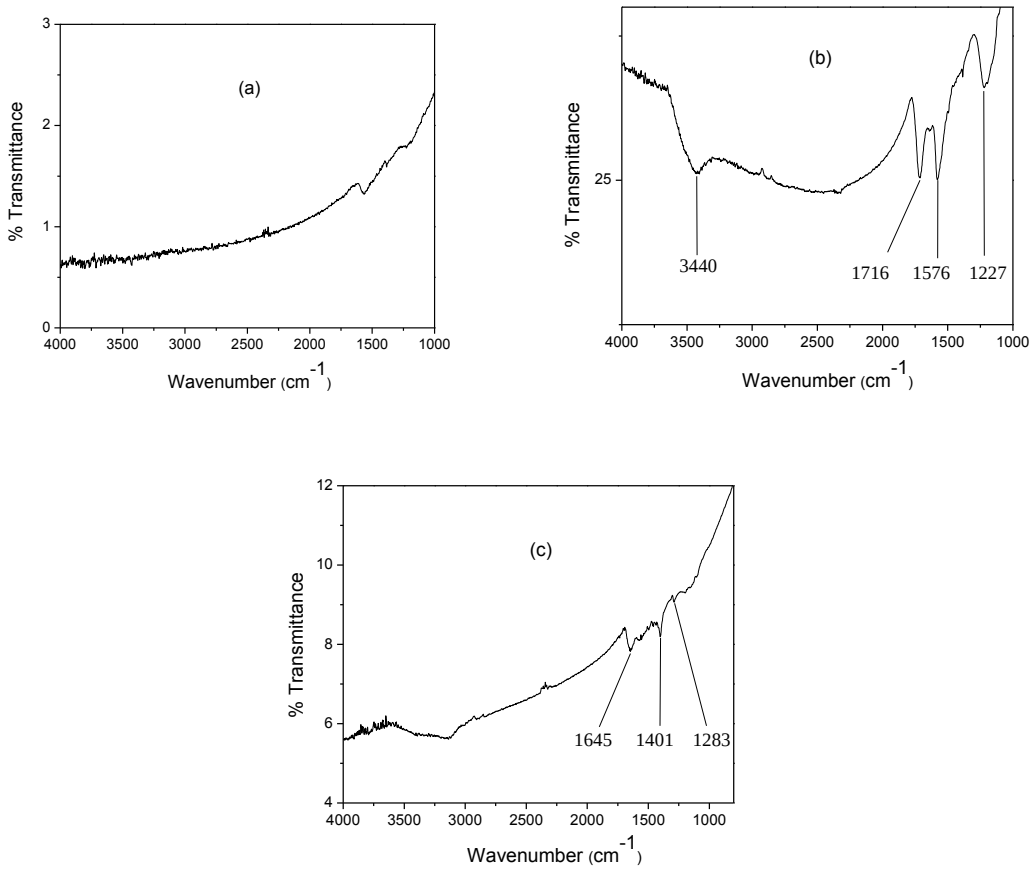

Figure 2.2 FTIR spectra of (a) purified MWCNT, (b) MWCNT-COOH and (c) MWCNT-PVP.

The TGA profile of MWCNT-PVP is presented in Figure 2.3c. It shows weight loss in the 200 ^{o}C to 350 ^{o}C region. This was attributed to the decomposition of the PVP wrapping on the CNT. A similar weight loss from 150 ^{o}C to 400 ^{o}C was observed in the MWCNT-COOH profile (Figure 2.3b) due to the loss of the carboxylic groups introduced through acid functionalization.

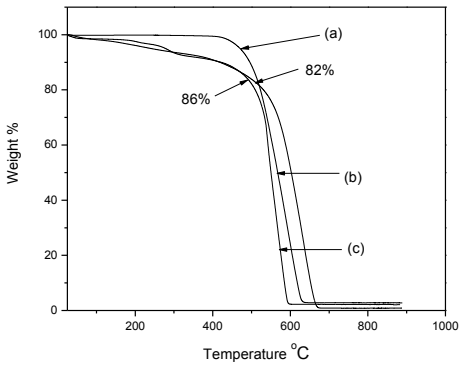

Figure 2.3 TGA profiles of (a) purified MWCNT, (b) MWCNT-COOH and (c) MWCNT-PVP.

2.2.2 Hydrophobicity

1-octanol/water partitioning was used to establish a hydrophobicity index (HI) for the two MWCNT derivatives. This index was calculated based on UV-Visible absorption of the F-CNT dispersions (at 252 nm) in the original water and after 1-octanol extraction. The HI was computed as:

$$\mathrm{HI}(\%) = \frac{A_o - A_i}{A_o} * 100 \qquad (2.1)$$

where, A_o is the UV-Visible absorbance of the F-CNTs before 1-octanol extraction and A_i is the absorbance after extraction (Wang et al., 2010). Visual inspection of the phase separation revealed that the tubes were homogeneously dispersed in the aqueous layer in both cases, and this is shown in Figure 2.4. The hydrophilicity of both MWCNT-COOH and MWCNT-PVP agreed with the relatively high negative surface charge, and the zeta potentials in water were -43.7 eV and -42.2 eV, respectively. Although the zeta potential values of the aqueous dispersions of the two F-CNTs were similar, their HI were quite

diverse (Table 1), making them fundamentally different materials. The results showed that both MWCNT-COOH and MWCNT-PVP had relatively low HI in deionized water, preferring to partition in the aqueous phase. Among the two, MWCNT-PVP was more hydrophilic.

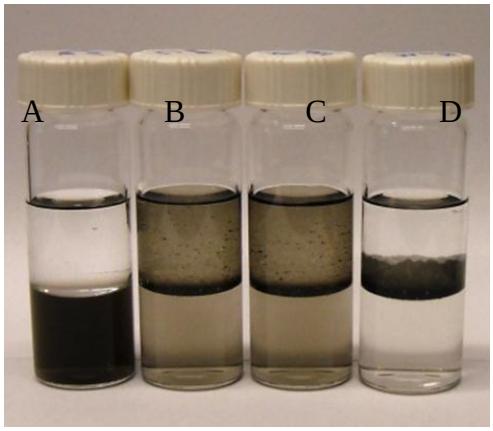

Figure 2.4 1-octanol extraction of MWCNT-COOH from A; deionized water, B; 25 mM NaCl, C; 25 mM NaOAc and D; 25 mM $MgCl_2.6H_2O$.

Table 1 compares the relative HI of the F-CNTs in deionized water, NaCl, NaOAc and $MgCl_2$. HI indices for the F-CNTs in the presence of the divalent Mg salt were higher than in the monovalent Na, which was consistent with the Schulze-Hardy Rule (Elimelech et al., 1995), where the critical coagulation concentration (*ccc*) depends upon the counterion valence *z* (ranges from -2 to -6). While NaCl is neutral in an aqueous environment (pKa 6.7-7.3), sodium acetate is basic (pKb 9.25). However, MWCNT-COOH is expected to be dissociated completely at both pH values accounting for the similarity in their HI. The HI of the MWCNT-COOH in the monovalent Na salt solutions was generally higher than those of MWCNT-PVP. This was attributed to the presence of relatively weaker charges on the MWCNT-PVP surface for neutralization by the metal

ions. On the other hand it is possible that PVP may partially unwrap (O'Connell et al., 2001) from the tube surface during 1-octanol extraction making the tubes hydrophobic, which may make them relatively insensitive to ionic strength.

It is known that the addition of an electrolyte to water changes the hydrogen-bonded structure of water. The effects of salt species in a polymer wrapped CNT depends on the interaction of the polymer with the solvent, the binding of water molecules to the polymer, changes in the hydrogen bonding and the alteration in the hydration sheath due to the added salt. PVP contains N-C=O units on the lactam rings, and these polar groups are involved in the association with water molecules by hydrogen bonding. The addition of salts into aqueous dispersions of MWCNT-PVP changed the association and/or hydration, and could disrupt the highly oriented water molecules surrounding the polymer leading to higher hydrophobicity (Schudel et al., 1997). MWCNT-PVP had a lower HI in the presence of sodium chloride than sodium acetate, which is consistent with previous reports where acetate ions were shown to be more effective in salting out PVP than the chloride (Schudel et al., 1997).

Table 2.1 Hydrophobicity Index of the F-CNTs

	Hydrophobicity Index %					
	DI Water	NaCl		NaOAc		$MgCl_2$
		25mM	100mM	25mM	100mM	25mM
MWCNT-COOH	-4.15	38.29	73.39	47.38	74.68	100
MWCNT-PVP	-62.57	26.31	10.27	40.64	39.38	100

2.2.3 Aggregation of the F-CNTs

Figure 2.5a shows the particle size distribution of MWCNT-COOH and MWCNT-PVP in water as a function of salt concentration. Agglomeration led to large particle size, which increased with salt concentration. The two functional forms showed markedly different behavior. The water dispersibility of MWCNT-COOH originates from the negatively charged oxygen-containing groups on the CNT surface. In aqueous phase, the electrostatic repulsive forces between negative surface charges of the oxygen-containing groups may lead to stability of the MWCNT-COOH in water. In the presence of electrolyte solutions, positively charged metal ions neutralized the surface charges on the MWCNT-COOH surface, and compressed the double layer of the dispersed nanotubes, which lead to agglomeration. On the other hand, the CNTs in the MWCNT-PVP dispersion were sterically stabilized by the presence of the hydrophilic polymer on the surface. The diameter of the MWCNT-COOH increased gradually at low monovalent salt concentration, but the size increased rapidly past a concentration of 100mM (Figure 2.5a). This was not observed in the case of PVP wrapped CNTs, where the size increase was gradual even at high salt concentrations. The anions did not appear to have any effect on the stability of the dispersions because the agglomeration in presence of NaOAc was similar to that of NaCl. The presence of acetate did not lead to any common ion effect in the case of MWNCT-COOH. It is interesting to note that in the case of MWCNT-COOH, as compared to the monovalent Na salt, the divalent Mg led to a marked increase in the particle size (nearly 4 times). The difference between the mono and the divalent salts was not as pronounced in the case of MWCNT-PVP, implying that the aggregation behavior was not as dependent on counterion valence in accordance to the Schulze-Hardy Rule

(Elimelech et al., 1995). In general, these observations were consistent with the zeta potential of the F-CNTs dispersions (Figure 2.5b), where an increase in salt concentration led to less negative values.

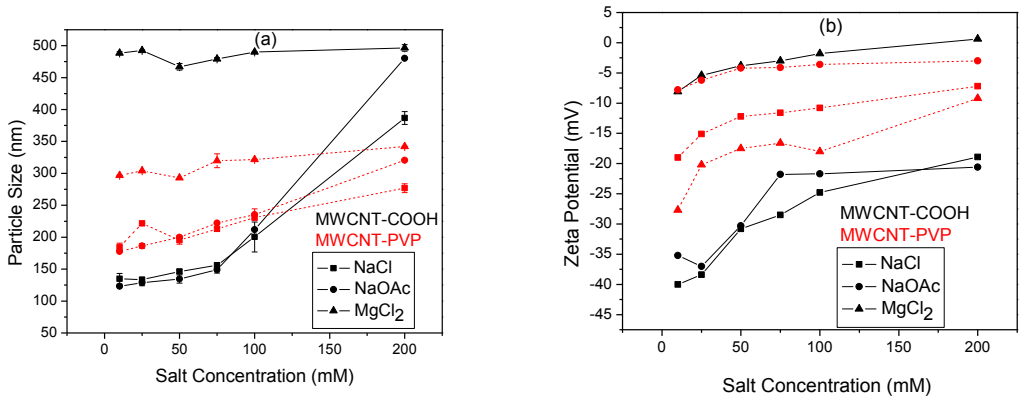

Figure 2.5 (a) Particle size distribution and (b) zeta potential of the F-CNTs as a function of salt concentration.

Figure 2.6 shows the particle size distribution as a function of zeta potential for the F-CNTs in the electrolyte media. It was observed that up to a point, the particle size of the F-CNTs generally increased as their zeta potential became less negative with increasing salt concentration. The size of the MWCNT-COOH showed a strong dependence on zeta potential in the presence of the sodium salts, where the particle size increased first linearly and then asymptotically. The effect was less pronounced in the case of MWCNT-PVP and significantly lesser in the presence of the Mg salt.

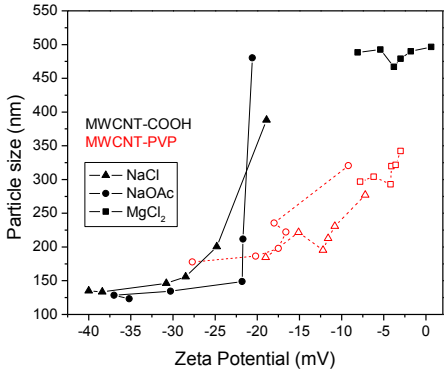

Figure 2.6 Particle size distribution as a function of zeta potential in the presence of (a) sodium chloride, (b) sodium acetate and (c) magnesium chloride.

The initial aggregation kinetics of the F-CNTs was investigated using time resolved dynamic light scattering. The initial rate of change in particle size (r_h) is proportional to kn_o where *k is* the initial aggregation rate constant and n_o is the initial concentration of the MWCNTs (Güner and Ataman, 1994). The reciprocal of stability ratio 1/W or the attachment efficiency α for suspensions with the same particle concentration were computed according to equation 2.2.

$$\alpha = \frac{\left(\frac{dR_h(t)}{dt}\right)_{t\to 0}}{\left(\frac{dR_h(t)}{dt}\right)_{t\to 0,fast}} \tag{2.2}$$

where the subscript "fast" represents favorable solution conditions, under which rapid, diffusion-limited aggregation takes place. The attachment efficiency, which is a measure of the ratio of the initial slope of the aggregation profile in a given electrolyte system to the slope obtained under fast aggregation conditions are shown in Figure 2.7. This shows

the attachment efficiencies of the F-CNTs in NaCl and $MgCl_2$ as a function of salt concentration.

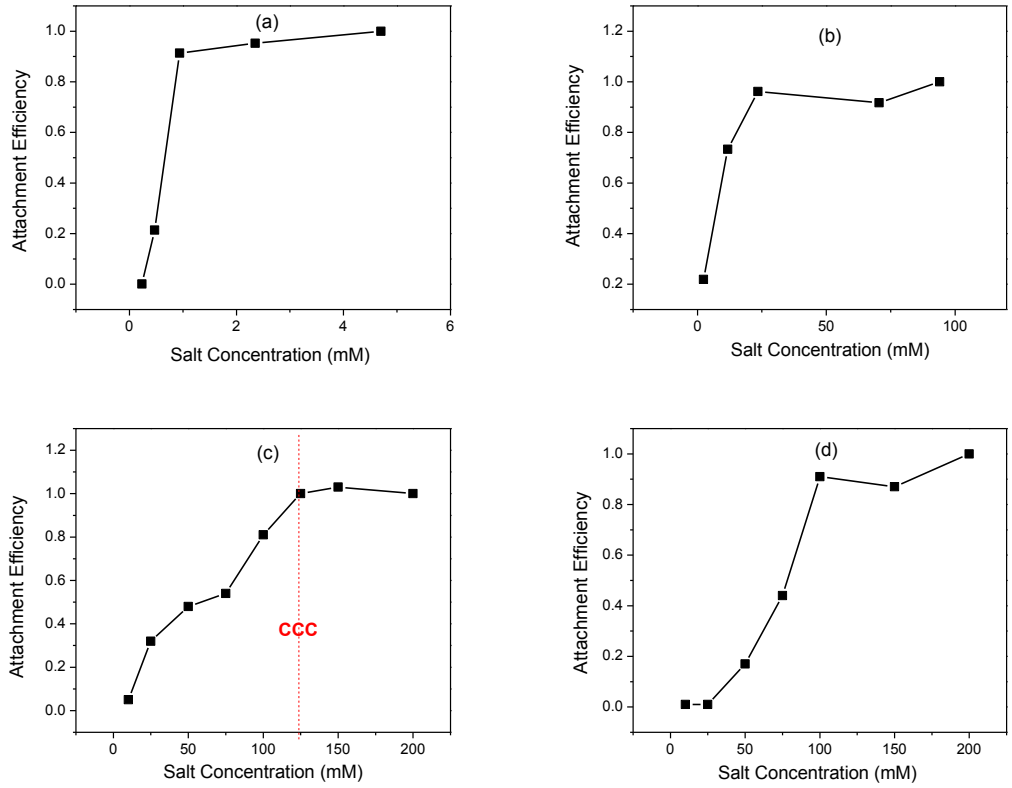

Figure 2.7 Attachment efficiency of the F-CNTs as a function of Electrolyte concentration. (a) MWCNT-COOH in $MgCl_2$, (b) MWCNT-PVP in $MgCl_2$, (c) MWCNT-COOH in NaCl, and (d) MWCNT-PVP in NaCl.

Distinct unfavorable and favorable aggregation kinetics regimes, demarcated by the critical coagulation concentration (*ccc*) (Figure 2.7) were observed. This indicated that electrostatic DLVO type interactions was the dominant mechanism for stabilization. At low ionic strengths, an increase in salt concentration led to a corresponding increase in attachment efficiency. This is in line with Figure 5b, where an increase in electrolyte concentration led to less negative zeta potential. At high concentrations, the attachment

efficiency was no longer a function of concentration and remained constant. This was similar to what had been reported previously (Saleh et al., 2008). Higher attachment efficiencies were observed in the presence of the divalent Mg ion [Figure 2.7(a and b)] which was also consistent with the zeta potential, where the latter became much less negative with even small increase in Mg concentration.

The *ccc* values were estimated from the plot of the attachment efficiencies against the salt concentration which shows the slow and fast aggregation regimes (Figure 2.7). The *ccc* values were obtained from the intersection of the interpolated lines through the slow and fast regimes. MWCNT-COOH showed higher attachment efficiencies than MWCNT-PVP [Figure 2.7 (c and d)], which was evident from the *ccc* values. For example, the *ccc* values were 0.6 mM and 18 mM of $MgCl_2$ for MWCNT-COOH and MWCNT-PVP, respectively, and the corresponding values in NaCl were 125 mM and 100 mM. The difference between $MgCl_2$ and NaCl was also quite apparent. With the exception of MWCNT-COOH in $MgCl_2$, previously reported *ccc* values are significantly lower than the present data which deals with highly water dispersible MWCNT (Saleh et al., 2008).

2.2.4 Long Term Stability of the F-CNTs

The time dependent stability of the nanoparticles dispersions are presented in Figure 2.8. It was observed that both MWCNT-COOH and MWCNT-PVP dispersions in deionized water were stable over the 24 hr measurement period. Aggregation and subsequent deposition of the nanoparticles was observed in the electrolytic environment. The higher the hydrophobic indexes of the F-CNTs, the less stable they became in aqueous solutions.

Therefore, the decreased long-term stability of the F-CNTs was in agreement with their hydrophobicity indexes (Table 2.1) in deionized water and electrolyte solution. Stability of MWCNT-COOH was better in the presence of the monovalent Na ions than the divalent Mg ions. This was consistent with the Schulze-Hardy Rule (Elimelech et al., 1995) where *ccc* is said to be dependent on counterion valence.

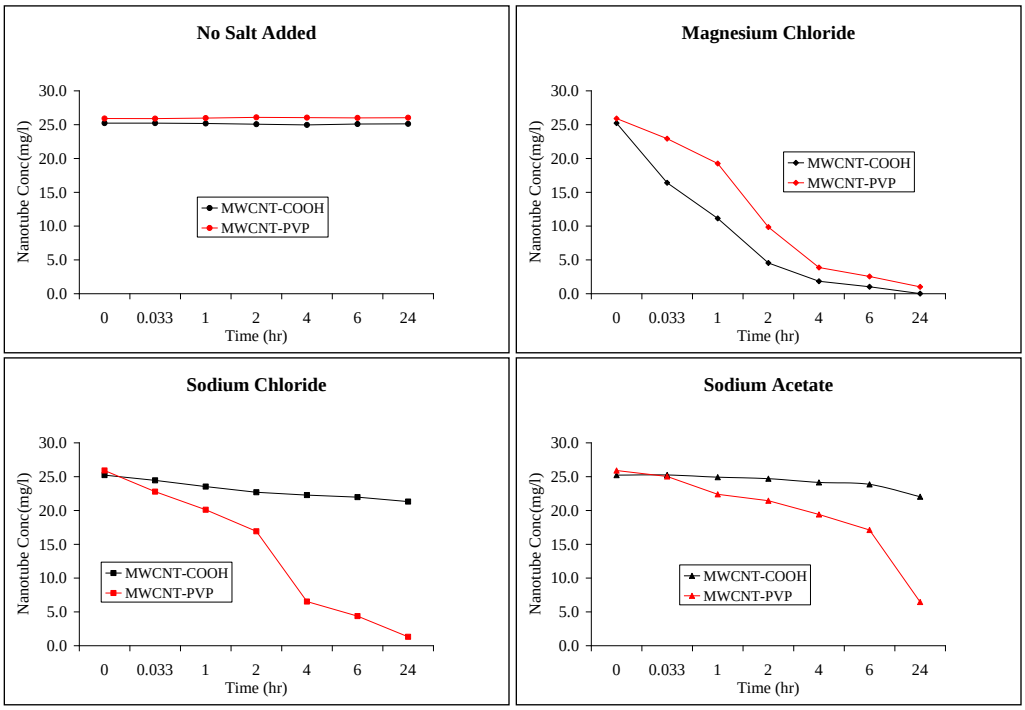

Figure 2.8 Colloidal stability as a function of time measured by UV absorbance at 252 nm wavelength.

MWCNT-PVP showed lower stability in the presence of electrolyte than MWCNT-COOH over the 24-hr period. This was attributed to the long term behavior of the PVP wrapped carbon nanotubes in the electrolytes. Wrapping of carbon nanotubes by water soluble polymers is driven largely by a thermodynamic drive to eliminate the hydrophobic interface between the tubes and their aqueous environment. Therefore,

changing the solvent system to remove the strong hydrophobic thermodynamic penalty would induce the polymer-CNT complexes to dissociate (O'Connell et al, 2001). It is therefore, possible that the PVP wrapping on the carbon nanotubes was partially removed after prolonged exposure to the electrolyte solution causing them to lose their hydrophilicity and subsequently they deposited out of the solution.

2.3 Conclusions

The colloidal behavior of carboxylated and polymer wrapped CNTs were markedly different in terms of hydrophobicity, particle size distribution and zeta potential. Aggregation of the polymer modified CNT was lower compared to the carboxylated CNTs, with orders of magnitude higher *ccc*. Since dispersion in the presence of NaOAc and NaCl followed similar patterns, it was concluded that the anions did not have any significant effect on stability. Both F-CNTs were highly stable in pure water, while MWCNT-PVP showed lower long term stability in the presence of electrolytes. The results suggest that these highly dispersible F-CNTs can be relatively stable in typical aquatic environments, and their behavior will depend upon the presence of other species.

CHAPTER 3

SIZE DEPENDENT AQUEOUS DISPERSIBILITY OF CARBOXYLATED MULTIWALL CARBON NANOTUBES

Several cytotoxicological studies have investigated the effect of size on the toxicity of nanoparticles and compared them to micrometer particles of the same composition. Metal oxides such as CuO and TiO_2 (Karlsson et al., 2009), gold (Pan et al., 2007), monodispersed amorphous spherical silica ((Napierska et al., 2009) as well as SiO_2 nanoparticles (Yuan et al., 2010) have shown size dependent cytotoxicity. In all these studies, the particles were observed to be more toxic in the smaller size ranges than the larger ones; only TiO_2 showed the opposite effect. At present there is no comprehensive data on the size dependent behavior of CNTs. It is important to realize that CNTs represent a diverse group of nanotubes that vary in size, shape and chirality. For example, in recent years there has been interest in shorter CNTs for high field quasiballistic electron transport (Javey et al., 2004), hydrogen storage (Liu et al., 2003), and energy storage systems such as in lithium batteries (Wang et al., 2007a). Since size alters many of the properties of CNTs, it may also affect its fate and transport and is an important parameter when CNTs are in consideration as pollutants. This Chapter presents the influence of tube dimensions on the aggregation behavior of carboxylated multiwall carbon nanotubes (c-MWCNTs) in electrolytic environments.

3.1 MWCNT Oxidation

The c-MWCNTs were functionalized in a Microwave Accelerated Reaction System (Mode: CEM Mars) fitted with internal temperature and pressure controls according to experimental procedures detailed in Section 2.1 of Chapter 2 (Chen et al., 2007b, Chen and Mitra, 2008). Carboxylic groups were formed on the surface of the CNTs through a microwave assisted reaction with a mixture of concentrated nitric and sulfuric acid, leading to high aqueous dispersibility.

The materials were characterized by scanning electron microscope (SEM), thermogravimetric analysis (TGA), and Fourier Transform Infrared spectroscopy (FTIR). SEM Data was collected on a LEO 1530 VP Scanning Electron Microscope equipped with an energy-dispersive X-ray analyzer. TGA was performed using a Pyris 1 TGA from Perkin-Elmer Inc from 30 °C to 900 °C under a flow of air at 10 mL min^{-1}, at a heating rate of 10 °C per min. FTIR measurements were carried out in purified KBr pellets using a Perkin-Elmer (Spectrum One) instrument.

3.1.1 Hydrophobicity and Stability Measurements

50 mg L^{-1} stock solutions of the c-MWCNTs and 400 mM stock solutions of salts were prepared according to procedures detailed in Section 2.1.1 in Chapter 2. Dilution was carried out as needed.

Hydrophobicity of the c-MWCNTs was determined in deionized water and in the presence of 100 mM salt solutions by measuring the UV absorbance at 500 nm before and after extraction with 1-octanol. The stability of 25mg L^{-1} dispersions of the c-MWCNTs over a 24-hr period was determined in the presence of 25 mM solutions of

sodium chloride and magnesium chloride using UV absorbance at 252 nm. Their dispersion stability indices were determined based on their UV-visible absorbance at 0 hr (Wang et al., 2010, Addo Ntim et al., 2011).

The hydrodynamic diameter of 1mg L^{-1} dispersions of the c-MWCNTs were measured in the presence of 100 mM salt concentration at 25 ^{o}C using dynamic light scattering (Beckman Coulter N4 Plus submicron particle size analyzer, operated at 90^{o} detector angle). The zeta potential of the c-MWCNT dispersions was measured at a concentration of 5 mg L^{-1} at 25 ^{o}C using a Malvern Instrument (Zetasizer nano ZS90). Measurements were made in deionized water and in the presence of 100 mM electrolyte solution. Aggregation data was collected using 1mg L^{-1} dispersions of the c-MWCNTs in the presence of electrolyte solutions whose concentrations ranged between 10 mM and 200 mM. The measurements were performed for a time period ranging from 180 s to 3 hrs.

3.2 Results and Discussion

3.2.1 Characterization

The physical characteristics of the c-MWCNTs such as outer diameter, length and aspect ratio are presented in Table 1. The c-MWCNTs studied had two length classes; short tubes with length of 0.5-2μm and long tubes with lengths of 10-30μm. Within those two length classes were five identical diameter classes (<8nm, 10-20nm, 20-30nm, 30-50nm and >50nm).

Table 3.1 Physical Characterization of the c-MWCNTs

CNT ID	OD (nm)	Length (μm)	Aspect Ratio	HI Index in DI Water (%)
$MWCNT_{20}$	>50	0.5-2	20	-22
$MWCNT_{31}$	30-50	0.5-2	31	3
$MWCNT_{50}$	20-30	0.5-2	50	-6
$MWCNT_{83}$	10-20	0.5-2	83	-3
$MWCNT_{250}$	<8	0.5-2	250	-23
$MWCNT_{300}$	>50	10-20	300	-6
$MWCNT_{375}$	30-50	10-20	375	-1
$MWCNT_{800}$	20-30	10-30	800	-4
$MWCNT_{1333}$	10-20	10-30	1333	-8
$MWCNT_{2608}$	8-15	10-50	2608	-7
$MWCNT_{4000}$	<8	10-30	4000	-6

SEM images of the c-MWCNTs are presented in Figure 3.1. These show that the CNTs remained intact with minimal visible tube damage. The shorter lengths of CNTs are apparent from the SEM images of $MWCNT_{20}$, $MWCNT_{31}$, $MWCNT_{50}$, $MWCNT_{83}$ and $MWCNT_{250}$, as are the relatively smaller diameters of $MWCNT_{250}$, $MWCNT_{2608}$ and $MWCNT_{4000}$.

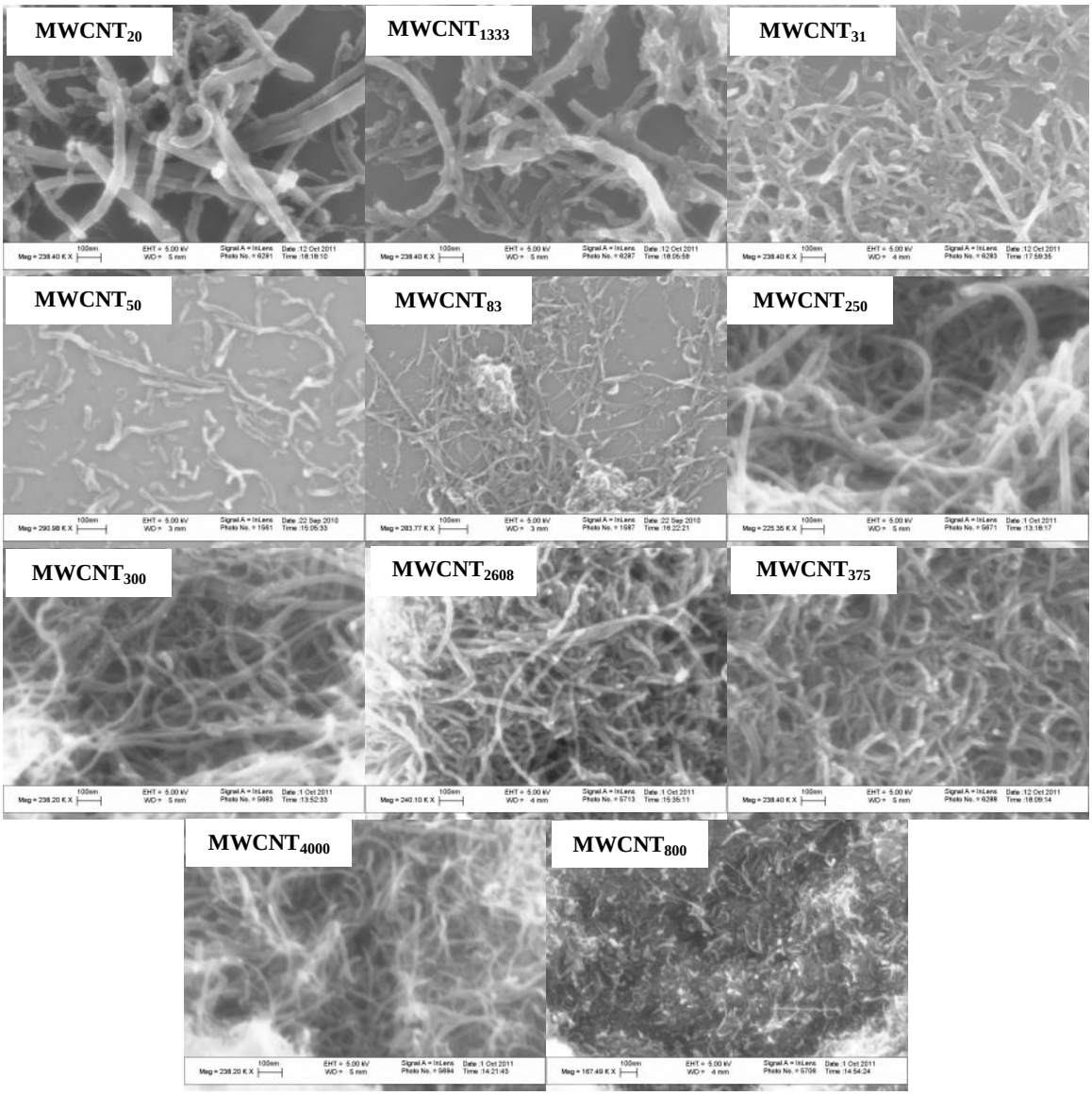

Figure 3.1 Scanning Electron microscope images of the c-MWCNTs.

The TGA profile of the c-MWCNTs is presented in Figure 3.2A. It shows weight loss in the 150 ^{o}C to 400 ^{o}C region (Figure 3.2A) which was absent from the purified MWCNT profile [Figure 3.2A(a)]. This weight loss was attributed to the decomposition of carboxylic groups introduced through acid functionalization. The CNTs were oxidized under the same controlled reaction conditions and based on the TGA profile, the mean

weight % of carboxylic groups on the CNT surface was 20.24 % with a standard deviation of 3.72 %.

The FTIR spectrum shown in Figure 3.2B confirmed the presence of functional groups in the c-MWCNTs. The carboxylic stretching frequency occurred around 1710 cm^{-1} for all the c-MWCNTs studied, indicating that they had all been oxidized. The stretching (C-O) vibration of the carboxylic group occurred around 1215 cm^{-1}. The peak around 1576 cm^{-1} was assigned to the C=C stretching of the carbon skeleton.

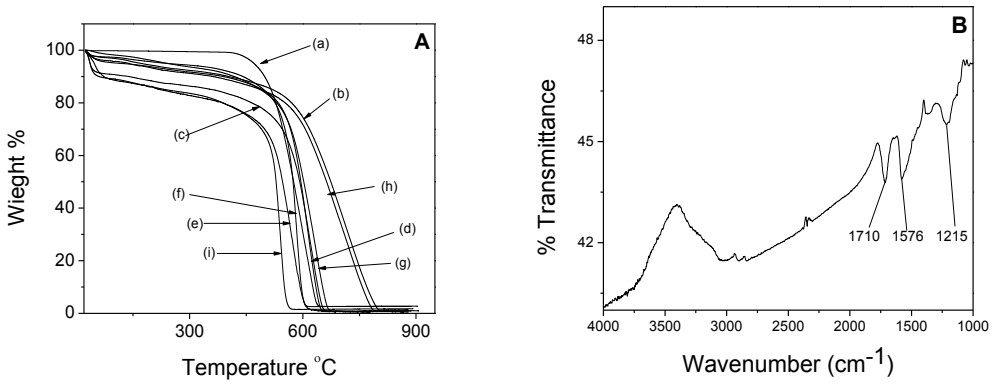

Figure 3.2 A. TGA data for (a) Purified MWCNT, (b) $MWCNT_{31}$, (c) $MWCNT_{50}$, (d) $MWCNT_{83}$, (e) $MWCNT_{250}$, (f) $MWCNT_{300}$, (g) $MWCNT_{800}$, (h) $MWCNT_{1333}$, (i) $MWCNT_{4000}$. **B.** FTIR spectra of the c-MWCNTs.

3.2.2 Hydrophobicity

1-octanol/water partitioning was used to establish a hydrophobicity index (HI) for the c-MWCNTs. This index was calculated based on UV-Visible absorption of the c-CNT dispersions (at 500 nm) in the original water and after 1-octanol extraction. The HI was computed according to equation 2.1. After the addition of salt some of the CNTs were extracted into the organic layer as shown in Figure 3.3(a, b, and c). This was attributed the neutralization of the negative surface charges on the c-MWCNTs by the metal ions

from the salt reducing the electrostatic repulsive forces that cause the tubes to disperse in aqueous solution and therefore, causing the c-MWCNTs to settle out of solution as shown in Figure 3.3 (d, e, and f). It is apparent from Figure 3.3f that the divalent Mg salt caused more aggregation in the c-MWCNTs than the monovalent sodium salts [Figure 3.3 (d, e]. Although the zeta potential values of the aqueous dispersions of the c-MWCNTs were similar, they had quite diverse HI suggesting a possible dependence on diameter and length (Figure 3.4).

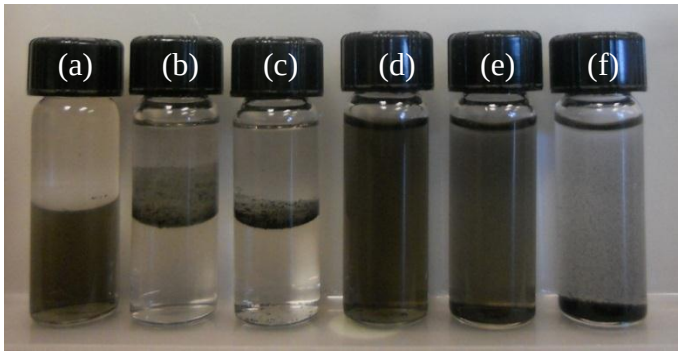

Figure 3.3 1-octanol extraction of the c-MWCNT in (a) DI Water, (b) 25 mM NaCl, and (c) 25 mM $MgCl_2$, and particle aggregation in the presence of (d) DI Water, (e) 25 mM NaCl, and (f) 25 mM $MgCl_2$.

Figure 3.4 shows the HI values of the c-MWCNTs in NaCl, and $MgCl_2$ as a function of tube diameter and length. In all the c-MWCNTs studied, the hydrophobicity index in deionized water was observed to be very low (Table 3.1), increasing with the addition of salt. HI values for the c-MWCNTs in the presence of the divalent Mg salt were higher than in the monovalent Na as shown in Figure 3.4b. This was consistent with the Schulze-Hardy Rule (Elimelech et al., 1995), where the critical coagulation concentration (*ccc*) depends upon the counterion valence *z* (ranges from -2 to -6).

The HI values showed no direct correlation with aspect ratio as presented in Figure 3.4(a). However, it showed improved correlation with length, based on which the CNTs were categorized into two length groups (short and long). Since all the c-MWCNTs were functionalized under the same conditions, and showed similar TGA results, it is assumed that they represented similar degree of carboxylation (20.24% ± 3.72%). Therefore, the difference in HI index was attributed to the differences in size. The HI values were generally higher for the longer CNTs than their shorter counterparts as presented in Figure 3.4 (b, c). The relatively higher HI values observed in the longer c-MWCNTs was attributed to the fact that they are more prone to increased intertube attraction due to van der Waals forces and π-π interactions and are thereby more likely to form agglomerates in comparison to the shorter c-MWCNTs (Heister et al., 2010). Dependence on CNT diameter was observed among the longer nanotubes. The higher diameter tubes probably led to the formation of denser particle aggregates because it is known that MWCNTs with larger diameter tend to comprise of more concentric tubes (Chiodarelli et al., 2012). These bigger diameter CNTs therefore, have a higher tendency to settle out of the colloidal system (Crowder et al., 2002), resulting in higher HI values. For the shorter c-MWCNTs the HI values were generally stable with increasing diameter.

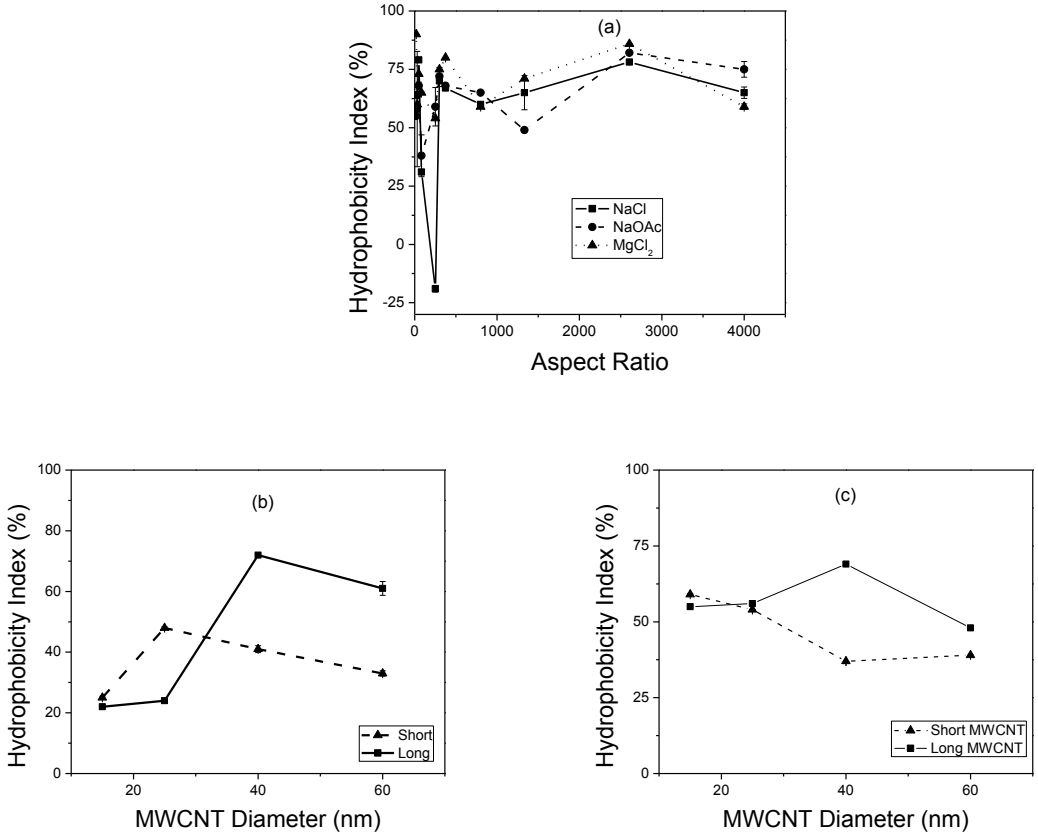

Figure 3.4 Hydrophobicity index of the c-MWCNT as a function of (a) aspect ratio; and as a function of diameter in the presence of 100 mM (b) NaCl and (c) $MgCl_2$.

3.2.3 Aggregation of the c-MWCNTs

The particle size distribution of the c-MWCNTs in the presence of salt as a function of diameter and length are presented in Figure 3.5. The water dispersibility of c-MWCNTs originates from the negatively charged oxygen-containing groups on the CNT surface. In aqueous phase, the electrostatic repulsive forces between negative surface charges of the oxygen-containing groups may lead to stability of the c-MWCNTs in water. In the presence of electrolyte solutions, positively charged metal ions neutralized the surface charges and compressed the double layer of the dispersed nanotubes, which led to agglomeration. The longer CNTs were observed to form significantly larger aggregates

than the shorter CNTs in the presence of salts (Figure 3.5) in agreement with the observed hydrophobicity index values [Figure 3.4 (b, c)]. This was attributed to relatively lower aspect ratios of the shorter c-MWCNTs, giving them a "stout" nature which is less prone to aggregation compared to the longer tubes with higher aspect ratio, which were more prone to intertube interactions which led to the formation of larger particle sizes. This observation was in agreement with recent data reported by Kim and co-workers on the effect of aspect ratio of CNTs on their toxicity (Kim et al., 2011a). Particle size was also observed to be dependent on tube diameter for the longer c-MWCNTs where an increase in diameter resulted in larger particles; this was attributed to the formation of larger aggregates as a result of higher number of concentric rings. Generally, the divalent Mg salt caused higher aggregation in the c-MWCNTs resulting in larger particle sizes than the monovalent Na salts consistent with HI data [Fig 3.4 (b, c)].

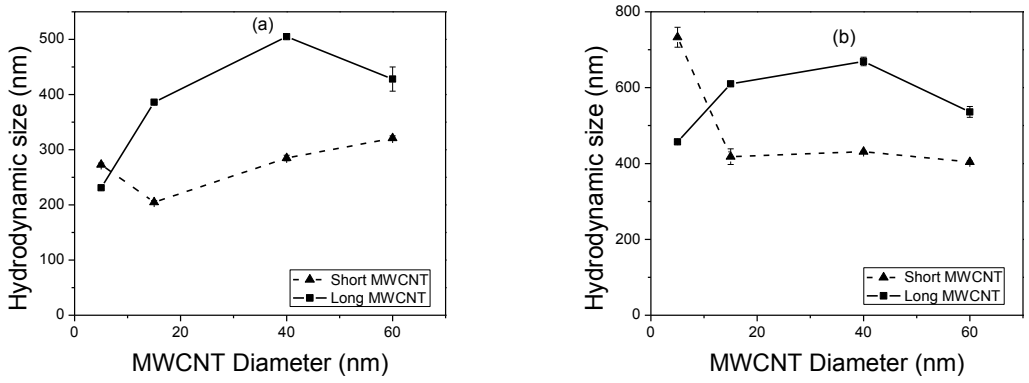

Figure 3.5 Particle size distribution in 100 mM electrolyte solution as a function of tube diameter for the c-MWCNTs in the presence of (a) NaCl and (b) $MgCl_2$.

Figure 3.6 shows the zeta potential of the c-MWCNTs in electrolytic media as a function of their diameter. The observed zeta potential values agreed very well with the observed particle aggregation shown in Figure 3.5. It was observed that the shorter tubes had slightly higher absolute zeta potential values than the longer tubes confirming that the longer CNTs were more prone to aggregation than their shorter counterparts. A similar dependence on CNT diameter was observed among the long tubes, where the absolute value of zeta potential decreased with increasing diameter, due to the formation of denser particle aggregates with increasing CNT diameter (Chiodarelli et al., 2012) The divalent Mg salt caused a significant decrease in the zeta potential values for all the c-MWCNTs which was in agreement with the larger particle sizes observed in the Mg environment as shown in Figure 3.5b.

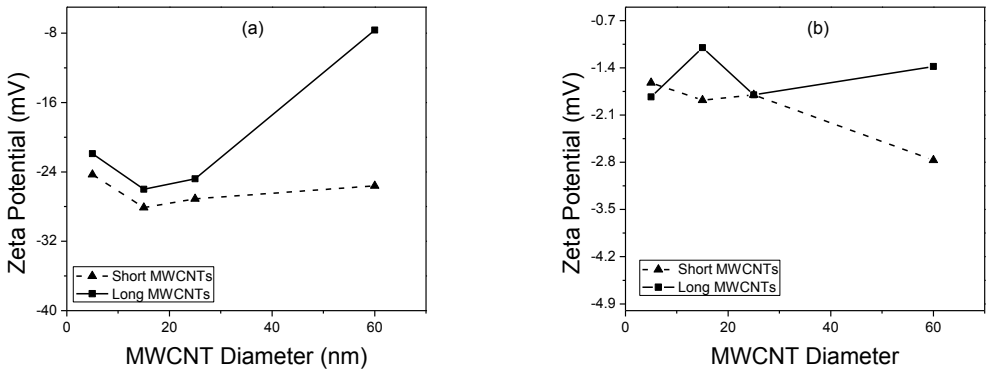

Figure 3.6 Zeta potential as a function of diameter for the c-MWCNTs in the presence of (a) NaCl and (b) $MgCl_2$.

The initial aggregation kinetics of the c-MWCNTs was investigated using time resolved dynamic light scattering. The initial rate of change in particle size (r_h) is proportional to kn_o where *k is* the initial aggregation rate constant and n_o is the initial

concentration of the c-MWCNTs (Schudel et al., 1997). The reciprocal of stability ratio 1/W or the attachment efficiency α for suspensions with the same particle concentration were computed as according to equation 2.2. The attachment efficiency, which is a measure of the ratio of the initial slope of the aggregation profile in a given electrolyte system to the slope obtained under fast aggregation conditions. Particle aggregation in electrolytic solution is presented as a function of time in Figure 3.7. It is evident that the slope of the diameter/time profiles increased with increasing electrolyte concentration.

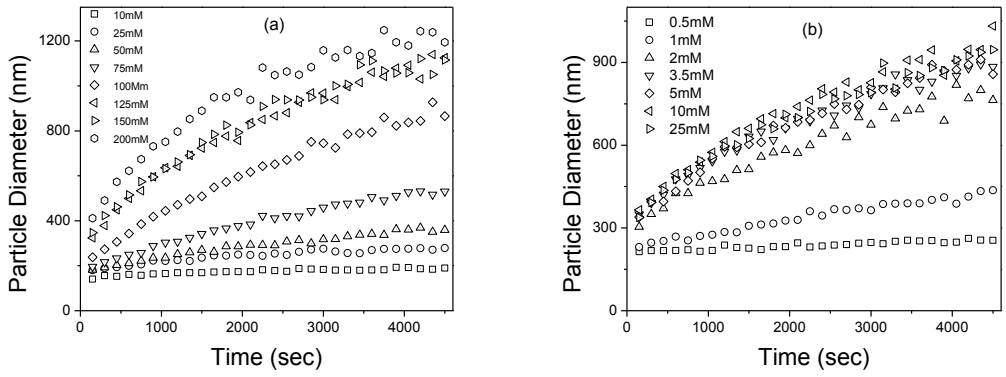

Figure 3.7 Particle size as a function of time in the presence of (a) NaCl and (b) $MgCl_2$.

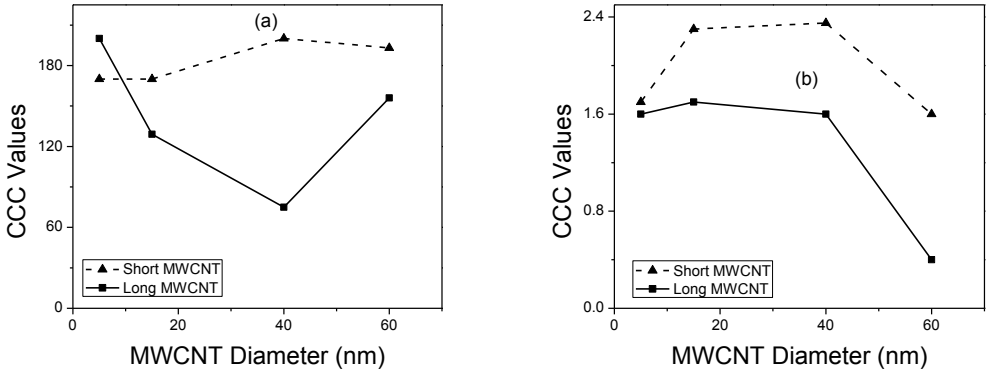

Figure 3.8 Attachment efficiency as a function of c-MWCNT diameter in the presence of (a) NaCl and (b) $MgCl_2$.

While a high concentration of sodium chloride was required for significant aggregation to be observed, magnesium chloride caused aggregation at concentration levels as low as 0.5 mM. The critical coagulation concentrations (*ccc*) of NaCl and $MgCl_2$ for aggregation of the c-MWCNTs were determined from the plot of attachment efficiencies against salt concentration (not shown) and are plotted against the diameters of the c-MWCNTs in Figure 3.8. Previously reported *ccc* values are significantly lower than the present data which deals with highly water dispersible MWCNTs (Elimelech et al., 1995). The shorter c-MWCNTs had relatively higher *ccc* values under both sodium and magnesium conditions than the longer ones implying that the shorter c-MWCNTs were better stabilized under the electrolytic conditions studied. The relatively lower *ccc* values observed in the longer c-MWCNTs was attributed to the fact that they are more prone to increased intertube attraction due to van der Waals forces and π-π interactions and are thereby more likely to form agglomerates and bundles in comparison to the shorter c-MWCNTs. While the *ccc* values were generally stable with increasing CNT diameter for the shorter tubes, they were observed to decrease with increasing diameter for the longer ones. This observation was in agreement with the observed HI values, particle size aggregation behavior and zeta potential values shown in Figures 3.4, 3.5 and 3.6, respectively. This was attributed to the phenomenon where the density of aggregates increased with increasing particle diameter (Chiodarelli et al., 2012) among the longer CNTs resulting in faster settling rates and therefore, lower *ccc* values. Significantly lower *ccc* values were observed in the presence of the divalent Mg ion [Figure 3.7 (c and d] which was also consistent with the HI, particle size and zeta potential in the presence of Mg, consistent with the Schulze-Hardy rule (Elimelech et al., 1995).

3.2.4 Long Term Stability of the c-MWCNTs

The time dependent stability of the nanotubes dispersions are presented in Figure 3.9. It was observed that c-MWCNTs dispersions in deionized water were stable over the 24 hour measurement period irrespective of diameter or length. In the presence of the sodium electrolytes however, the shorter tubes were generally stable with increasing tube diameter unlike the longer CNTs where stability was observed to decrease with increasing diameter, in perfect agreement with the observed HI values, particle size aggregation behavior and zeta potential values. This highlights the greater tendency for the longer tubes to aggregate due to van der Waals intertube attraction and π-π interactions and confirms the formation of larger denser particle aggregates with increasing CNT diameter as a result of the higher number of concentric rings associated with larger diameter MWCNTs (Chiodarelli et al., 2012), settling out of the colloidal system faster (Crowder et al., 2002). In the presence of the Mg salt the all the c-MWCNTs become destabilized within 24 hrs, this was also in agreement with the relatively higher HI values observed in the Mg environment.

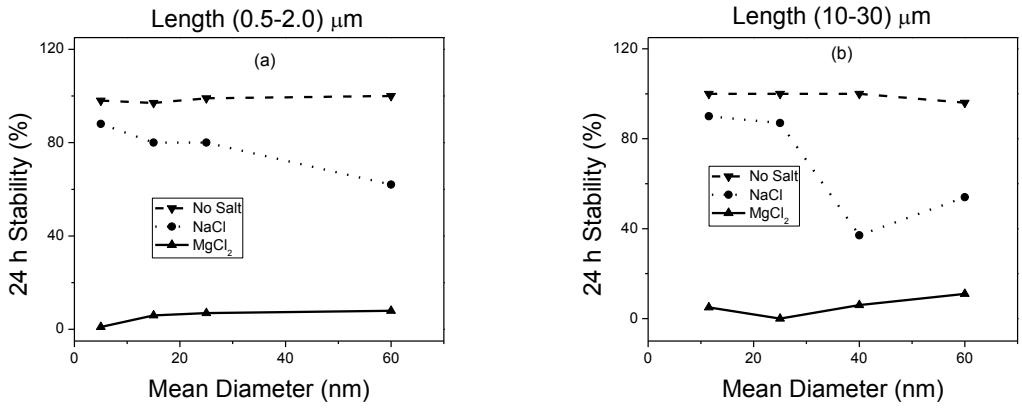

Figure 3.9 Colloidal stability as a function of c-MWCNT diameter for (a) short c-MWCNTs and (b) long c-MWCNTs.

3.3 Conclusions

The colloidal behavior of c-MWCNTs of different sizes was found to be different in terms of hydrophobicity, particle size distribution, zeta potential and aggregation kinetics. The hydrophobicity indices of the c-MWCNTs showed a dependence on the length of the c-MWCNTs, where the shorter tubes showed relatively lower HI values. Zeta potential values of the c-MWCNTs showed a similar dependence on tube length where the shorter c-MWCNTs showed more negative values. This was consistent with the particle size aggregation behavior and the initial aggregation kinetics, where the longer c-MWCNTs showed significantly larger aggregates than the shorter ones, with corresponding lower *ccc* values. It was observed the shorter the c-MWCNTs were less prone to aggregation. The effect of CNT diameter was not very pronounced among the shorter c-MWCNTs as all the parameters investigated did not vary significantly with diameter. The colloidal behavior of the longer c-MWCNTs however, showed a dependence on diameter where stability appeared to decrease with increasing CNT diameter. The higher diameter tubes led to the formation of denser particle aggregates due to the presence of more concentric tubes, with greater tendency to settle out of the colloidal system. There was no apparent correlation between the parameters investigated and the aspect ratio of the MWCNTs. All the c-MWCNTs were quite stable in pure water for the twenty-four hr period studied here.

CHAPTER 4

REMOVAL OF TRACE ARSENIC TO MEET DRINKING WATER STANDARDS USING IRON OXIDE COATED MULTIWALL CARBON NANOTUBES

Arsenic in natural waters is a problem that affects many parts of the world including North America and Asia (Chatterjee et al., 1995, Mondal et al., 2006). Arsenic is listed as a carcinogenic contaminant which is responsible for other health effects such as spontaneous abortion (Richardson, 2006) and diabetes (Navas-Acien et al., 2008). As a result of this, more stringent standards are being established by the US-EPA. Typically, arsenite [As(III)], which is neutral, uncharged and a soluble molecule, is considered more toxic than arsenate or As(V) (Knowles and Benson, 1983, Pattanayak et al., 2000).

Existing technologies for arsenic removal include oxidation/precipitation, coagulation/coprecipitation, nanofiltration, reverse osmosis, electrodialysis, adsorption, ion exchange, foam flotation, solvent extraction and bioremediation (Mohan and Pittman Jr, 2007). Most of these techniques are well established, and have their merits and inherent limitations such as the generation of toxic waste, low arsenic removal efficiencies and/or high cost (Mohan and Pittman Jr, 2007).

Adsorption has proven to be an efficient method for arsenic removal and a wide range of materials including lanthanum/iron compounds, mineral oxides, and biological materials (Elizalde-González et al., 2001) have been studied. The use of polymeric resins, activated carbon, activated alumina, iron coated sand (Thirunavukkarasu et al., 2003), hydrous ferric oxide (Wilkie and Hering, 1996), and natural ores have generated much interest and novel metal modified adsorbents have demonstrated superior performance (Chen et al., 2007a, Schmidt et al., 2008). At present there is a need for the development

of higher capacity sorbents for arsenic removal that will be effective at trace As levels so that they may be used for drinking water purification.

Carbon nanotubes (CNTs) are made from graphene sheets seamlessly rolled into cylindrical tubes, and are found as single-walled (SWCNT) and multiwall carbon nanotubes (MWCNT), with the latter being relatively inexpensive (Iijima, 1991, Iijima, 2002). Their unique characteristics such as high aspect ratio, superior mechanical, electrical and thermal properties make them well suited for many applications. CNTs also exhibit exceptional sorption properties towards various organic compounds and inorganic ions (Trojanowicz, 2006). The potential for sidewall functionalization and surface modification make them attractive as support phases for water treatment (Wang et al., 2005a, Wang et al., 2005b, Wang et al., 2006). Carbon nanotubes functionalized with tetragonal zirconyl oxide particles has recently been reported, which have proven effective in water defluoridation (Ramamurthy et al., 2011). A recent study has reported the implementation of a fabric supported magnetite multiwalled carbon nanotube composite based supercapacitor for removal of sodium chloride and arsenic at high mg L^{-1} levels from sea water (Mishra and Ramaprabhu, 2010). From the standpoint of practical applications, the CNTs can be implemented in water treatment as a replacement for activated carbon with the added advantage that they can be self-assembled on supports via chemical vapor deposition (Karwa et al., 2006), and can also be immobilized in membranes (Hylton et al., 2008, Roy et al., 2011) and filters (Mishra and Ramaprabhu, 2010). However, cost and other factors need to be taken into consideration before such a process could be commercialized.

The goal here was to synthesize iron oxide-MWCNT hybrid (Fe-MWCNT) using highly functionalized nanotubes and study the removal of μg L^{-1} levels of arsenic from water to meet the US EPA drinking water standard of 10 μg L^{-1}.

4.1 Synthesis and Characterization of Fe–MWCNT

The MWCNT was functionalized in a Microwave Accelerated Reaction System (Mode: CEM Mars) fitted with internal temperature and pressure controls according to an experimental procedure previously published by our laboratory (Chen et al., 2007b, Chen and Mitra, 2008). Weighed amounts of purified MWCNT were treated with a mixture of concentrated H_2SO_4 and HNO_3 solution by subjecting them to microwave radiation at 120 °C for (20 to 40) min. This led to the formation of carboxylic groups on the surface along with some sulphonation and nitration. The resulting solid was filtered through a 10 μm membrane filter, washed with water to a neutral pH and dried under vacuum at 80 °C to a constant weight. This product (f-MWCNT) was used in the subsequent synthesis of the Fe-MWCNT composite.

The iron oxide coated hybrid (Fe-MWCNT) was synthesized using a method reported previously (Zhang et al., 2007). This was accomplished by dispersing a weighed amount of the f-MCWNT in a 2:1 aqueous solution of $FeCl_3$: $FeSO_4$ under ultrasonication at room temperature. The dispersion was gently stirred at 70 °C for 5 minutes, after which 5 M NaOH solution was added and stirred vigorously at 85 °C for 1 hour. The pH of the reaction was kept between 5 and 11 with the final pH being 10. The composite thus formed was filtered through a 10 μm membrane filter paper, washed and

acidified to pH 5 with 1 M hydrochloric acid and dried under vacuum at 105 °C for 24 hours.

The Fe-MWCNT was characterized using a scanning electron microscope (SEM) fitted with an energy dispersive x-ray spectrometer (EDS), thermogravimetric analysis (TGA), Fourier Transform Infrared spectroscopy (FTIR) and BET surface area. SEM data was collected on a LEO 1530 VP scanning electron microscope equipped with an energy-dispersive X-ray analyzer. Energy dispersive spectroscopic (EDS) data was collected on the EDAX silicon drift detector (SDD) (Apollo XV) mounted on a Hitachi S-3000N electron microscope with specific light element performance. TGA was performed using a Pyris 1 TGA from Perkin-Elmer Inc from 30 °C to 900 °C under a flow of air at 10 mL/min, at a heating rate of 10 °C per min. FTIR measurements were carried out in purified KBr pellets using a Perkin-Elmer (Spectrum One) instrument. Specific surface area, micropore volume, and average pore radius were measured using a Quantachrome NOVA 3000 series (Model N32-11) High Speed Gas Sorption Analyzer at 77.40 K. Before each experiment, the samples were heated at 180 °C and degassed at this temperature until constant vacuum for four hours. The pH of point of zero charge (pHpzc) was determined based on a previously published procedure (Chen et al., 2007a).

4.2 Kinetics and Adsorption Isotherms

10 mg L^{-1} stock solutions of As(III) and As(V) were prepared by dissolving weighed amounts of $NaAsO_2$ and Na_2HAsO_4, respectively in measured volumes of deionized water. The stock solutions were preserved with 1% trace metal grade HNO_3. 1 mg L^{-1} working solutions were then prepared from the stock for analysis. pH values were

maintained constant during the analysis using 100 mM acetate buffer (pH 4 and 5) and 0.1 M Tris buffer (pH 6 – 8). 10 mL of 100 μg L^{-1} arsenic solution [As(III) and As(V)] was contacted with 0.01 g of the adsorbent in a series of conical flasks and samples were collected at (5, 10, 15, 30, and 45) min and (1, 3, 6, 12, 15 and 24) hrs for kinetic studies. The mass of the adsorbent was varied from (0.01 to 0.1) g in the isothermal adsorption studies keeping all other parameters constant (equilibrium contact time 1 hr and 12 hrs for As(V) and As(III), respectively and pH 4). The arsenic solutions and the adsorbents were mixed thoroughly at a speed of 175 rpm on a platform shaker (Lab systems Wellmix). The mixture was filtered through a 0.45 μm membrane syringe filter.

Residual arsenic was measured using Agilent 7500 ICP-MS. All standards were prepared from multi-element solution 2A, Ten mg L^{-1} (Spex Certiprep) with addition of an internal standard mix (Li6, Ge, Y, In, Tb, Bi). A Buffer solution was used for all dilutions. Multi-element instrument calibration standard (No. 1, 20 mg/L (Spex Certiprep)) was used for the verification of the calibration.

4.3 Results and Discussion

4.3.1 Sorbent Characterization

The different oxide forms expected in the Fe-MWCNT composite are: magnetite (Fe_3O_4), maghemite (γ-Fe_2O_3), hematite (α-Fe_2O_3) and goethite (α-FeO(OH)) (Zhang et al., 2007). Acid functionalization of the carbon nanotubes produced carboxylic groups on the surface and this enhanced iron oxide loading. The Brunauer, Emmett, and Teller (BET) surface area of MWCNT and Fe-MWCNT were 110 m^2 g^{-1} and 153 m^2 g^{-1}, respectively, which shows that the surface area of the carbon nanotubes was increased by

approximately 40 % with the iron oxide coating. The pH at zero point charge (pH_{ZPC}) for MWCNT, f-MWCNT and Fe-MWCNT was 6.8, 3.91 and 7.35, respectively. This is the point where the surface charge of the carbon nanotube is independent of the electrolyte concentration. Therefore, the carboxylic groups on the f-MWCNT had been replaced in the Fe-MWCNT.

SEM images of f-MWCNT and the Fe-MWCNT hybrid are shown in Figure 4.1. The original MWCNTs had a diameter in the range of (20 to 40) nm and the length was about (10 to 30) µm. There was no detectable change in tube morphology after acid treatment or iron oxide coating, implying minimal damage to the tube structure. It is quite evident from Figure 4.1b that in the case of Fe-MWCNT, the surface was heavily coated with iron oxide.

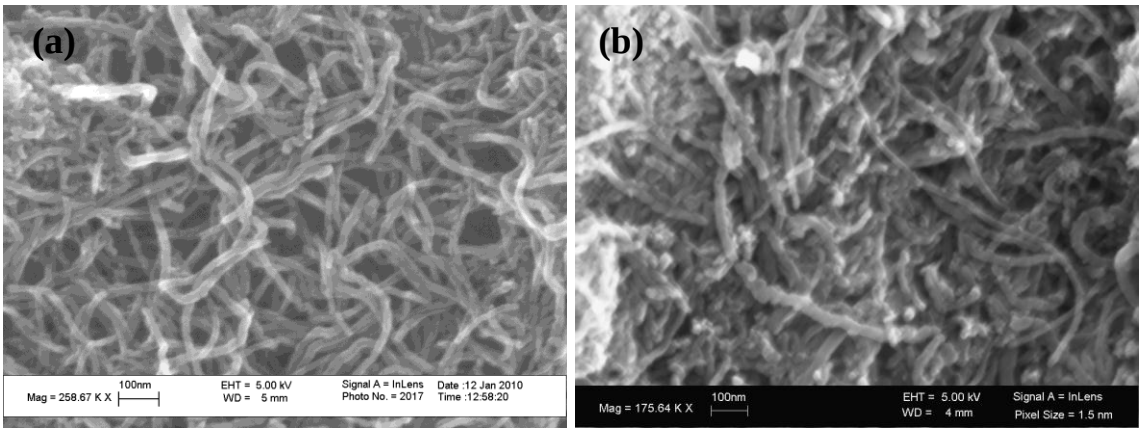

Figure 4.1 SEM Image of (a) acid functionalized MWCNT, (b) the Fe-MWCNT Composite.

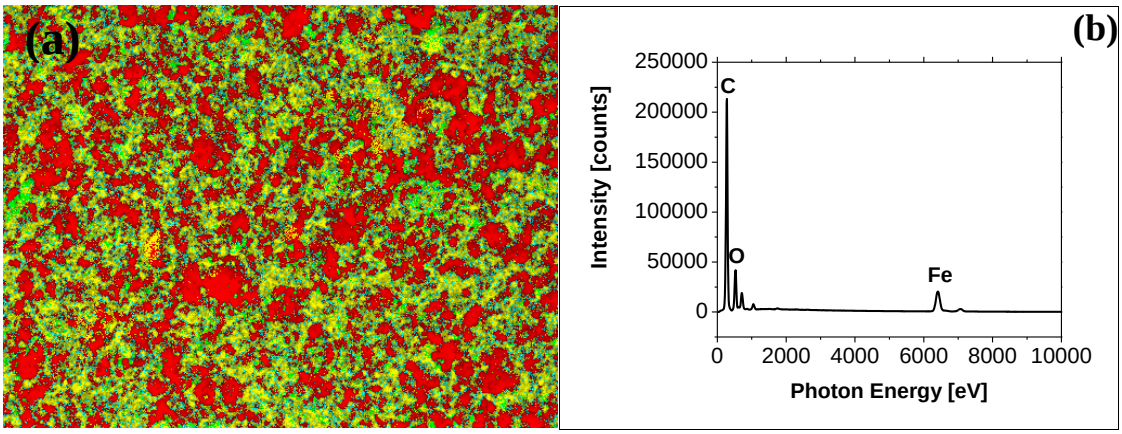

Figure 4.2 EDS (a) map(red – carbon, green – oxygen, and yellow – iron, (b) spectra [carbon (C), oxygen (O), and iron (Fe)].

The EDS data shown in Figure 4.2 also confirmed the presence of relatively large amounts of iron oxide on the surface of the carbon nanotubes. TGA was used to quantify the iron oxide loading in the MWCNT as shown in Figure 4.3. The resulting weight above 600 °C was attributed to the weight of residual metal or metal oxide. The Fe-MWCNT hybrid was found to contain as much as 40 % (by weight) of iron implying an approximate atomic ratio between Fe and carbon of 11:100. The catalytic activity of the iron is evident from the TGA data, where it altered the thermal stability of the MWCNT. The Fe-MWCNT hybrid degraded at a significantly lower temperature (by nearly 200 °C) compared to the original carbon nanotubes, because the iron catalyzed its oxidation, consistent with previous observation (Brukh and Mitra, 2007).

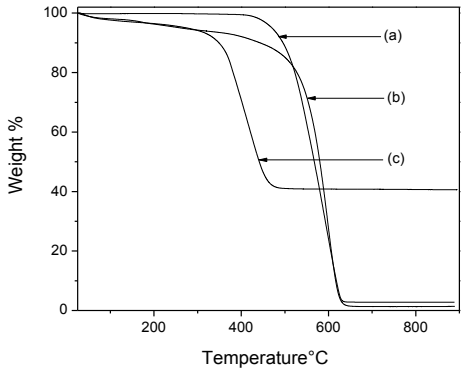

Figure 4.3 TGA data for (a) MWCNT, (b) f-MWCNT, and (c) Fe-MWCNT.

The FTIR spectrum (Figure 4.4) confirmed the presence of functional groups in MWCNT, f-MWCNT and the Fe-MWCNT hybrid. The carboxylic stretching frequency in f-MCWNT occurred at 1715 cm^{-1} (C=O) and 1218 cm^{-1} (C – O). The stretching (O – H) vibration occurred at 3424 cm^{-1} in the f-MWCNT spectrum (Figure 4.4b) which is clearly absent from the MWCNT spectrum (Figure 4.4a). In the Fe-MWCNT spectrum, the characteristic peaks at 1715 cm^{-1}, 1218 cm^{-1} and 1400 cm^{-1} belonging to the C=O, C–O and O–H vibrations of carboxylic acid disappear. This may be due to the binding of iron oxide onto the oxidized MWCNTs surface. Based on the disappearance of the C–O and O–H peaks, it is evident that the iron oxide particles are anchored to the MWCNTs by an ester-like bond (Yan and Lian, 2005). In all the samples, the peak around 1576 cm^{-1} was assigned to the C=C stretching of the carbon skeleton. The appearance of two new bands at (636 and 565) cm^{-1} in Figure 4.4c confirmed the formation of the Fe-O bonds.

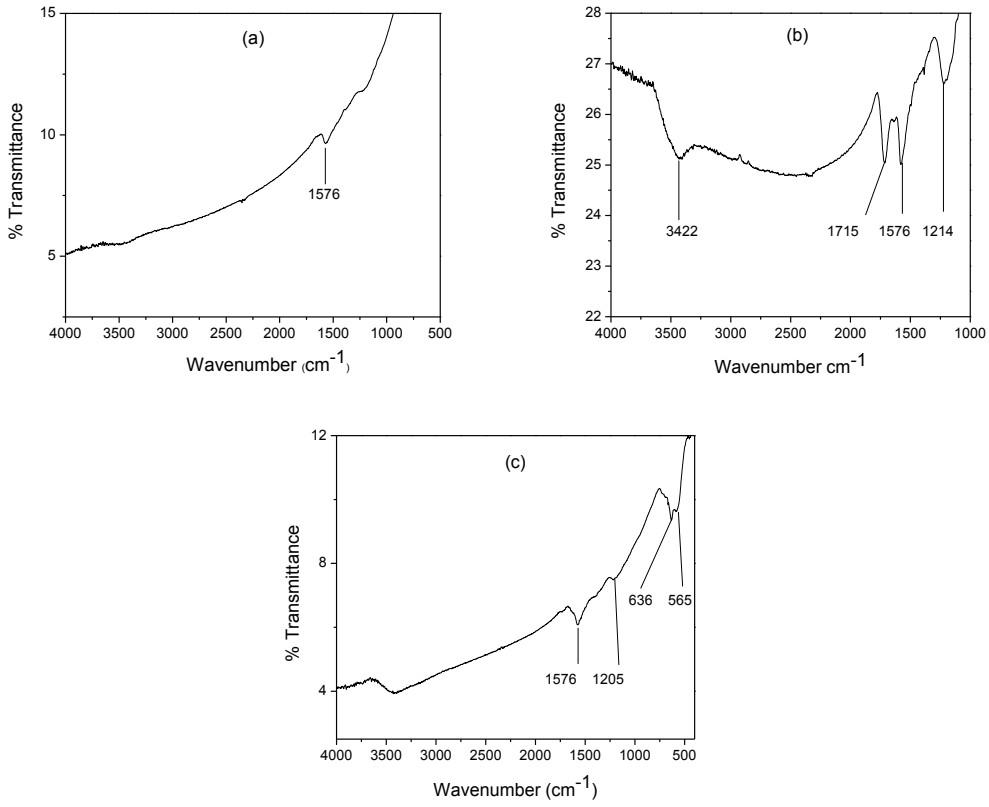

Figure 4.4 FTIR spectra of (a) MWCNT, (b) f-MWCNT, and (c) Fe-MWCNT.

4.3.2 Arsenic Removal and its Kinetics

The arsenic removal capacity of Fe-MWCNT was compared to those of the original multiwall carbon nanotubes (MWCNT) and functionalized multiwall carbon nanotubes (f-MWCNT). The adsorption capacity for arsenic shown by Fe-MWCNT for both As(III) and As(V) (1723 µg g^{-1} and 189 µg g^{-1}, respectively) was much higher than the values obtained for MWCNT (10 µg g^{-1} and 23 µg g^{-1}, respectively) and f-MWCNT (3 µg g^{-1} and 9 µg g^{-1}, respectively). The adsorption capacity for As(III) and As(V) using Fe-MWCNT was also found to be higher than that for iron coated sand (Thirunavukkarasu et al., 2003, Gupta et al., 2005), ferrihydrite, and hardened paste of Portland cement (Kundu

et al., 2004). It was higher than the values reported for iron oxide-coated biomass (Pokhrel and Viraraghavan, 2008) but less than those shown by activated carbon and activated alumina, mostly due to the fact that the initial concentrations of arsenic in these studies were as high as 100 mg L^{-1}.

Oxyanionic arsenic species such as arsenate and arsenite adsorb at the iron oxyhydroxide surface by forming complexes with the surface sites (Edwards, 1994). This assertion is supported by the poor adsorption capacities obtained from analysis with MWCNT and f-MCWNT. As(V) and As(III) showed different sorption behavior as can be seen from the isothermal and kinetic data. This difference in their sorption characteristics may be due to their ionic forms at a pH of 4. In the pH range studied, As(V) existed in the anionic form $H_2AsO_4^-$, whereas As(III) is partially ionized below pH 9.22, existed in the molecular form (H_3AsO_3). This may account for the better adsorption of As(V) compared to As(III). Anionic arsenic species ($H_2AsO_3^-$, $H_2AsO_4^-$) are reported to be adsorbed with the positively charged iron oxide-coated adsorbents through electrostatic attraction. There are also reports of the surface potential of iron loaded adsorbents becoming less negative with increasing iron loading (Huang and Vane, 1989). It was therefore, postulate that arsenic removal with Fe-MWCNT may occur via multiple mechanisms. Negatively charged arsenic species may adsorb onto positively charged sites on the adsorbent surface resulting in their removal from water.

When the iron oxide was exposed to water, metal ions on the oxide surface completed their coordination shells with OH groups (Kingston et al., 1972), which either bound to or released H^+ ions depending on the pH, and in the process developed a surface charge. The adsorption properties of oxides are due to the existence of these OH_2^+, OH

and O^- functional groups (Sposito, 1984). Arsenic may be removed by ligand exchange with OH and OH_2^+ functional groups on the surface forming an inner-sphere complex. An incompletely dissociated acid $H_2AsO_4^-$ is required to provide a proton for complexation with the OH group to form H_2O and providing space for anion adsorption (Kingston et al., 1972). Therefore, arsenic species may be removed through complexation with oxyhydroxide sites on the adsorbent surface according to equations 4.1 and 4.2 (Pokhrel and Viraraghavan, 2008).

$$\alpha\text{-FeOOH} + H_2AsO_4^- + 3H^+ \rightarrow FeH_2AsO_4 + 2H_2O \quad (4.1)$$

$$\alpha\text{-FeOOH} + H_3AsO_3 + 2H^+ \rightarrow FeH_2AsO_3 + 2H_2O \quad (4.2)$$

The kinetics of arsenic uptake was investigated by the Lagergren (Lagergren, 1898) and Ho and McKay (Ho and McKay, 1999) kinetic models. Lagergren models the rate of adsorption of pollutants on an adsorbent after a pseudo-first order equation:

$$\frac{dq_t}{dt} = k_1(q_e - q_t) \quad (4.3)$$

where q_e and q_t are the sorption capacity (μg g^{-1}) of the adsorbent at equilibrium and at time t (h), respectively and k_1 is the pseudo-first order sorption rate constant (h^{-1}). Ho and McKay proposed a pseudo-second order equation of the form:

$$\frac{dq_t}{dt} = k_2(q_e - q_t)^2 \quad (4.4)$$

where k_2 is the pseudo-second order sorption rate constant (g h μg^{-1}) and t is time (h).

Figure 4.5a shows the residual As(III) and As(V) concentrations versus time at pH 4. After 10 minutes of contacting the adsorbent with 100 μg L^{-1} arsenic solution, 96 % of As(V) was removed, whereas only 45 % of As(III) was removed. 99 % of As(V) and 80 % of As(III) were removed after 30 minutes of contact. Ho and McKay's pseudo-second kinetic equation was a better fit for adsorption of both As(III) and As(V) than the Lagergren's pseudo-first order equation. The pseudo-second order kinetic parameters for As(III) and As(V) removal are presented in Table 1. The R^2 values for both As (III) and As (V) were close to unity implying that their adsorption can best be described by the pseudo-second order kinetic model with chemisorption being the rate limiting step. This means that the adsorption rate is proportional to the amount of adsorbent and the square of the number of free sites. The latter corresponds to the term $(q_e - q_t)^2$ in the pseudo second order model.

Table 4.1 Pseudo-second Order Kinetic Parameters for As(III) and As(V) Adsorption

	q_e (μg g^{-1})	k_2 (g $(\min \mu g)^{-1}$)	h (μg $(g \min)^{-1}$)	R^2
As(III)	97.09	$7.8 * 10^{-4}$	7.353	0.9999
As(V)	103.84	$7.4 * 10^{-3}$	79.79	0.9992

The rate of As(V) removal was faster than that of As(III) as shown by the pseudo-second order kinetic parameters in Table 4.1. Faster adsorption of arsenate than arsenite has also been attributed to the smaller radius of the arsenate ion [(4.0 to 4.2) Å] compared with that of the arsenite ion (4.8 Å) (Kim et al., 2004).

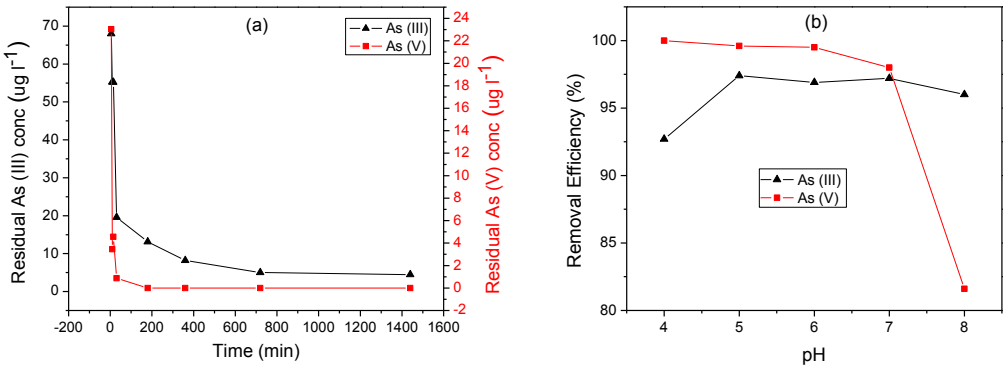

Figure 4.5 (a) Residual Arsenic concentration as a function of time, (b) effect of pH on As(III) and As(V) adsorption.

The optimum pH for As(V) removal was determined to be 4, the equilibrium adsorption q_e (μg g^{-1}) of As(V) was found to decrease slightly from pH 4 through 8 as presented in Figure 4(b). On the contrary the equilibrium adsorption of As(III) was found to increase slightly from pH 4 to pH 6 and remained constant from pH 6 to pH 8 (Figure 4.5b). As(III) is dominant in the form of neutral species (H_3AsO_3) below pH 9.22, accounting for the relatively constant As(III) adsorption. A reduced removal of As(V) at pH 8 may be because OH^- ion becomes dominant at alkaline pH and this ion competes with arsenic species [$H_2AsO_4^-$]. The pH range studied here was within what is normally encountered in water resources.

4.3.3 Adsorption Isotherms for As(III) and As(V) Removal

The capacity of arsenic removal by the adsorbent was evaluated with the Langmuir (Langmuir, 1916) and Freundlich (Freundlich, 1906) isotherms. The linear form of the Langmuir adsorption isotherm is presented in equation 4.5:

$$\frac{1}{q_e} = \frac{1}{q_m} + \frac{1}{bq_mC_e} \quad (4.5)$$

where q_m (μg/g) is the maximum sorption capacity for monolayer coverage of the adsorbent, C_e (μg/L) is the equilibrium concentration of arsenic and the Langmuir constant b (L/μg) is indirectly related to the enthalpy of adsorption. The linearized form of the Freundlich isotherm involves a plot of log q_e and log C_e with n and log k_f being the slope and y-intercept, respectively.

$$\log q_e = \log k_f + \mathrm{n}\log \mathrm{C_e} \quad (4.6)$$

The Freundlich constants k_f and $1/n$ measure the adsorption capacity and intensity, respectively. The bond energy increases proportionally with surface density for $n<1$ and vice a versa for n>1.

The Langmuir isotherm parameters presented in Table 4.2 indicate a high maximum sorption capacity for monolayer adsorption (q_m) for the adsorbent in the removal of As(III). The adsorption of As(III) and As(V) fit both the Langmuir and Freundlich equations; however, the coefficient of determination (R^2) value for the Freundlich model in both instances were higher than that of the Langmuir equation. Hence the Freundlich isotherm model effectively explained the removal of As(III) and As(V) by the adsorbent with coefficient of determination (R^2) values of 0.9907 and 0.9997, respectively.

Table 4.2. Adsorption Isotherm Parameters for the Removal of As(III) and As(V) by Fe-MWCNT

	Langmuir			Freundlich		
	q_m (µg g^{-1})	b (L μg^{-1})	R^2	k_f (L μg^{-1})	n	R^2
As(III)	1723	0.013	0.9899	21.89	1.181	0.9907
As(V)	189	0.373	0.9900	50.83	1.946	0.9997

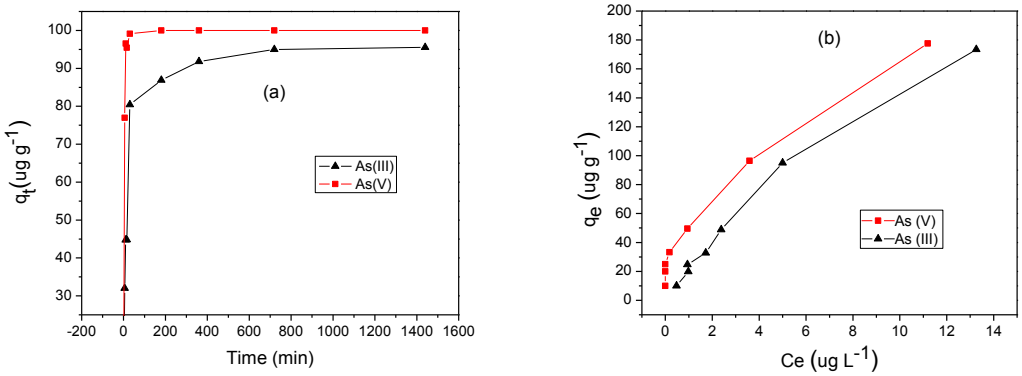

Figure 4.6 (a) Kinetic and (b) equilibrium data at pH 4 for As(III) and As(V) adsorption by Fe-MWCNT.

The Freundlich constants log k_f and n were obtained from the y-intercept and slope, respectively. The constants k_f (mg g^{-1}) and $1/n$ provide a measure of adsorption capacity and intensity, respectively are presented in Table 4.2. The bond energy increases proportionally with surface density for $n<1$ and vice a versa for n>1 (Freundlich, 1906). The adsorption capacity for the adsorbent in As(V) removal was much higher than As(III) as was the intensity. The Freundlich isotherm model effectively explained the removal of As(V) by the adsorbent with a coefficient of determination of 0.9995. The value of the constant 1/n (0 – 1) is also indicative of the heterogeneity of the adsorbent

surface, with 1/n closer to 0 implying a heterogeneous surface. The kinetic and equilibrium data at pH 4 for As(III) and As(V) adsorption are shown in Figure 4.6.

4.3.4 Effect of Temperature on Arsenic Removal

The effect of temperature on arsenic removal efficiency was investigated at pH 4, 1 g L^{-1} adsorbent dose, 180 rpm agitation, and 1 hr and 12 hrs equilibration time for As(V) and As(III), respectively. The temperature was varied from 28°C to 40°C. It was found that Arsenic removal efficiency was fairly constant over the temperature range. A plot of arsenic removal versus temperature is presented in Figure 4.7. A study using Fe^{3+}-impregnated granular activated carbon (GAC) reported a decrease in arsenic As(III) and As(V) removal efficiency with increasing temperature from (30 to 60) °C (Mondal et al., 2007) but the decrease did not seem substantial.

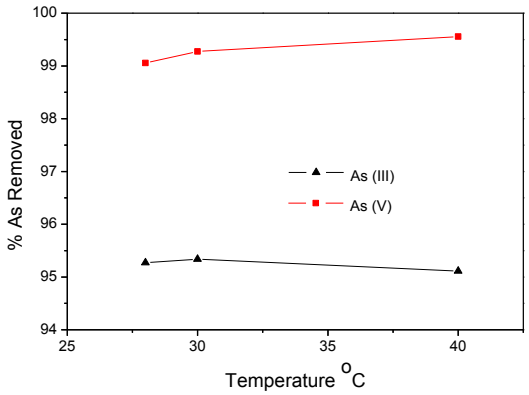

Figure 4.7 Arsenic removal efficiency as a function of temperature**.**

4.4 Conclusions

The iron oxide-multi-walled carbon nanotube (Fe-MWCNT) hybrid was effective as a sorbent material for arsenic removal from water. Controlled assembly of iron oxide was possible and the MWCNT served as an effective support for the oxide. The kinetics of As(III) and As(V) removal was explained by the pseudo-second order rate equation and their adsorption by the Langmuir and Freundlich models. It is conceivable that MWCNT with appropriate surface modification can provide a platform for developing potentially useful environmental remediation tools.

CHAPTER 5

ADSORPTION OF ARSENIC ON MULTIWALL CARBON NANOTUBE–ZIRCONIA NANOHYBRID FOR POTENTIAL DRINKING WATER PURIFICATION

Zirconium oxides/hydroxides have been extensively investigated as adsorbents for the removal of cationic and anionic pollutants from water. They have been shown to be effective in the removal of dyes, fluoride, uranium (IV), phosphate, mercury, and selenium (Zheng et al., 2009). While iron oxides represent some of the most common sorbents for As removal (Mohan and Pittman Jr, 2007, Liu et al., 2012), the potential for using zirconium based compounds is also being investigated. Preliminary investigations using zirconium loaded materials such as activated charcoal, porous resin, chelating resin with lysine-Na and orange waste, have shown promising results for As removal (Zheng et al., 2009). In general, for use as an environmental adsorbent, zirconium needs to be impregnated or loaded on a support because it has poor physical properties and moreover this also lowers the overall cost of this expensive material. Therefore, the development of effective support materials is of utmost importance.

Effective arsenic removal with iron oxide coated MWCNT has been previously reported as discussed in Chapter 4 (Mishra and Ramaprabhu, 2010, Addo Ntim and Mitra, 2011). Here the iron oxides were protonated forming OH_2^+ groups on the adsorbent surface at low pH values, and the arsenic species were removed by covalent ligand exchange. Zirconia coated multiwall carbon nanotubes synthesized in our laboratory have shown excellent efficiency for fluoride removal from water with sorption capacity significantly higher than other conventional sorbents (Ramamurthy et al., 2011).

It is anticipated that Zirconium oxide supported on MWCNT may remove arsenic species through a synergistic combination of chemisorption and physisorption.

The objective here was to study the adsorption capacity of a MWCNT–Zirconia nanohybrid in the removal of arsenite and arsenate from water to meet drinking water standards.

5.1 Synthesis and Characterization of MWCNT-ZrO_2

The MWCNT was functionalized in a Microwave Accelerated Reaction System (Mode: CEM Mars) fitted with internal temperature and pressure controls according to an experimental procedures detailed in Section 4.1. This product (f-MWCNT) was used in the subsequent synthesis of the MWCNT-ZrO_2 composite.

The MWCNT-ZrO_2 hybrid was synthesized by dispersing a weighed amount of the f-MWCNT in 0.008M $ZrOCl_2$ (Anand et al., 2011). The reaction was carried out in a Microwave Accelerated Reaction System (Mode: CEM Mars) fitted with internal temperature and pressure controls at 150 ^oC for 1 hr. The product was vacuum filtered through a 10 μm membrane filter paper and thoroughly washed with DI water until all the unreacted $ZrOCl_2 \cdot 8H_2O$ was removed. The resultant product was dried in a vacuum oven at 80 ^oC for 12 hrs.

The MWCNT-ZrO_2 was characterized using a scanning electron microscope (SEM) fitted with an Energy Dispersive X-ray spectrometer (EDS), Thermogravimetric analysis (TGA), X-ray diffraction (XRD), Fourier Transform Infrared spectroscopy (FTIR) and BET surface area. SEM Data was collected on a LEO 1530 VP Scanning Electron Microscopy equipped with an energy-dispersive X-ray analyzer, which was used

in collecting EDS data. TGA was performed using a Pyris 1 TGA from Perkin-Elmer Inc from 30 °C to 900 °C under a flow of air at 10 mL min^{-1}, at a heating rate of 10 °C per min. X-ray diffraction (XRD) was performed on a Philips X'Pert PW3040-MPD (Netherlands) diffractometer using Cu Kα radiation (λ = 1.5406 Å) at 25 °C. FTIR measurements were carried out in purified KBr pellets using a Perkin-Elmer (Spectrum One) instrument. Specific surface area, micropore volume, and average pore radius were measured using Quantachrome NOVA 3000 series (Model N32-11) High Speed Gas Sorption Analyzer at 77.40 K. Before each experiment, the samples were heated at 200°C and degassed at this temperature until constant vacuum for four hours. pH of Point of Zero Charge (pHpzc) was determined based on a previously published procedure (Chen et al., 2007a).

5.2 Adsorption Studies

Stock and working solutions of As (III) and As (V) were prepared according to procedures detailed in Section 4.2 of Chapter 4. 10 ml of 100µg l^{-1} arsenic solution [As (III) and As (V)] was contacted with 0.01 g of the adsorbent in a series of conical flasks at pHs ranging between 5 and 8, and samples were collected at 5, 10, 15, 30, and 45 min 1, 3, 6, 12, 15 and 24 h for kinetic studies. Equilibrium contact time and pH were determined to be 6 h and pH 6, respectively. The mass of the adsorbent was varied from 0.01 to 0.1 g in the isothermal adsorption studies at pH 6 for 6 hours. The arsenic solutions and the adsorbents were mixed thoroughly at a speed of 175 rpm on a platform

shaker, (Labsystems Wellmix). The mixture was filtered through a 0.45μm membrane syringe filter.

Residual Arsenic was measured using Agilent 7500 ICP-MS. All standards were prepared from multi-element solution 2A, 10 mg/L (Spex Certiprep) with addition of internal standard mix (Li6, Ge, Y, In, Tb, Bi). Buffer solution was used for all dilutions. Multi-element instrument calibration standard 1, 20 mg/L (Spex Certiprep) was used for the verification of calibration.

5.2.1 Effects of Competing Anions

To determine the effects of co-existing anions on arsenic adsorption, three types of oxyanions (CO_3^{2-}, SO_4^{2-} and NO_3^-) were evaluated individually. The experiments were conducted at 25 °C and pH 6.0 with initial Arsenic concentration of 100 μg L^{-1}. Concentration of the oxyanions was controlled at three levels (0.1, 1 and 5 mM).

5.3 Results and Discussion

5.3.1 Characterization of Adsorbent

The BET surface area of MWCNT, f-MWCNT and the MWCNT-ZrO_2 hybrid were 110 m^2g^{-1}, 162 m^2g^{-1} and 152 m^2g^{-1}, respectively. BET surface area increased significantly after acid treatment as the value for f-MWCNT was an approximate 40 % higher than that of original MWCNT. This increase may be due to defects on the surface of f-MWCNT as a result of the acid treatment. BET surface area of the MWCNT-ZrO_2 hybrid was however, not significantly different from f-MWCNT. Zirconia has a relatively small surface area which slightly decreased the surface area of the hybrid. The acid

functionalization of the carbon nanotubes produced carboxylic groups on the surface enhancing zirconia loading. The pH at zero point charge (pH_{ZPC}) for MWCNT, f-MWCNT and the MWCNT-ZrO_2 hybrid were 6.8, 3.91 and 9.6, respectively. This is the point where the surface charge of the carbon nanotube is independent of the electrolyte concentration. Therefore, it is evident that the carboxylic groups on the f-MWCNT had been replaced in the MWCNT-ZrO_2 hybrid.

SEM images of f-MWCNT and the MWCNT-ZrO_2 hybrid are shown in Figure 5.1(a, b). The original MWCNTs had diameters in the range of 20-40 nm and the length was about 10-30 μm. There was no detectable change in tube morphology after acid treatment or zirconia loading, implying minimal damage to the tube structure. It is quite evident from Figure 5.1b that the CNT surface was coated with zirconia.

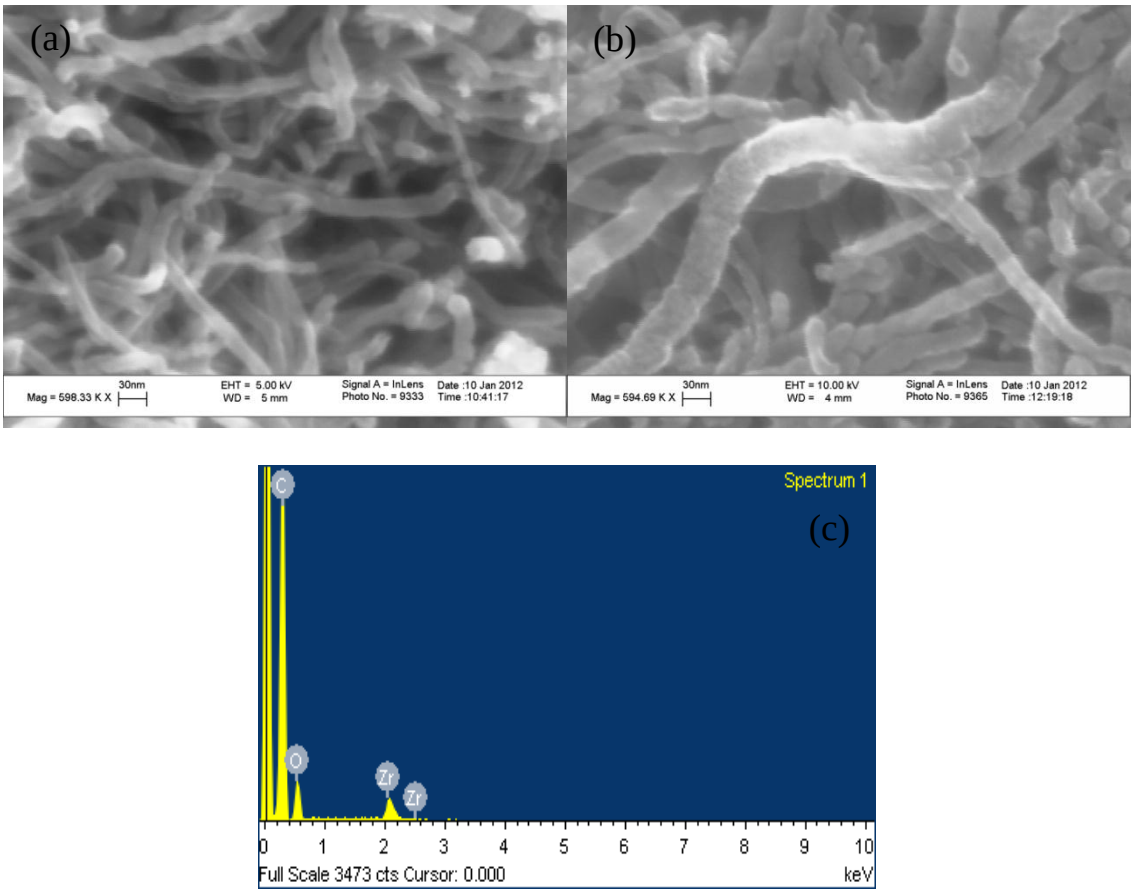

Figure 5.1 SEM Images of (a) carboxylated MWCNT, (b) the MWCNT- ZrO_2 Composite, (c) EDS spectra of the MWCNT-ZrO_2 Composite.

The EDS data shown in Figure 5.1c confirmed the presence of zirconia on the surface of the CNTs. TGA was used to quantify the zirconia loading in the MWCNT as shown in Figure 5.2. The resulting weight above 600 °C was attributed to the weight of residual metal or metal oxide. The MWCNT-ZrO_2 hybrid was found to contain 4.85 % zirconia.

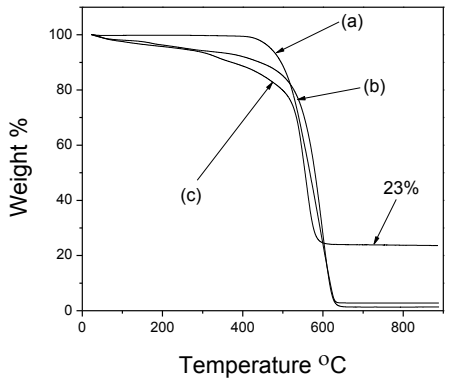

Figure 5.2 TGA data for (a) MWCNT, (b) f-MWCNT, and (c) MWCNT-ZrO_2.

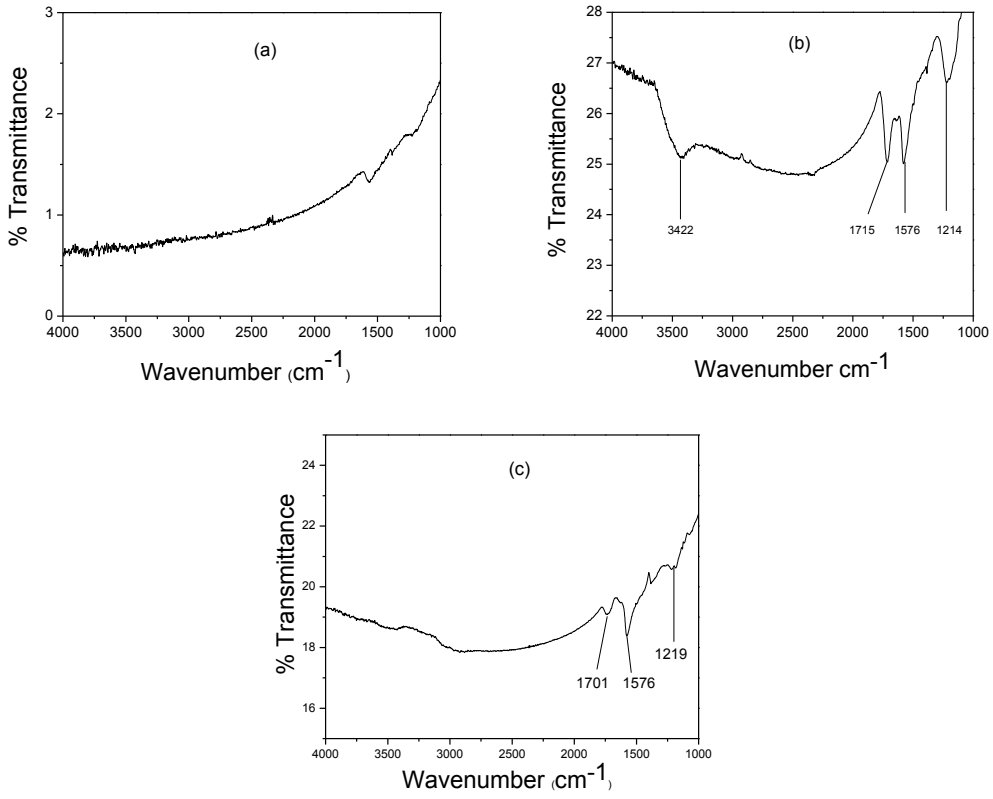

Figure 5.3 FTIR data for (a) MWCNT, (b) f-MWCNT, and (c) MWCNT-ZrO_2.

The FTIR spectrum (Figure 5.3) confirmed the presence of functional groups in MWCNT, f-MWCNT, and MWCNT-ZrO_2. The carboxylic stretching frequency in f-MCWNT occurred at 1715 cm^{-1} (C=O) and 1221cm^{-1} (C–O). The stretching (O–H)

vibration occurred at 3424 cm^{-1} in the f-MWCNT spectrum (Figure 5.3b) which was clearly absent from the MWCNT spectrum (Figure 5.3a). In all the samples, the peak around 1576 cm^{-1} was assigned to the C=C stretching of the carbon skeleton. From the MWCNT-ZrO_2 (Figure 5.3c) spectrum, it can be seen that the characteristic peaks of the carboxyl groups of the MWCNTs shifted from 1715 to 1701 cm^{-1} and the relative intensity decreased significantly. The peak at 3440cm^{-1} belonging to the O–H vibration of carboxylic acid also disappeared. The disappearance of the peak of O–H vibration of carboxylic acid was attributed to the fact that ZrO_2 is anchored to the MWCNTs through an esterification process forming C–O–Zr bonds, in line with previous observations (Yan and Lian, 2005).

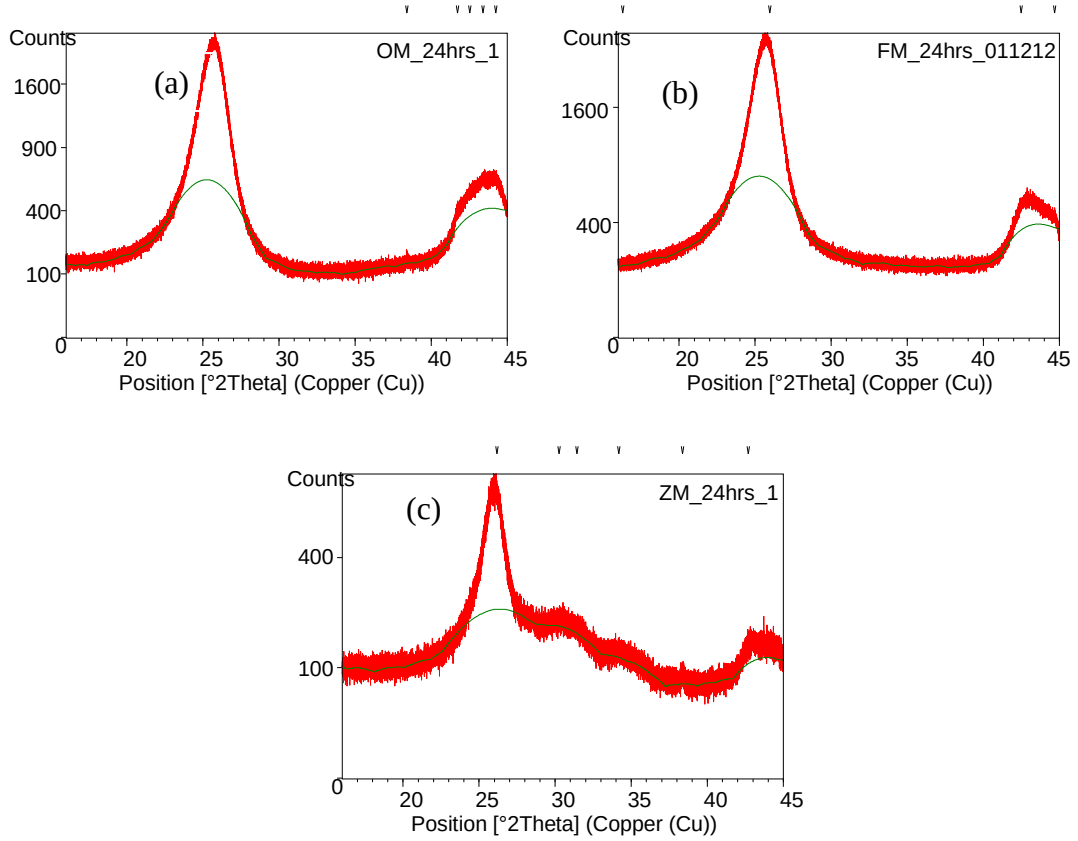

Figure 5.4 X-ray powder diffraction patterns of (a) MWCNT (b) f-MWCNT, (c) MWCNT- ZrO_2 hybrid.

Figure 5.4 shows the x-ray powder diffraction pattern of MWCNT, f-MWCNT and the MWCNT-ZrO_2 hybrid. The peak around 30.2° in 2θ in the XRD pattern of the MWCNT-ZrO_2 hybrid (Figure 5.4c) indicated the presence of zirconia (Yan and Lian, 2005) which was clearly absent from the diffraction patterns of MWCNT and f-MWWNT [Figure 5.4(a and b)]. The intense peak around 26° in 2θ in all the XRD patterns was due to the MWCNT.

5.3.2 Arsenic Removal by MWCNT-ZrO_2

It was found that no arsenic was adsorbed on the MWCNT and the carboxylated MWCNT; however, the MWCNT-ZrO_2 hybrid was effective in removing arsenic from water. It occurred through a synergistic combination of chemisorption and physisorption processes on the Zr immobilized on the MWCNT backbone. Schmidt et al. (2008) have reported the surface speciation for Zirconium and arsenate adsorption using the GRFIT model, determining that they formed two surface complexes represented by equations 5.1 and 5.2, with reaction 5.1 being practically negligible (Schmidt et al., 2008).

$$ZrOH + H_3AsO_4 \leftrightarrow ZrOAsO_2(OH)^- + H^+, \log K = -2.5, \quad (5.1)$$

$$ZrOH + H_3AsO_4 \leftrightarrow ZrOAsO_3^{2-} + 2H^+, \log K = 1.4. \quad (5.2)$$

Ion exchange and non-covalent H-bonding interactions may also play a role in the arsenic removal process (Ramamurthy et al., 2011). This was somewhat different from the iron oxide coated MWCNTs where the former protonated forming OH_2^+ groups on

the adsorbent surface at low pH values, and the arsenic species were removed by covalent ligand exchange with OH and OH_2^+ functional groups (Addo Ntim and Mitra, 2011).

The kinetics of As uptake was investigated by the Lagergren (Lagergren, 1898) and Ho and McKay (Ho and McKay, 2000) kinetic models. These kinetic models are represented in Chapter 4 by equations 4.3 and 4.4, respectively. Figure 5(a) shows As(III) and As(V) removal efficiencies as a function of time at the different pH values. After 10 mins of contact with the adsorbent over 50% of As (V) was removed as compared to 17% of As (III). 99% of As(V) and 92% of As(III) were removed after 60 minutes of contact. Relative to MWCNT-ZrO_2 nearly twice the amount of both As(III) and As(V) were removed in the presence of Fe-MWCNT (Addo Ntim and Mitra, 2011) after 10 mins of contact, with (80-99)% removed after only 30mins of contact. The kinetics of As(III) and As(V) adsorption using the MWCNT-ZrO_2 was relatively slower compared to that observed with iron oxide coated MWCNT (Addo Ntim and Mitra, 2011).

Ho and Mckay's pseudo-second kinetic equation was a better fit than the Lagergren's pseudo-first order equation for adsorption of both oxidation states of arsenic on MWCNT-ZrO_2. The pseudo-second order kinetic parameters at the pH range studied are presented in Table 5.1. The R^2 values for both As (III) and As (V) were close to unity implying that their adsorption can best be described by the pseudo-second order kinetic model with chemisorption being the rate limiting step. This means that the adsorption rate is proportional to the amount of adsorbent and the square of the number of free sites. The latter corresponds to the term $(q_e - q_t)^2$ in the pseudo second order model.

Table 5.1 Pseudo-second Order Kinetic Parameters for As(III) and As(V) Adsorption

	As (III)				As (V)			
pH	q_e (µg g^{-1})	k_2 (g (min µg)$^{-1}$)	h (µg (g min)$^{-1}$)	R^2	q_e (µg g^{-1})	k_2 (g (min µg)$^{-1}$)	h (µg (g min)$^{-1}$)	R^2
5	95.4	2.5E-04	2.3	0.9987	101.1	1.0E-03	10.5	0.9999
6	98.6	3.1E-04	3.0	0.9993	100.5	1.3E-03	13.6	1.0000
7	95.4	4.1E-04	3.7	0.9997	101.1	1.7E-03	16.9	1.0000
8	97.5	3.6E-04	3.4	0.9999	101.7	7.0E-04	7.2	0.9999

The rate of As(V) removal was an order of magnitude faster than that of As(III) as shown by the pseudo-second order kinetic parameters in Table 5.,1 as was the removal efficiency (Figure 5.5). This was similar to what was observed for arsenic adsorption on Fe-MWCNT. The higher removal rate of As(V) relative to As(III) may be due to the rate-limiting oxidation of As(III) to As(V) catalyzed by surficial carbon compounds preceding the adsorption reaction (Schmidt et al., 2008).

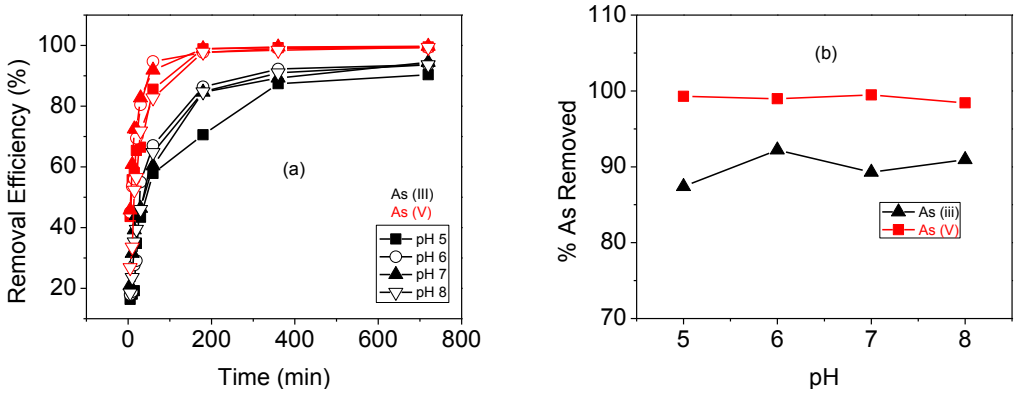

Figure 5.5 (a) Arsenic removal efficiency as a function of time, (b) Effect of pH on As(III) and As(V) adsorption.

The optimum pH for As(V) removal was determined to be 6. The equilibrium adsorption q_e (μg g^{-1}) of both As(V) and As(III) was found to be fairly constant over the pH range studied as presented in Figure 5.5(b). This was contrary to As(V) removal on Fe-MWCNT, where q_e was observed to decrease with increasing pH due to interference from dominant OH^- ions at basic pH. As(III) is dominant in the form of neutral species (H_3AsO_3) below pH 9.22, accounting for the relatively constant As(III) adsorption in both instances. This implies that unlike Fe-MWCNT, MWCNT-ZrO_2 has the advantage of effective arsenic removal over a wide range of pH.

5.3.3 Adsorption Isotherms for As(III) and As(V) Removal

The capacity of arsenic removal by the adsorbent was evaluated with the Langmuir (Langmuir, 1916), and Freundlich (Freundlich, 1906) isotherms, represented in Chapter 4 by equations 4.5 and 4.6, respectively. From the Langmuir isotherm parameters presented in Table 5.2, the maximum sorption capacity for monolayer adsorption (q_m) for the adsorbent in the removal of As(V) was much higher than that of As(III). The adsorption capacity, estimated by the Langmuir isotherm model was 2000µg g^{-1} and 5000µg g^{-1} for As(III) and As(V), respectively. These values were significantly higher than the q_m values obtained with Fe-MWCNT (Addo Ntim and Mitra, 2011). The Langmuir constant, b, the ratio of the adsorption rate constant to the desorption rate constant, is an indication of the affinity of the sorbent material toward arsenic (Patnukao et al., 2008). The Langmuir b values for arsenic sorption by MWCNT-ZrO_2, presented in Table 5.2 were approximately an order of magnitude lower than those observed for Fe-MWCNT (Addo Ntim and Mitra, 2011) in the presence of both As(III) and As(V), indicating a higher affinity of Fe-MWCNT for arsenic. This also implies that the rate of desorption of adsorbed arsenic species during sorbent regeneration will be higher in the case of MWCNT-ZrO_2.

The adsorption of As(III) and As(V) fit both the Langmuir and Freundlich equations with correlation coefficient R^2 values close to unity, as was observed with Fe-MWCNT (Addo Ntim and Mitra, 2011). The applicability of the two isotherms to the arsenic sorption shows that both monolayer sorption and heterogeneous energetic distribution of active sites on the surface of the sorbent are possible.

Table 5.2 Adsorption Isotherm Parameters for the Removal of As(III) and As(V) by MWCNT- ZrO_2

	Langmuir			Freundlich		
	q_m (µg g^{-1})	b (L µg^{-1})	R^2	k_f (L µg^{-1})	n	R^2
As(III)	2000	0.0049	1.0000	9.9	1.0204	0.9999
As(V)	5000	0.038	0.8801	274.09	1.2048	0.9916

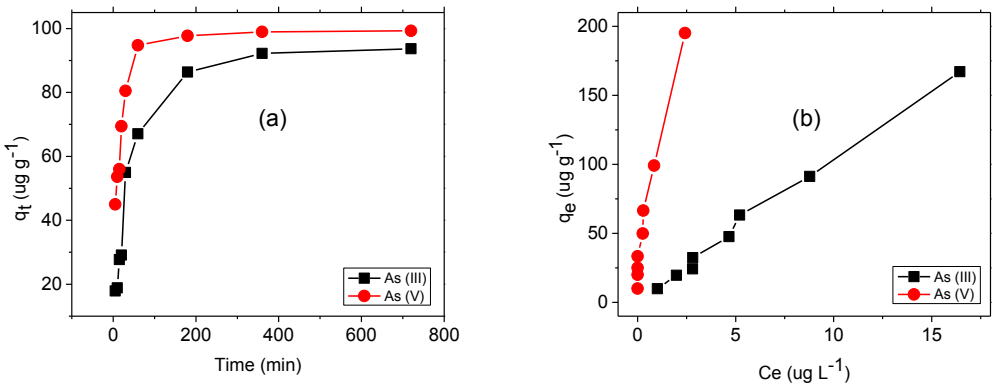

Figure 5.6 (a) Kinetic, and (b) Equilibrium data at pH 6 for As(III) and As(V) adsorption by MWCNT-ZrO_2.

The Freundlich constants k_f and n were obtained from the y-intercept and slope, respectively. The constants k_f (L µg^{-1}) and 1/n providing a measure of adsorption capacity and intensity, respectively are presented in Table 5.2. The bond energy increases proportionally with surface density for n<1 and vice a versa for n>1 (Freundlich, 1906). The adsorption capacity for the adsorbent in As(V) removal was much higher than As(III) as was the intensity. The value of the constant 1/n (0 – 1) is indicative of the heterogeneity of the adsorbent surface, with 1/n closer to 0 implying heterogeneous surface. The values the freundlich isotherm parameter 1/n for arsenic adsorption on MWCNT-ZrO_2 were less than 1 for both As(III) and As(V) as was observed for the

adsorption on Fe-MWCNT, indicating favorable adsorption on both sorbents (Patnukao et al. 2008). However, the values were closer to zero in the case of Fe-MWCNT than MWCNT-ZrO_2, implying a more favorable process in the presence of the iron coated MWCNTs. This was consistent with the values of Langmuir constant b observed. The kinetic and kquilibrium data at pH 6 for As(III) and As(V) adsorption are shown in Figure 5.6.

5.3.4 Effect of Competing Anions

Sulfates, carbonates and nitrates are ionic components often present in many surface and subsurface aquatic systems, and have been reported to exert varied levels of influence on the adsorption of both arsenate and arsenite depending on pH and concentration of anions. In this study, the presence of these anions had negligible effects on the removal of As(V) over the concentration range investigated (0.1 mM – 5 mM), as presented in Figure 5.7. Contrary to the above observation, the removal efficiency of As(III) decreased to various degrees in the presence of these anions. While the decrease in As(III) removal efficiency was not statistically significant in the presence of carbonate ions, sulfate and nitrate ions showed a statistically significant effect. This was contrary to what has been observed in literature for iron-modified sorbents, where the presence of sulfate and carbonate had negligible effects on the removal of both As(III) and As(V) at various pHs and ionic strengths (Jain and Loeppert, 2000, Meng et al., 2000, Su and Puls, 2001). An increase in anion concentration from 1 mM to 5 mM did not result in a corresponding larger decrease in removal efficiency, indicating the saturation of sites

accessible to the anions. The results suggest that the binding affinity of these anions for zirconia was weaker than As(V), but comparable to that of As(III).

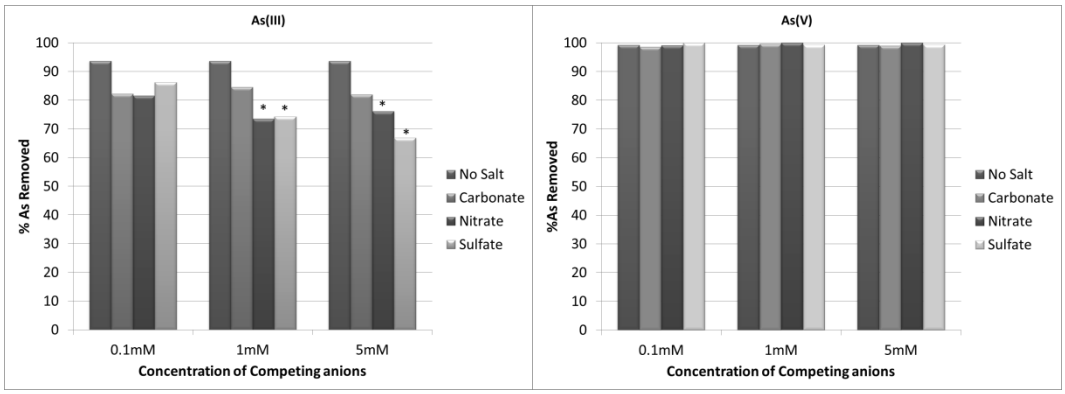

Figure 5.7 Effects of oxyanions on Arsenic removal by MWCNT-ZrO_2 after 24 h at pH 6 and 25 °C for initial Arsenic concentration of 100 µg/L. (* difference significant at 95% confidence level).

5.4 Conclusions

The MWCNT-ZrO_2 was effective as a sorbent material for arsenic removal from drinking water. A major advantage of this material is that the sorption capacity was independent of pH over the range studied. The kinetics of As (III) and As (V) removal was explained by the pseudo-second order rate equation and their adsorption by Langmuir and Freundlich models. Although the rate of Arsenic removal by MWCNT-ZrO_2 was two to three times slower than that for iron coated MWCNTs, the adsorption capacity was nearly two to five times higher. While the removal efficiency of As(V) was not affected by the presence of competing anions, As(III) removal was reduced by the presence of sulfate and nitrate ions.

CHAPTER 6

REGENERATION OF THE MWCNT-METAL OXIDE NANOHYBRIDS AFTER ARSENIC REMOVAL

Adsorptive removal of arsenic has proven to be one of the most reliable and somewhat less expensive methods and therefore, several sorbent materials have been tested for their arsenic sorption capacity. One of the main issues raised with adsorption is the cyclability of the sorbent material which will reduce the cost of removal and the generation of toxic waste. It is therefore, imperative to develop specially designed, tailor-made adsorbents for selective removal of arsenic from drinking water especially addressing the issue of regeneration.

Once the sorbent becomes exhausted, the metals must be recovered and the sorbent regenerated. Desorption and sorbent regeneration is a critical consideration and contributor to process costs and metal(s) recovery in a concentrated form. A successful desorption process must restore the sorbent close to its initial properties for effective reuse. Desorption can be improved by gaining insight into the metal sorption mechanism. Most of the arsenic sorption studies in the literature do not discuss desorption or regeneration of the spent sorbent. The few studies in literature discussing arsenic desorption to regenerate the exhausted sorbent have used eluents, such as sodium hydroxide (NaOH)(Cumbal et al., 2003, Guo and Chen, 2005, Kundu and Gupta, 2006), hydrogen peroxide (H_2O_2) and strong acids (HNO_3) (Manju et al., 1998, Say et al., 2003), with NaOH being the most commonly used. Selection of eluent depends on the arsenic adsorption mechanism and nature of the adsorbent.

The effective removal of both As(III) and As(V) using metal oxide coated carbon nanotubes has recently been reported (Addo Ntim and Mitra, 2011, Addo Ntim and Mitra, 2012). Iron oxide coated MWCNT was observed to remove arsenic species by covalent ligand exchange where hydroxyl groups on the iron oxide (protonated to form OH_2^+ groups on the adsorbent surface at low pH values) were exchanged for negatively charged arsenic species (Addo Ntim and Mitra, 2011). Zirconia coated MWCNT nanohybrid (MWCNT-ZrO_2) was observed to remove arsenic through a synergistic combination of chemisorption and physisorption processes on the ZrO_2 immobilized on the MWCNT backbone, with Ion exchange and non-covalent H-bonding interactions playing a minor role in the arsenic removal process (Addo Ntim and Mitra, 2012).

The objective of this Chapter was to determine the optimal conditions for sorbent regeneration using NaOH by varying pH, concentration of base, volume of base, and duration of contact. The arsenic sorption capacity of the regenerated sorbent was also investigated.

6.1 Adsorption Studies

10 ml of 1 mg L^{-1} arsenic solution [As (III) and As (V)] was contacted with 0.04 g of the adsorbent in a series of conical flasks at pH 6. The arsenic solutions and the adsorbents were mixed thoroughly at a speed of 175 rpm on a platform shaker, (Labsystems Wellmix). The mixture was filtered through a 0.45μm membrane syringe filter after 24 hrs of contact. The sorbent material was isolated, washed with DI water to remove any residual arsenic and dried for regeneration studies.

Residual arsenic was measured using Agilent 7500 ICP-MS. All standards were prepared from multi-element solution 2A, 10mg/L (Spex Certiprep) with addition of internal standard mix (Li6, Ge, Y, In, Tb, Bi). Buffer solution was used for all dilutions. Multi-element instrument calibration standard 1, 20 mg/L (Spex Certiprep) was used for the verification of calibration.

6.2 Desorption Studies

The dried sorbent materials from the adsorption studies were investigated for their regenerative ability. To investigate the effect of pH, aqueous solutions of HCl and NaOH with pH ranging from 4 to 13 was used to desorb the adsorbed arsenic. Typically, 10 mL of the solutions were contacted with 0.04 g of the adsorbent for a period of 24 hrs. The mixture was then filtered using a 0.45μm membrane syringe filter and the filtrate was analyzed for the presence of As.

NaOH concentration was varied between (0.001 – 0.5) M to determine the effect of concentration on arsenic desorption after 24 hrs of contact. Effect of contact time was investigated by varying the time of contact between the sorbent and NaOH at pH 13 from (5 – 1440) mins. The effect of 0.1 M $NaHCO_3$ solution was compared with that of 0.1 M NaOH solution for the arsenic desorption efficiency by contacting 10 mL of their aqueous solutions at 0.1 M concentration with 0.04 g of the sorbent over a period of 24 hrs.

The arsenic sorption capacity of the regenerated nanohybrids was investigated by contacting 10 ml of 0.1 mg L^{-1} arsenic solution [As (III) and As (V)] at pH 6 with 0.01 g

of the regenerated sorbent. The mass of the adsorbent was varied from 0.001 to 0.1 g in the isothermal adsorption studies at pH 6 for 6 hours.

6.3 Results and Discussion

6.3.1 Desorption Kinetics

The reduced sorption capacities of As(III) and As(V) on CNT-metal oxide nanohybrid at alkaline pH is indicative of the fact that adsorbed arsenic species can be desorbed from the loaded sorbent material. Therefore, desorption studies were performed using NaOH. Experimental desorption data was fitted to both the Lagergren and Ho and Mckay kinetics models presented in Chapter 4 as equations 4.3 and 4.4, respectively (Ho and McKay, 2000, Lagergren, 1898). Figure 6.1 shows the As(III) and As(V) desorption efficiencies as a function of time in NaOH at pH 13. Desorption efficiency was observed to increase with increasing time of contact to an equilibrium after 6 hrs. The kinetics of As desorption was similar for both MWCNT-ZrO_2 and Fe-MWCNT, where As(V) was desorbed to a higher efficiency than As(III). Ho and McKay's pseudo-second kinetic equation was a better fit for desorption of both As(III) and As(V) than the Lagergren's pseudo-first order equation. The pseudo-second order kinetic parameters for As(III) and As(V) desorption are presented in Table 6.1. The R^2 values for both As (III) and As (V) were close to unity, implying that their desorption can best be described by the pseudo-second order kinetic model.

Table 6.1 Pseudo-second Order Kinetic Parameters of Arsenic Desorption

		q_e (µg g^{-1})	k_2 (g (min µg)$^{-1}$)	h (µg (g min)$^{-1}$)	R^2
Fe-MWCNT	As(III)	730	6.95E-06	3.70	0.9867
	As(V)	855	3.07E-05	22.42	0.9988
MWCNT-ZrO_2	As(III)	826	4.61E-06	3.15	0.9895
	As(V)	746	7.32E-05	40.77	0.9995

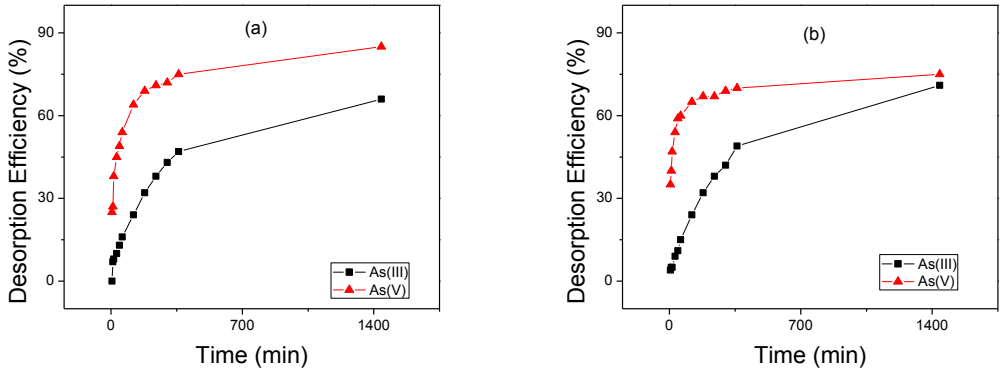

Figure 6.1 Kinetics of arsenic desorption by (a) Fe-MWCNT and (b) MWCNT-ZrO_2.

The optimum pH for As(V) desorption was determined to be 13. Desorption efficiency increased with increasing pH for both sorbent materials as presented in Figure 6.2. The apparent insensitivity of arsenic adsorption on MWCNT-ZrO_2 to pH changes ranging from 4 to 8 (Addo Ntim and Mitra, 2012) was evident in the low desorption efficiency between pH 4 and 10. The desorption efficiencies observed for Fe-MWCNT also agreed well with the effect of pH on its arsenic adsorption capacity (Addo Ntim and Mitra, 2011).

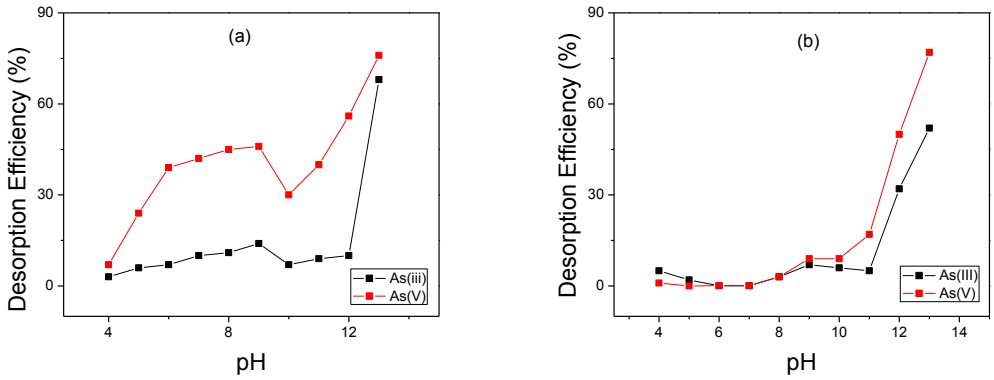

Figure 6.2 Effect of initial pH of desorption medium on the efficiency of arsenic desorption from (a) Fe-MWCNT and (b) MWCNT-ZrO_2.

The results indicate that the mechanism of arsenic adsorption proceeds by the arsenic species being removed from aqueous phase through ligand exchange with OH^- and OH_2^+ groups formed on the nanohybrid surface on contact with water. Desorption, on the other hand, involves the attack of OH^- ions on the metal-oxygen bond of the metal-arsenate/arsenite complex leading the release of arsenic species into the liquid phase. Therefore, an increase in OH^- ion concentration is expected to cause a corresponding increase in arsenic desorption efficiency. Data presented in Figure 6.3 show an increase in desorption efficiency with increasing NaOH concentration to a 0.1 M equilibrium after which an increase in NaOH concentration did not cause any increase in efficiency. This concentration was thus noted as the effective NaOH concentration for arsenic desorption for both nanohybrid sorbent materials.

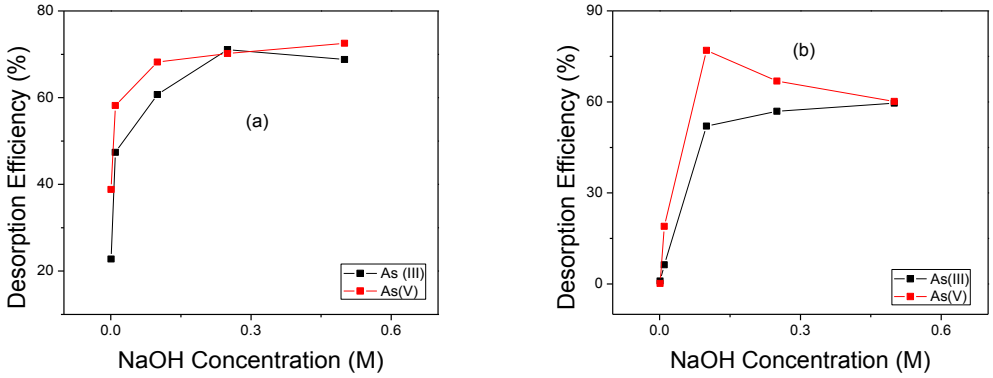

Figure 6.3 Effect of NaOH concentration on arsenic desorption from (a) Fe-MWCNT and (b) MWCNT-ZrO_2.

6.3.2 Adsorption Efficiency of the Regenerated Sorbent

The adsorption efficiency of the used Fe-MWCNT for As(III) and As(V) was observed to reduce after the sorbent material was regenerated by 10% and 8%, respectively. The adsorption efficiency for MWCNT-ZrO_2 was reduced to a much greater extent, approximately 25% and 16% for As(III) and As(V), respectively. The reduction in sorption capacity was attributed to loss of iron oxide or zirconia from the nanohybrid during regeneration.

6.4 Conclusions

Batch desorption analysis of arsenic species loaded onto CNT-metal oxide nanohybrid sorbents indicated that the effective NaOH concentration required for arsenic desorption was 0.1 M with an optimal pH of 13. The kinetics of arsenic desorption followed the pseudo-second order kinetic model with desorption efficiencies up to 85%. Fe-MWCNT was observed to show higher desorption efficiency than MWCNT-ZrO_2. The adsorption efficiency of the recycled material was slightly reduced with Fe-MWCNT showing better

regeneration ability than MWCNT-ZrO_2. This shows that the CNT-metal oxide nanohybrids have the capacity to remove arsenic from water with the potential for cyclable use.

REFERENCES

ADDO NTIM, S. & MITRA, S. 2011. Removal of Trace Arsenic to Meet Drinking Water Standards Using Iron Oxide Coated Multiwall Carbon Nanotubes. *J Chem Eng Data,* 56**,** 2077-2083.

ADDO NTIM, S. & MITRA, S. 2012. Adsorption of Arsenic on Multiwall Carbon Nanotube–Zirconia Nanohybrid for Potential Drinking Water Purification. *J Colloid Interface Sci,* 375**,** 154-159.

ADDO NTIM, S., SAE-KHOW, O., WITZMANN, F. A. & MITRA, S. 2011. Effects of Polymer Wrapping and Covalent Functionalization on the Stability of MWCNT in Aqueous Dispersions. *J Colloid Interface Sci,* 355**,** 383-388.

AITCHISON, T. J., GINIC-MARKOVIC, M., MATISONS, J. G., SIMON, G. P. & FREDERICKS, P. M. 2007. Purification, Cutting, and Sidewall Functionalization of Multiwalled Carbon Nanotubes Using Potassium Permanganate Solutions. *J Phys Chem C,* 111**,** 2440-2446.

ANAND, B., ADDO NTIM, S., SAI MUTHUKUMAR, V., SIVA SANKARA SAI, S., PHILIP, R. & MITRA, S. 2011. Improved Optical Limiting in Dispersible Carbon Nanotubes and Their Metal Oxide Hybrids. *Carbon,* 49**,** 4767-4773.

BISHNOI, N. R., BAJAJ, M., SHARMA, N. & GUPTA, A. 2004. Adsorption of Cr(Vi) on Activated Rice Husk Carbon and Activated Alumina. *Bioresource Technol,* 91**,** 305-307.

BRUKH, R. & MITRA, S. 2007. Kinetics of Carbon Nanotube Oxidation. *J Mater Chem,* 17**,** 619-623.

BUFFLE, J., WILKINSON, K. J., STOLL, S., FILELLA, M. & ZHANG, J. 1998. A Generalized Description of Aquatic Colloidal Interactions: The Three-Colloidal Component Approach. *Environ Sci Technol,* 32**,** 2887-2899.

CHATTERJEE, A., DAS, D., MANDAL, B. K., CHOWDHURY, T. R., SAMANTA, G. & CHAKRABORTI, D. 1995. Arsenic in Ground Water in Six Districts of West Bengal, India: The Biggest Arsenic Calamity in the World. Part I. Arsenic Species in Drinking Water and Urine of the Affected People. *Analyst,* 120**,** 643-650.

CHEN, K. L. & ELIMELECH, M. 2007. Influence of Humic Acid on the Aggregation Kinetics of Fullerene (C60) Nanoparticles in Monovalent and Divalent Electrolyte Solutions. *J Colloid Interface Sci,* 309**,** 126-134.

CHEN, R. J., BANGSARUNTIP, S., DROUVALAKIS, K. A., WONG SHI KAM, N., SHIM, M., LI, Y., KIM, W., UTZ, P. J. & DAI, H. 2003. Noncovalent Functionalization of Carbon Nanotubes for Highly Specific Electronic Biosensors. *P Natl Acad Sci,* 100**,** 4984-4989.

CHEN, R. J., ZHANG, Y., WANG, D. & DAI, H. 2001. Noncovalent Sidewall Functionalization of Single-Walled Carbon Nanotubes for Protein Immobilization. *J Am Chem Soc,* 123**,** 3838-3839.

CHEN, W., PARETTE, R., ZOU, J., CANNON, F. S. & DEMPSEY, B. A. 2007a. Arsenic Removal by Iron-Modified Activated Carbon. *Wat Res,* 41**,** 1851-1858.

CHEN, Y., IQBAL, Z. & MITRA, S. 2007b. Microwave-Induced Controlled Purification of Single-Walled Carbon Nanotubes without Sidewall Functionalization. *Adv Funct Mater,* 17**,** 3946-3951.

CHEN, Y. & MITRA, S. 2008. Fast Microwave-Assisted Purification, Functionalization and Dispersion of Multi-Walled Carbon Nanotubes. *J Nanosci Nanotechnol,* 8**,** 5770-5775.

CHIANG, I. W., BRINSON, B. E., SMALLEY, R. E., MARGRAVE, J. L. & HAUGE, R. H. 2001. Purification and Characterization of Single-Wall Carbon Nanotubes. *J Phys Chem B,* 105**,** 1157-1161.

CHIODARELLI, N., RICHARD, O., BENDER, H., HEYNS, M., DE GENDT, S., GROESENEKEN, G. & VEREECKEN, P. M. 2012. Correlation between Number of Walls and Diameter in Multiwall Carbon Nanotubes Grown by Chemical Vapor Deposition. *Carbon,* 50**,** 1748-1752.

COLEMAN, K. S., BAILEY, S. R., FOGDEN, S. & GREEN, M. L. H. 2003. Functionalization of Single-Walled Carbon Nanotubes Via the Bingel Reaction. *J Am Chem Soc,* 125**,** 8722-8723.

CROWDER, T. M., ROSATI, J. A., SCHROETER, J. D., HICKEY, A. J. & MARTONEN, T. B. 2002. Fundamental Effects of Particle Morphology on Lung Delivery: Predictions of Stokes' Law and the Particular Relevance to Dry Powder Inhaler Formulation and Development. *Pharmaceutical Research,* 19**,** 239-245.

CUMBAL, L., GREENLEAF, J., LEUN, D. & SENGUPTA, A. K. 2003. Polymer Supported Inorganic Nanoparticles: Characterization and Environmental Applications. *React Funct Polym,* 54**,** 167-180.

DĄBROWSKI, A., HUBICKI, Z., PODKOŚCIELNY, P. & ROBENS, E. 2004. Selective Removal of the Heavy Metal Ions from Waters and Industrial Wastewaters by Ion-Exchange Method. *Chemosphere,* 56**,** 91-106.

DANIEL, S., RAO, T. P., RAO, K. S., RANI, S. U., NAIDU, G. R. K., LEE, H. Y. & KAWAI, T. 2007. A Review of DNA Functionalized/Grafted Carbon Nanotubes and Their Characterization. *Sensor Actuat B-Chem,* 122**,** 672-682.

DERJAGUIN, B. & LANDAU, L. 1993. Theory of the Stability of Strongly Charged Lyophobic Sols and of the Adhesion of Strongly Charged Particles in Solutions of Electrolytes. *Prog Surf Sci,* 43**,** 30-59.

DESAI, C., ADDO NTIM, S. & MITRA, S. 2012. Antisolvent Precipitation of Hydrophobic Functionalized Multiwall Carbon Nanotubes in an Aqueous Environment. *J Colloid Interface Sci,* 368**,** 115-120.

EDWARDS, M. 1994. Chemistry of Arsenic Removal During Coagulation and Fe-Mn Oxidation. *J Am Water Works Ass,* 86**,** 64-78.

ELIMELECH, M., GREGORY, J., JIA, X. & WILLIAMS, R. 1995. *Particle Deposition and Aggregation: Measurement, Modelling and Simulation,* Oxford United Kingdom, Butterworth-Heinemann.

ELIZALDE-GONZÁLEZ, M. P., MATTUSCH, J., EINICKE, W. D. & WENNRICH, R. 2001. Sorption on Natural Solids for Arsenic Removal. *Chem Eng J,* 81**,** 187-195.

ESUMI, K., ISHIGAMI, M., NAKAJIMA, A., SAWADA, K. & HONDA, H. 1996. Chemical Treatment of Carbon Nanotubes. *Carbon,* 34**,** 279-281.

FREUNDLICH, H. M. F. 1906. Over the Adsorption in Solution. *Z. Phys. Chem., Stoechiom. Verwandtschaftsl.,* 57A**,** 385-471.

GEORGAKILAS, V., KORDATOS, K., PRATO, M., GULDI, D. M., HOLZINGER, M. & HIRSCH, A. 2002. Organic Functionalization of Carbon Nanotubes. *J Am Chem Soc,* 124**,** 760-761.

GIRIFALCO, L. A., HODAK, M. & LEE, R. S. 2000. Carbon Nanotubes, Buckyballs, Ropes, and a Universal Graphitic Potential. *Phys Rev B,* 62**,** 13104-13110.

GÜNER, A. & ATAMAN, M. 1994. Effects of Inorganic Salts on the Properties of Aqueous Poly(Vinylpyrrolidone) Solutions. *Colloid Polym Sci,* 272**,** 175-180.

GUO, X. & CHEN, F. 2005. Removal of Arsenic by Bead Cellulose Loaded with Iron Oxyhydroxide from Groundwater. *Environ Sci Technol,* 39**,** 6808-6818.

GUPTA, V. K., SAINI, V. K. & JAIN, N. 2005. Adsorption of as(Iii) from Aqueous Solutions by Iron Oxide-Coated Sand. *J Colloid Interface Sci,* 288**,** 55-60.

HEIDMANN, I., CHRISTL, I. & KRETZSCHMAR, R. 2004. Aggregation Kinetics of Kaolinite−Fulvic Acid Colloids as Affected by the Sorption of Cu and Pb. *Environ Sci Technol,* 39**,** 807-813.

HEISTER, E., LAMPRECHT, C., NEVES, V., TILMACIU, C., DATAS, L., FLAHAUT, E., SOULA, B., HINTERDORFER, P., COLEY, H. M., SILVA, S. R. & MCFADDEN, J. 2010. Higher Dispersion Efficacy of Functionalized Carbon Nanotubes in Chemical and Biological Environments. *ACS Nano,* 4**,** 2615-2626.

HIRSCH, A. & VOSTROWSKY, O. 2005. Functionalization of Carbon Nanotubes Functional Molecular Nanostructures. *In:* SCHLÜTER, A. D. (ed.). Germany: Springer Berlin / Heidelberg.

HO, Y. S. & MCKAY, G. 1999. The Sorption of Lead(II) Ions on Peat. *Wat Res,* 33**,** 578-584.

HO, Y. S. & MCKAY, G. 2000. The Kinetics of Sorption of Divalent Metal Ions onto Sphagnum Moss Peat. *Wat Res,* 34**,** 735-742.

HU, C., LIAO, H., LI, F., XIANG, J., LI, W., DUO, S. & LI, M. 2008. Noncovalent Functionalization of Multi-Walled Carbon Nanotubes with Siloxane Polyether Copolymer. *Mater Lett,* 62**,** 2585-2588.

HU, H., YU, A., KIM, E., ZHAO, B., ITKIS, M. E., BEKYAROVA, E. & HADDON, R. C. 2005. Influence of the Zeta Potential on the Dispersability and Purification of Single-Walled Carbon Nanotubes. *J Phys Chem B,* 109**,** 11520-11524.

HUANG, C. P. & VANE, L. M. 1989. Enhancing As^{5+} Removal by a Fe^{2+}-Treated Activated Carbon. *J Water Pollut Control Fed,* 61**,** 1596–1603.

HUANG, W., TAYLOR, S., FU, K., LIN, Y., ZHANG, D., HANKS, T. W., RAO, A. M. & SUN, Y.-P. 2002. Attaching Proteins to Carbon Nanotubes Via Diimide-Activated Amidation. *Nano Lett,* 2**,** 311-314.

HYLTON, K., CHEN, Y. & MITRA, S. 2008. Carbon Nanotube Mediated Microscale Membrane Extraction. *J Chromatogr A,* 1211**,** 43-48.

HYUNG, H., FORTNER, J. D., HUGHES, J. B. & KIM, J. H. 2007. Natural Organic Matter Stabilizes Carbon Nanotubes in the Aqueous Phase. *Environ Sci Technol,* 41**,** 179-184.

HYUNG, H. & KIM, J. H. 2008. Natural Organic Matter (NOM) Adsorption to Multi-Walled Carbon Nanotubes: Effect of NOM Characteristics and Water Quality Parameters. *Environ Sci Technol,* 42**,** 4416-4421.

IIJIMA, S. 1991. Helical Microtubules of Graphitic Carbon. *Nature,* 354**,** 56-58.

IIJIMA, S. 2002. Carbon Nanotubes: Past, Present, and Future. *Physica B,* 323**,** 1-5.

ISLAM, M. F., ROJAS, E., BERGEY, D. M., JOHNSON, A. T. & YODH, A. G. 2003. High Weight Fraction Surfactant Solubilization of Single-Wall Carbon Nanotubes in Water. *Nano Lett,* 3**,** 269-273.

ISRAELACHVILI, J. N. 2010. *Intermolecular and Surface Forces,* London, Academic Press.

JAIN, A. & LOEPPERT, R. H. 2000. Effect of Competing Anions on the Adsorption of Arsenate and Arsenite by Ferrihydrite. *J Environ Qual,* 29**,** 1422-1430.

JAVEY, A., GUO, J., PAULSSON, M., WANG, Q., MANN, D., LUNDSTROM, M. & DAI, H. 2004. High-Field Quasiballistic Transport in Short Carbon Nanotubes. *Phys Rev Lett,* 92**,** 106804.

JIA, G., WANG, H., YAN, L., WANG, X., PEI, R., YAN, T., ZHAO, Y. & GUO, X. 2005. Cytotoxicity of Carbon Nanomaterials: Single-Wall Nanotube, Multi-Wall Nanotube, and Fullerene. *Environ Sci Technol,* 39**,** 1378-1383.

JIANG, L., GAO, L. & SUN, J. 2003. Production of Aqueous Colloidal Dispersions of Carbon Nanotubes. *J Colloid Interface Sci,* 260**,** 89-94.

JUNG, D.-H., KOAN KO, Y. & JUNG, H.-T. 2004. Aggregation Behavior of Chemically Attached Poly(Ethylene Glycol) to Single-Walled Carbon Nanotubes (SWNTs) Ropes. *Mat Sci Eng C-Biomim,* 24**,** 117-121.

KARAJANAGI, S. S., VERTEGEL, A. A., KANE, R. S. & DORDICK, J. S. 2004. Structure and Function of Enzymes Adsorbed onto Single-Walled Carbon Nanotubes. *Langmuir,* 20**,** 11594-11599.

KARLSSON, H. L., GUSTAFSSON, J., CRONHOLM, P. & MÖLLER, L. 2009. Size-Dependent Toxicity of Metal Oxide Particles—A Comparison between Nano- and Micrometer Size. *Toxicol Lett,* 188**,** 112-118.

KARWA, M., IQBAL, Z. & MITRA, S. 2006. Scaled-up Self-Assembly of Carbon Nanotubes inside Long Stainless Steel Tubing. *Carbon,* 44**,** 1235-1242.

KHARISOV, B. I., KHARISSOVA, O. V., LEIJA GUTIERREZ, H. & ORTIZ MÉNDEZ, U. 2008. Recent Advances on the Soluble Carbon Nanotubes. *Ind Eng Chem Res,* 48**,** 572-590.

KIM, J., LEE, K., LEE, Y., CHO, H., KIM, K., CHOI, K., LEE, S., SONG, K., KANG, C. & YU, I. 2011a. Aspect Ratio Has No Effect on Genotoxicity of Multi-Wall Carbon Nanotubes. *Arch Toxicol,* 85**,** 775-786.

KIM, J., SONG, K., LEE, J. & YU, I. 2011b. Evaluation of Biocompatible Dispersants for Carbon Nanotube Toxicity Tests. *Arch Toxicol,* 85**,** 1499-1508.

KIM, Y., KIM, C., CHOI, I., RENGARAJ, S. & YI, J. 2004. Arsenic Removal Using Mesoporous Alumina Prepared Via a Templating Method. *Environ Sci Technol,* 38**,** 924-931.

KINGSTON, F. J., POSNER, A. M. & QUIRK, J. P. 1972. Anion Adsorption by Goethite and Gibbsite. *J Soil Sci,* 23**,** 177-192.

KNOWLES, F. C. & BENSON, A. A. 1983. The Biochemistry of Arsenic. *Trends Biochem Sci,* 8**,** 178-180.

KONG, J., FRANKLIN, N. R., ZHOU, C., CHAPLINE, M. G., PENG, S., CHO, K. & DAI, H. 2000. Nanotube Molecular Wires as Chemical Sensors. *Science,* 287**,** 622-625.

KUNDU, S. & GUPTA, A. K. 2006. Arsenic Adsorption onto Iron Oxide-Coated Cement (Iocc): Regression Analysis of Equilibrium Data with Several Isotherm Models and Their Optimization. *Chem Eng J,* 122**,** 93-106.

KUNDU, S., KAVALAKATT, S. S., PAL, A., GHOSH, S. K., MANDAL, M. & PAL, T. 2004. Removal of Arsenic Using Hardened Paste of Portland Cement: Batch Adsorption and Column Study. *Wat Res,* 38**,** 3780-3790.

LAGERGREN, S. 1898. About the Theory of So-Called Adsorption of Soluble Substances. *Kungliga Svenska Vetenskapsakademiens Handlingar,* 24**,** 1-39.

LAM, C.-W., JAMES, J. T., MCCLUSKEY, R. & HUNTER, R. L. 2004. Pulmonary Toxicity of Single-Wall Carbon Nanotubes in Mice 7 and 90 Days after Intratracheal Instillation. *Toxicol Sci,* 77**,** 126-134.

LANGMUIR, I. 1916. The Constitution and Fundamental Properties of Solids and Liquids. Part I. Solids. *J Am Chem Soc,* 38**,** 2221-2295.

LEE, K. M., LI, L. & DAI, L. 2005. Asymmetric End-Functionalization of Multi-Walled Carbon Nanotubes. *J Am Chem Soc,* 127**,** 4122-4123.

LI, H., ZHOU, B., LIN, Y., GU, L., WANG, W., FERNANDO, K. A., KUMAR, S., ALLARD, L. F. & SUN, Y. P. 2004. Selective Interactions of Porphyrins with Semiconducting Single-Walled Carbon Nanotubes. *J Am Chem Soc,* 126**,** 1014-1015.

LIN, D. & XING, B. 2008. Tannic Acid Adsorption and Its Role for Stabilizing Carbon Nanotube Suspensions. *Environ Sci Technol,* 42**,** 5917-5923.

LIN, Y., ZHOU, B., SHIRAL FERNANDO, K. A., LIU, P., ALLARD, L. F. & SUN, Y.-P. 2003. Polymeric Carbon Nanocomposites from Carbon Nanotubes Functionalized with Matrix Polymer. *Macromolecules,* 36**,** 7199-7204.

LISUNOVA, M. O., LEBOVKA, N. I., MELEZHYK, O. V. & BOIKO, Y. P. 2006. Stability of the Aqueous Suspensions of Nanotubes in the Presence of Nonionic Surfactant. *J Colloid Interface Sci,* 299**,** 740-746.

LIU, F., ZHANG, X., CHENG, J., TU, J., KONG, F., HUANG, W. & CHEN, C. 2003. Preparation of Short Carbon Nanotubes by Mechanical Ball Milling and Their Hydrogen Adsorption Behavior. *Carbon,* 41**,** 2527-2532.

LIU, X., AO, H., XIONG, X., XIAO, J. & LIU, J. 2012. Arsenic Removal from Water by Iron-Modified Bamboo Charcoal. *Water Air Soil Poll,* 223**,** 1033-1044.

LIU, Z., CHEN, K., DAVIS, C., SHERLOCK, S., CAO, Q., CHEN, X. & DAI, H. 2008. Drug Delivery with Carbon Nanotubes for in Vivo Cancer Treatment. *Cancer Res,* 68**,** 6652-6660.

LIU, Z., SUN, X., NAKAYAMA-RATCHFORD, N. & DAI, H. 2007. Supramolecular Chemistry on Water-Soluble Carbon Nanotubes for Drug Loading and Delivery. *ACS Nano,* 1**,** 50-56.

MANIVANNAN, S., JEONG, I. O., RYU, J. H., LEE, C. S., KIM, K. S., JANG, J. & PARK, K. C. 2009. Dispersion of Single-Walled Carbon Nanotubes in Aqueous and Organic Solvents through a Polymer Wrapping Functionalization. *J Mater Sci-Mater El,* 20**,** 223-229.

MANJU, G. N., RAJI, C. & ANIRUDHAN, T. S. 1998. Evaluation of Coconut Husk Carbon for the Removal of Arsenic from Water. *Wat Res,* 32**,** 3062-3070.

MENG, X., BANG, S. & KORFIATIS, G. P. 2000. Effects of Silicate, Sulfate, and Carbonate on Arsenic Removal by Ferric Chloride. *Wat Res,* 34**,** 1255-1261.

MERCER, R. R., SCABILLONI, J., WANG, L., KISIN, E., MURRAY, A. R., SCHWEGLER-BERRY, D., SHVEDOVA, A. A. & CASTRANOVA, V. 2008. Alteration of Deposition Pattern and Pulmonary Response as a Result of Improved Dispersion of Aspirated Single-Walled Carbon Nanotubes in a Mouse Model. *Am J Physiol-Lung C,* 294**,** L87-L97.

MICKELSON, E. T., CHIANG, I. W., ZIMMERMAN, J. L., BOUL, P. J., LOZANO, J., LIU, J., SMALLEY, R. E., HAUGE, R. H. & MARGRAVE, J. L. 1999. Solvation of Fluorinated Single-Wall Carbon Nanotubes in Alcohol Solvents. *J Phys Chem B,* 103**,** 4318-4322.

MISHRA, A. K. & RAMAPRABHU, S. 2010. Magnetite Decorated Multiwalled Carbon Nanotube Based Supercapacitor for Arsenic Removal and Desalination of Seawater. *J Phys Chem C,* 114**,** 2583-2590.

MOGHADDAM, M. J., TAYLOR, S., GAO, M., HUANG, S., DAI, L. & MCCALL, M. J. 2003. Highly Efficient Binding of DNA on the Sidewalls and Tips of Carbon Nanotubes Using Photochemistry. *Nano Lett,* 4**,** 89-93.

MOHAN, D. & PITTMAN JR, C. U. 2007. Arsenic Removal from Water/Wastewater Using Adsorbents—A Critical Review. *J Hazard mater,* 142**,** 1-53.

MONDAL, P., BALOMAJUMDER, C. & MOHANTY, B. 2007. A Laboratory Study for the Treatment of Arsenic, Iron, and Manganese Bearing Ground Water Using Fe^{3+} Impregnated Activated Carbon: Effects of Shaking Time, pH and Temperature. *J Hazard Mater,* 144**,** 420-426.

MONDAL, P., MAJUMDER, C. B. & MOHANTY, B. 2006. Laboratory Based Approaches for Arsenic Remediation from Contaminated Water: Recent Developments. *J Hazard Mater,* 137**,** 464-479.

MULLER, J., HUAUX, F., MOREAU, N., MISSON, P., HEILIER, J. F., DELOS, M., ARRAS, M., FONSECA, A., NAGY, J. B. & LISON, D. 2005. Respiratory Toxicity of Multi-Wall Carbon Nanotubes. *Toxicol Appl Pharmacol,* 207**,** 221-231.

MURUGESAN, S., PARK, T.-J., YANG, H., MOUSA, S. & LINHARDT, R. J. 2006. Blood Compatible Carbon Nanotubes − Nano-Based Neoproteoglycans. *Langmuir,* 22**,** 3461-3463.

NAKAYAMA-RATCHFORD, N., BANGSARUNTIP, S., SUN, X., WELSHER, K. & DAI, H. 2007. Noncovalent Functionalization of Carbon Nanotubes by Fluorescein−Polyethylene Glycol: Supramolecular Conjugates with Ph-Dependent Absorbance and Fluorescence. *J Am Chem Soc,* 129**,** 2448-2449.

NAPIERSKA, D., THOMASSEN, L. C. J., RABOLLI, V., LISON, D., GONZALEZ, L., KIRSCH-VOLDERS, M., MARTENS, J. A. & HOET, P. H. 2009. Size-Dependent Cytotoxicity of Monodisperse Silica Nanoparticles in Human Endothelial Cells. *Small,* 5**,** 846-853.

NAVAS-ACIEN, A., SILBERGELD, E. K., PASTOR-BARRIUSO, R. & GUALLAR, E. 2008. Arsenic Exposure and Prevalence of Type 2 Diabetes in US Adults. *J Am Med Assoc,* 300**,** 814-822.

NIYOGI, S., BOUKHALFA, S., CHIKKANNANAVAR, S. B., MCDONALD, T. J., HEBEN, M. J. & DOORN, S. K. 2007. Selective Aggregation of Single-Walled Carbon Nanotubes Via Salt Addition. *J Am Chem Soc,* 129**,** 1898-1899.

NOGUCHI, Y., FUJIGAYA, T., NIIDOME, Y. & NAKASHIMA, N. 2008. Single-Walled Carbon Nanotubes/DNA Hybrids in Water are Highly Stable. *Chem Phys Lett,* 455**,** 249-251.

O'CONNELL, M. J., BOUL, P., ERICSON, L. M., HUFFMAN, C., WANG, Y., HAROZ, E., KUPER, C., TOUR, J., AUSMAN, K. D. & SMALLEY, R. E. 2001. Reversible Water-Solubilization of Single-Walled Carbon Nanotubes by Polymer Wrapping. *Chem Phys Lett,* 342**,** 265-271.

PAN, Y., NEUSS, S., LEIFERT, A., FISCHLER, M., WEN, F., SIMON, U., SCHMID, G., BRANDAU, W. & JAHNEN-DECHENT, W. 2007. Size-Dependent Cytotoxicity of Gold Nanoparticles. *Small,* 3**,** 1941-1949.

PASTORIN, G., WU, W., WIECKOWSKI, S., BRIAND, J.-P., KOSTARELOS, K., PRATO, M. & BIANCO, A. 2006. Double Functionalisation of Carbon Nanotubes for Multimodal Drug Delivery. *Chem Comm***,** 1182-1184.

PATNUKAO, P., KONGSUWAN, A. & PAVASANT, P. 2008. Batch Studies of Adsorption of Copper and Lead on Activated Carbon from Eucalyptus Camaldulensis Dehn. Bark. *J Environ Sci,* 20**,** 1028-1034.

PATTANAYAK, J., MONDAL, K., MATHEW, S. & LALVANI, S. B. 2000. A Parametric Evaluation of the Removal of As(V) and As(III) by Carbon-Based Adsorbents. *Carbon,* 38**,** 589-596.

PENG, X., JIA, J., GONG, X., LUAN, Z. & FAN, B. 2009. Aqueous Stability of Oxidized Carbon Nanotubes and the Precipitation by Salts. *J Hazard Mater,* 165**,** 1239-1242.

PETROV, P., LOU, X., PAGNOULLE, C., JÉRÔME, C., CALBERG, C. & JÉRÔME, R. 2004. Functionalization of Multi-Walled Carbon Nanotubes by Electrografting of Polyacrylonitrile. *Macromol Rapid Comm,* 25**,** 987-990.

POKHREL, D. & VIRARAGHAVAN, T. 2008. Arsenic Removal from an Aqueous Solution by Modified A. Niger Biomass: Batch Kinetic and Isotherm Studies. *J Hazard Mater,* 150**,** 818-825.

POMPEO, F. & RESASCO, D. E. 2002. Water Solubilization of Single-Walled Carbon Nanotubes by Functionalization with Glucosamine. *Nano Lett,* 2**,** 369-373.

PORTER, D., SRIRAM, K., WOLFARTH, M., JEFFERSON, A., SCHWEGLER-BERRY, D., ANDREW, M. E. & CASTRANOVA, V. 2008. A Biocompatible Medium for Nanoparticle Dispersion. *Nanotoxicology,* 2**,** 144-154.

RAMAMURTHY, S. S., CHEN, Y., KALYAN, M. K., RAO, G. N., CHELLI, J. & MITRA, S. 2011. Carbon Nanotube-Zirconium Dioxide Hybrid for Defluoridation of Water. *J Nanosci Nanotechnol,* 11**,** 3552-3559.

RICHARDSON, S. D. 2006. Environmental Mass Spectrometry: Emerging Contaminants and Current Issues. *Anal Chem,* 78**,** 4021-4046.

ROMO-HERRERA, J. M., TERRONES, M., TERRONES, H., DAG, S. & MEUNIER, V. 2006. Covalent 2D and 3D Networks from 1D Nanostructures: Designing New Materials. *Nano Lett,* 7**,** 570-576.

ROY, S., ADDO NTIM, S., MITRA, S. & SIRKAR, K. K. 2011. Facile Fabrication of Superior Nanofiltration Membranes from Interfacially Polymerized CNT-Polymer Composites. *J Mem Sci,* 375**,** 81-87.

SAGER, T. M., PORTER, D. W., ROBINSON, V. A., LINDSLEY, W. G., SCHWEGLER-BERRY, D. E. & CASTRANOVA, V. 2007. Improved Method to Disperse Nanoparticles for In Vitro and In Vivo Investigation of Toxicity. *Nanotoxicology,* 1**,** 118-129.

SALEH, N. B., PFEFFERLE, L. D. & ELIMELECH, M. 2008. Aggregation Kinetics of Multiwalled Carbon Nanotubes in Aquatic Systems: Measurements and Environmental Implications. *Environ Sci Technol,* 42**,** 7963-7969.

SALEH, N. B., PFEFFERLE, L. D. & ELIMELECH, M. 2010. Influence of Biomacromolecules and Humic Acid on the Aggregation Kinetics of Single-Walled Carbon Nanotubes. *Environ Sci Technol,* 44**,** 2412-2418.

SANO, M., KAMINO, A. & SHINKAI, S. 2000. Critical Coagulation of Langmuir Monolayers: 2D Schulze−Hardy Rule. *J Phys Chem B,* 104**,** 10339-10347.

SANO, M., OKAMURA, J. & SHINKAI, S. 2001. Colloidal Nature of Single-Walled Carbon Nanotubes in Electrolyte Solution: The Schulze−Hardy Rule. *Langmuir,* 17**,** 7172-7173.

SAY, R., YıLMAZ, N. & DENIZLI, A. 2003. Biosorption of Cadmium, Lead, Mercury, and Arsenic Ions by the Fungus Penicillium Purpurogenum. *Sep Sci Technol,* 38**,** 2039-2053.

SCHIPPER, M. L., NAKAYAMA-RATCHFORD, N., DAVIS, C. R., KAM, N. W. S., CHU, P., LIU, Z., SUN, X., DAI, H. & GAMBHIR, S. S. 2008. A Pilot Toxicology Study of Single-Walled Carbon Nanotubes in a Small Sample of Mice. *Nat Nano,* 3**,** 216-221.

SCHMIDT, G. T., VLASOVA, N., ZUZAAN, D., KERSTEN, M. & DAUS, B. 2008. Adsorption Mechanism of Arsenate by Zirconyl-Functionalized Activated Carbon. *J Colloid Interface Sci,* 317**,** 228-234.

SCHUDEL, M., BEHRENS, S. H., HOLTHOFF, H., KRETZSCHMAR, R. & BORKOVEC, M. 1997. Absolute Aggregation Rate Constants of Hematite Particles in Aqueous Suspensions: A Comparison of Two Different Surface Morphologies. *J Colloid Interface Sci,* 196**,** 241-253.

SHI KAM, N. W., JESSOP, T. C., WENDER, P. A. & DAI, H. 2004. Nanotube Molecular Transporters: Internalization of Carbon Nanotube−Protein Conjugates into Mammalian Cells. *J Am Chem Soc,* 126**,** 6850-6851.

SHIEH, Y.-T., LIU, G.-L., WU, H.-H. & LEE, C.-C. 2007. Effects of Polarity and pH on the Solubility of Acid-Treated Carbon Nanotubes in Different Media. *Carbon,* 45**,** 1880-1890.

SHIM, M., SHI KAM, N. W., CHEN, R. J., LI, Y. & DAI, H. 2002. Functionalization of Carbon Nanotubes for Biocompatibility and Biomolecular Recognition. *Nano Lett,* 2**,** 285-288.

SHVEDOVA, A., CASTRANOVA, V., KISIN, E., SCHWEGLER-BERRY, D., MURRAY, A., GANDELSMAN, V., MAYNARD, A. & BARON, P. 2003. Exposure to Carbon Nanotube Material: Assessment of Nanotube Cytotoxicity Using Human Keratinocyte Cells. *J Toxicol Env Heal A,* 66**,** 1909-1926.

SHVEDOVA, A. A., KISIN, E. R., MERCER, R., MURRAY, A. R., JOHNSON, V. J., POTAPOVICH, A. I., TYURINA, Y. Y., GORELIK, O., AREPALLI, S., SCHWEGLER-BERRY, D., HUBBS, A. F., ANTONINI, J., EVANS, D. E., KU, B. K., RAMSEY, D., MAYNARD, A., KAGAN, V. E., CASTRANOVA, V. & BARON, P. 2005. Unusual Inflammatory and Fibrogenic Pulmonary Responses to Single-Walled Carbon Nanotubes in Mice. *Am J Physiol Lung Cell Mol Physiol,* 289**,** L698-L708.

SINANI, V. A., GHEITH, M. K., YAROSLAVOV, A. A., RAKHNYANSKAYA, A. A., SUN, K., MAMEDOV, A. A., WICKSTED, J. P. & KOTOV, N. A. 2005. Aqueous Dispersions of Single-Wall and Multiwall Carbon Nanotubes with Designed Amphiphilic Polycations. *J Am Chem Soc,* 127**,** 3463-3472.

SMITH, B., WEPASNICK, K., SCHROTE, K. E., BERTELE, A. R., BALL, W. P., O'MELIA, C. & FAIRBROTHER, D. H. 2009. Colloidal Properties of Aqueous Suspensions of Acid-Treated, Multi-Walled Carbon Nanotubes. *Environ Sci Technol,* 43**,** 819-825.

SPOSITO, G. 1984. *The Surface Chemistry of Soils,* Oxford, United Kingdom, Oxford University Press.

SU, C. & PULS, R. W. 2001. Arsenate and Arsenite Removal by Zerovalent Iron: Effects of Phosphate, Silicate, Carbonate, Borate, Sulfate, Chromate, Molybdate, and Nitrate, Relative to Chloride. *Environ Sci Technol,* 35**,** 4562-4568.

SUD, D., MAHAJAN, G. & KAUR, M. P. 2008. Agricultural Waste Material as Potential Adsorbent for Sequestering Heavy Metal Ions from Aqueous Solutions – a Review. *Bioresource Technol,* 99**,** 6017-6027.

TAGMATARCHIS, N. & PRATO, M. 2004. Functionalization of Carbon Nanotubes Via 1,3-Dipolar Cycloadditions. *J Mater Chem,* 14**,** 437-439.

TAN, Y. & RESASCO, D. E. 2005. Dispersion of Single-Walled Carbon Nanotubes of Narrow Diameter Distribution. *J Phys Chem B,* 109**,** 14454-14460.

TASIS, D., TAGMATARCHIS, N., BIANCO, A. & PRATO, M. 2006. Chemistry of Carbon Nanotubes. *Chem Rev,* 106**,** 1105-1136.

TERASHIMA, M. & NAGAO, S. 2007. Solubilization of [C60]Fullerene in Water by Aquatic Humic Substances. *Chem Lett,* 36**,** 302-303.

THESS, A., LEE, R., NIKOLAEV, P., DAI, H., PETIT, P., ROBERT, J., XU, C., LEE, Y. H., KIM, S. G., RINZLER, A. G., COLBERT, D. T., SCUSERIA, G. E., TOMANEK, D., FISCHER, J. E. & SMALLEY, R. E. 1996. Crystalline Ropes of Metallic Carbon Nanotubes. *Science,* 273**,** 483-487.

THIRUNAVUKKARASU, O. S., VIRARAGHAVAN, T. & SUBRAMANIAN, K. S. 2003. Arsenic Removal from Drinking Water Using Iron Oxide-Coated Sand. *Water Air Soil Poll,* 142**,** 95-111.

TIPPING, E. & OHNSTAD, M. 1984. Colloid Stability of Iron Oxide Particles from a Freshwater Lake. *Nature,* 308**,** 266-268.

TRIPATHY, S. S., BERSILLON, J.-L. & GOPAL, K. 2006. Removal of Fluoride from Drinking Water by Adsorption onto Alum-Impregnated Activated Alumina. *Sep Purif Technol,* 50**,** 310-317.

TROJANOWICZ, M. 2006. Analytical Applications of Carbon Nanotubes: A Review. *Trends Anal Chem,* 25**,** 480-489.

TU, X. & ZHENG, M. 2008. A DNA-Based Approach to the Carbon Nanotube Sorting Problem. *Nano Res,* 1**,** 185-194.

UMEYAMA, T., TEZUKA, N., FUJITA, M., MATANO, Y., TAKEDA, N., MURAKOSHI, K., YOSHIDA, K., ISODA, S. & IMAHORI, H. 2007. Retention of Intrinsic Electronic Properties of Soluble Single-Walled Carbon Nanotubes after a Significant Degree of Sidewall Functionalization by the Bingel Reaction. *J Phys Chem C,* 111**,** 9734-9741.

VÁCLAVÍKOVÁ, M., VITALE, K., GALLIOS, G. P. & IVANICOVÁ, L. 2009. *Water Treatment Technologies for the Removal of High-Toxity Pollutants,* Berlin, Germany, Springer.

VERWEY, E. J. W. & OVERBEEK, J. T. G. 1999. *Theory of the Stability of Lyophobic Colloids,* New York USA, Dover Publications.

VIDYASAGAR, D. 2007. Global Minute: Water and Health - Walking for Water and Water Wars. *J Perinatol,* 27**,** 56-58.

VIGOLO, B., PENICAUD, A., COULON, C., SAUDER, C., PAILLER, R., JOURNET, C., BERNIER, P. & POULIN, P. 2000. Macroscopic Fibers and Ribbons of Oriented Carbon Nanotubes. *Science,* 290**,** 1331-1334.

WANG, X., XIA, T., ADDO NTIM, S., JI, Z., GEORGE, S., MENG, H., ZHANG, H., CASTRANOVA, V., MITRA, S. & NEL, A. E. 2010. Quantitative Techniques for Assessing and Controlling the Dispersion and Biological Effects of Multiwalled Carbon Nanotubes in Mammalian Tissue Culture Cells. *ACS Nano,* 4**,** 7241-7252.

WANG, X., XIA, T., ADDO NTIM, S., JI, Z., LIN, S., MENG, H., CHUNG, C.-H., GEORGE, S., ZHANG, H., WANG, M., LI, N., YANG, Y., CASTRANOVA, V., MITRA, S., BONNER, J. C. & NEL, A. E. 2011. Dispersal State of Multiwalled Carbon Nanotubes Elicits Profibrogenic Cellular Responses That Correlate with Fibrogenesis Biomarkers and Fibrosis in the Murine Lung. *ACS Nano,* 5**,** 9772-9787.

WANG, X. X., WANG, J. N., CHANG, H. & ZHANG, Y. F. 2007a. Preparation of Short Carbon Nanotubes and Application as an Electrode Material in Li-Ion Batteries. *Adv Funct Mater,* 17**,** 3613-3618.

WANG, Y., IQBAL, Z. & MITRA, S. 2005a. Microwave-Induced Rapid Chemical Functionalization of Single-Walled Carbon Nanotubes. *Carbon,* 43**,** 1015-1020.

WANG, Y., IQBAL, Z. & MITRA, S. 2005b. Rapidly Functionalized, Water-Dispersed Carbon Nanotubes at High Concentration. *J Am Chem Soc,* 128**,** 95-99.

WANG, Y., IQBAL, Z. & MITRA, S. 2006. Rapid, Low Temperature Microwave Synthesis of Novel Carbon Nanotube–Silicon Carbide Composite. *Carbon,* 44**,** 2804-2808.

WANG, Z., LIU, Q., ZHU, H., LIU, H., CHEN, Y. & YANG, M. 2007b. Dispersing Multi-Walled Carbon Nanotubes with Water-Soluble Block Copolymers and Their Use as Supports for Metal Nanoparticles. *Carbon,* 45**,** 285-292.

WARHEIT, D. B., LAURENCE, B. R., REED, K. L., ROACH, D. H., REYNOLDS, G. A. & WEBB, T. R. 2004. Comparative Pulmonary Toxicity Assessment of Single-Wall Carbon Nanotubes in Rats. *Toxicol Sci,* 77**,** 117-125.

WHITE, B., BANERJEE, S., O'BRIEN, S., TURRO, N. J. & HERMAN, I. P. 2007. Zeta-Potential Measurements of Surfactant-Wrapped Individual Single-Walled Carbon Nanotubes. *J Phys Chem C,* 111**,** 13684-13690.

WICK, P., MANSER, P., LIMBACH, L. K., DETTLAFF-WEGLIKOWSKA, U., KRUMEICH, F., ROTH, S., STARK, W. J. & BRUININK, A. 2007. The Degree and Kind of Agglomeration Affect Carbon Nanotube Cytotoxicity. *Toxicol Lett,* 168**,** 121-131.

WIESNER, M. R., LOWRY, G. V., ALVAREZ, P., DIONYSIOU, D. & BISWAS, P. 2006. Assessing the Risks of Manufactured Nanomaterials. *Environ Sci Technol,* 40**,** 4336-4345.

WILKIE, J. A. & HERING, J. G. 1996. Adsorption of Arsenic onto Hydrous Ferric Oxide: Effects of Adsorbate/Adsorbent Ratios and Co-Occurring Solutes. *Colloids Surface A,* 107**,** 97-110.

WISE, E. L. & RAYMENT, I. 2004. Understanding the Importance of Protein Structure to Nature's Routes for Divergent Evolution in Tim Barrell Enzymes. *ChemInform,* 35.

WU, P., CHEN, X., HU, N., TAM, U. C., BLIXT, O., ZETTL, A. & BERTOZZI, C. R. 2008. Biocompatible Carbon Nanotubes Generated by Functionalization with Glycodendrimers. *Angew Chem Int Edit,* 47**,** 5022-5025.

YADANAPARTHI, S. K. R., GRAYBILL, D. & VON WANDRUSZKA, R. 2009. Adsorbents for the Removal of Arsenic, Cadmium, and Lead from Contaminated Waters. *J Hazard Mater,* 171**,** 1-15.

YAN, S. & LIAN, G. 2005. Synthesis and Characterization of Phase Controllable Zro2–Carbon Nanotube Nanocomposites. *Nanotechnology,* 16**,** 625-630.

YU, J., GROSSIORD, N., KONING, C. E. & LOOS, J. 2007. Controlling the Dispersion of Multi-Wall Carbon Nanotubes in Aqueous Surfactant Solution. *Carbon,* 45**,** 618-623.

YUAN, H., GAO, F., ZHANG, Z., MIAO, L., YU, R., ZHAO, H. & LAN, M. 2010. Study on Controllable Preparation of Silica Nanoparticles with Multi-Sizes and Their Size-Dependent Cytotoxicity in Pheochromocytoma Cells and Human Embryonic Kidney Cells. *J Health Sci,* 56**,** 632-640.

YUN, Y., SHANOV, V., TU, Y., SCHULZ, M. J., YARMOLENKO, S., NERALLA, S., SANKAR, J. & SUBRAMANIAM, S. 2006. A Multi-Wall Carbon Nanotube Tower Electrochemical Actuator. *Nano Lett,* 6**,** 689-693.

YUREKLI, K., MITCHELL, C. A. & KRISHNAMOORTI, R. 2004. Small-Angle Neutron Scattering from Surfactant-Assisted Aqueous Dispersions of Carbon Nanotubes. *J Am Chem Soc,* 126**,** 9902-9903.

ZHANG, Q. L., LIN, Y. C., CHEN, X. & GAO, N. Y. 2007. A Method for Preparing Ferric Activated Carbon Composites Adsorbents to Remove Arsenic from Drinking Water. *J Hazard Mater,* 148**,** 671-678.

ZHAO, B., HU, H., YU, A., PEREA, D. & HADDON, R. C. 2005. Synthesis and Characterization of Water Soluble Single-Walled Carbon Nanotube Graft Copolymers. *J Am Chem Soc,* 127**,** 8197-8203.

ZHENG, Y. M., LIM, S. F. & CHEN, J. P. 2009. Preparation and Characterization of Zirconium-Based Magnetic Sorbent for Arsenate Removal. *J Colloid Interface Sci,* 338**,** 22-29.

ZHOU, O., SHIMODA, H., GAO, B., OH, S., FLEMING, L. & YUE, G. 2002. Materials Science of Carbon Nanotubes: Fabrication, Integration, and Properties of Macroscopic Structures of Carbon Nanotubes. *Acct Chem Res,* 35**,** 1045-1053.